

UNIVERSITY OF CALIFORNIA
SANTA CRUZ

**MICROCLIMATIC CONTROLS ON CRITICAL ZONE
DEVELOPMENT AND ECOHYDROLOGIC FUNCTIONS**

A dissertation submitted in partial satisfaction of the
requirements for the degree of

DOCTOR OF PHILOSOPHY

in

EARTH SCIENCES

by

Amanda M. Donaldson

September 2024

The Dissertation of Amanda M. Donaldson
is approved:

Dr. Margaret Zimmer, Chair

Dr. Andrew Fisher

Dr. Noah Finnegan

Dr. Michael Loik

Peter F. Biehl
Vice Provost and Dean of Graduate Studies

Copyright © by
Amanda M. Donaldson
2024

Table of Contents

List of Figures	v
List of Tables	vii
Abstract	viii
Dedication	xii
Acknowledgments	xiii
1 Aspect Differences in Vegetation Type Drive Higher Evapotranspiration on a Pole-facing Slope in a California Oak Savanna	1
Abstract	2
1.1 Introduction	3
1.2 Methods	5
1.2.1 Site description and instrumentation	5
1.2.2 Field-based transpiration measurements	7
1.2.3 Remotely-sensed NDVI and ET	9
1.2.4 Subsurface water storage deficit calculations	10
1.3 Results	11
1.3.1 Field-based estimates of grass and oak transpiration	11
1.3.2 Remotely-sensed NDVI and ET	13
1.3.3 Subsurface water storage deficit	15
1.4 Discussion	16
1.4.1 Oak and grass transpiration in rain-dominated mediterranean climates	16
1.4.2 Ecohydrologic implications for higher ET on PFS	19
1.4.3 Multi-tool approaches to quantify oak savanna ET	20
1.5 Conclusion	22
1.6 References	24
1.7 Supplementary Materials	33
1.7.1 Grass transpiration methods	33

1.7.2	Sapflow methods	36
1.7.3	OpenET methods	39
1.7.4	Sapflow results	40
1.7.5	Open ET results	41
1.7.6	Supplementary References	43
2	Subsurface Weathering and Vadose Zone Water Storage Between Hillslopes with Opposing Aspects	45
2.1	Abstract	46
2.2	Introduction	47
2.3	Methods	50
2.3.1	Site description	50
2.3.2	Drilling, standard penetration tests and borehole completion	53
2.3.3	Core characterization, matrix porosity and geochemistry	54
2.3.4	Vadose zone hydrologic monitoring	56
2.4	Results	57
2.4.1	Core description, standard penetration tests, matrix porosity	57
2.4.2	Bulk geochemistry and chemical depletion	58
2.4.3	Mineral assemblages and evolution	64
2.4.4	Water storage in the weathered bedrock	66
2.5	Discussion	69
2.5.1	Subsurface chemical weathering and water storage patterns within Arbor Creek catchment	69
2.5.2	Controls on weathering and water cycling between hillslopes with opposing aspects	70
2.5.3	Weathering across sites underlain by clastic sedimentary rocks	73
2.5.4	Nuances and limitations of study	75
2.6	Conclusion	76
2.7	References	78
2.8	Supplementary Materials	91
3	Symmetry in Hillslope Steepness and Saprolite Thickness Between Hillslopes with Opposing Aspects	96

List of Figures

1.1	Location of study area and instrumentation	6
1.2	Field-based grass transpiration	11
1.3	Field-based tree transpiration	12
1.4	Remotely-sensed NDVI and ET	14
1.5	Slope-averaged soil water storage deficit	16
1.6	Monthly root-zone storage deficit	17
1.7	Annotated image of the constructed chamber	35
1.8	Image of grass density	35
1.9	Inter-model ET comparison	42
2.1	Site map with boreholes delineated	51
2.2	Depth profiles of matrix porosity and core images of recovered rock samples	59
2.3	Sulfur concentrations with depth between aspects	60
2.4	Absolute geochemical compositions	62
2.5	Chemical depletion and enrichment plots of individual elements	63
2.6	XRD and identified mineral peak intensities	65
2.7	Depth profiles of neutron count difference	67
2.8	Depth profile comparisons between changes in neutron counts and chemical depletion	68
2.9	Standard penetration tests for all boreholes	91
2.10	Mineralogical comparison between unweathered samples	93
2.11	Individual neutron probe surveys	94
2.12	Image of rock core with fine woody root	95
3.1	Site map	99
3.2	Seismic refraction survey and instrumentation	99
3.3	Slope distribution for Arbor Creek and broader region	102
3.4	Soil pit images with soil horizons	103
3.5	Seismic refraction velocity model	104
3.6	Average saprolite depth	104
3.7	Precipitation and soil moisture time series	105

3.8	Groundwater time series	106
3.9	Frameworks to explain similarities in hillslope steepness and saprolite thickness	107

List of Tables

S1.1 Study tree characteristics	37
S1.2 Tree survey	38
S1.3 Total sapflow comparison	40
S2.1 Protolith percent average geochemistry	92
3.1 Geometric information for the seismic refraction surveys	101

Abstract

Microclimatic controls on critical zone development and ecohydrologic functions

by

Amanda M. Donaldson

The Earth's critical zone (CZ) extends from the top of vegetation canopies to the base of weathered bedrock. Within this region, rock meets life, as water is stored and released to streams, groundwater and vegetation. However, understanding the complex interactions between vegetation, water cycling, and bedrock weathering remains a grand challenge in forecasting and managing freshwater resources and ecosystem health. The research presented here is motivated by the need to more accurately quantify how small changes in climate will alter the relationship between aboveground vegetation and belowground water cycling and subsurface weathering. It addresses this need by utilizing a natural experiment provided by aspect, or the direction a hillslope faces, which produces different amounts of direct solar radiation between adjacent hillslopes. Specifically, pole-facing slopes (north-facing in the northern hemisphere) receive less direct solar radiation compared to equator-facing slopes (south-facing in the northern hemisphere) which often lead to distinct vegetation structures (e.g. density, composition). Current models of how aspect mediates the relationship between vegetation, water cycling and the subsurface have been limited to snow-dominated landscapes with woody vegetation on either hillslope (e.g. trees). Furthermore, most studies have focused on the shallow soil, owing to the difficulty to directly characterize the physical and chemi-

cal properties of the weathered bedrock below. To overcome this limitation and explore how microclimates regulate critical zone form and ecohydrologic function, I established and continuously monitored Arbor Creek Experimental Catchment, a rain-dominated catchment that is dominated by oak trees on the pole-facing slope and only has grasses on the equator-facing slope.

In my first chapter, I investigated how the interplay between microclimates and vegetation type (e.g. grass versus tree) regulate the timing and magnitude of evapotranspiration (combined evaporation and plant water use). Within Arbor Creek Catchment, I combined oak tree sapflow, grass transpiration, and soil moisture monitoring with tree survey based evapotranspiration scaling, and remote sensing techniques to quantify hillslope-scale evapotranspiration. My research revealed that despite receiving less direct solar radiation, the pole-facing slope with oak trees has higher evapotranspiration than warmer equator-facing slopes. This research highlights the importance of adequately representing hillslope-scale vegetation dynamics to more accurately predict evapotranspiration, which is the largest and most difficult component of the terrestrial water cycle to constrain. Furthermore, these findings suggest that due to oak tree transpiration on pole-facing slopes, the subsurface root-zone water storage deficit may be higher (i.e. pole-facing slopes are drier) compared to the equator-facing slope with grasses which has important consequences for groundwater recharge and streamflow generation.

In my second chapter, I used deep drilling (6 - 40 m) to determine how differences in vegetation type (e.g. rooting structures and water use) influence the relationship

between subsurface bedrock weathering and water storage dynamics between hillslopes with opposing aspects. Extensive geochemical, physical and hydrologic measurements within near-ridge boreholes on the pole-facing and equator-facing slope reveal a coupling between the depth and extent of vadose zone water storage and bedrock weathering. Specifically, the subsurface bedrock within the pole-facing slope has a higher degree of chemical and physical alteration compared to the equator-facing slope. This is likely driven by both "bottom-up" and "top-down" drivers including a higher degree of protholith fracturing, larger change in vadose zone water storage, and deeper extent to roots which may promote rock weathering through root growth and enhanced microbial processes.

Lastly, in my third chapter, I combined topographic analyses, soil pits, and seismic refraction measurements to characterize the shallow (top 6 m) subsurface structure (e.g. thickness, porosity) from the ridge tops to the stream between hillslopes with opposing aspects. To determine the biophysical controls on shallow water storage and movement, I paired this physical characterization with soil moisture and transient, perched, groundwater measurements. My research showed that the average slope, soil, and saprolite thickness were similar between hillslopes with opposing aspects. The similarities in slope, soil thickness and saprolite thickness may also be a consequence of past weathering processes when this landscape was likely not precipitation-limited and woody vegetation was dominant across the catchment. Additionally, my results show a depth-dependent relationship between aspect and subsurface water storage. Specifically, while the soil moisture suggested similarities in soil water storage capacity, between rain

events the pole-facing slope soil remained wetter than the equator-facing slope soil due to less evaporative demand. However, we observed a higher occurrence of a perched, transient, groundwater response on the grass-dominated equator-facing slope, which was likely due to a lower root-zone storage deficit because of overall lower evapotranspiration.

Together, these dissertation chapters highlight the importance of past and present-day vegetation dynamics to mediate the effects of microclimate on water cycling and subsurface weathering. This work demonstrates the critical need to better refine vegetation type, rooting architecture, and water use patterns within Earth system models to more accurately predict hillslope-scale subsurface weathering and hydrologic processes. Furthermore, this research reveals the importance of root-zone water storage, below the soil and into weathered bedrock, to serve as an important control on hydrologic refugia, groundwater recharge, and ecosystem health within oak savannas.

To resilient and compassionate people, especially my parents,

Scott Donaldson and Angel Apodaca.

Acknowledgments

Here, I wish share my sincerest gratitude to the people that have filled my graduate school journey with support, laughter, and love. Without which this dissertation would not be possible.

I am forever grateful for my advisor Dr. Margaret Zimmer. I remember sitting with Margaret over breakfast during my prospective student visit to Santa Cruz. We sketched out a grand plan about how we were going to characterize the entire critical zone of two hillslopes and shared in a giddy excitement for the future. Now six years later, we have accomplished more than we could have even imagined on that day due to Margaret's unwavering leadership. Her leadership is only made stronger by her ability to bring together diverse ideas and people to build a scientific community. Thank you for the wonderful gift this graduate school experience has been. I look forward to many more chai lattes and collaborations. I also am grateful to my academic role models and committee members, Drs. Andrew Fisher, Noah Finnegan, and Michael Loik. Their insightful feedback has truly shaped this dissertation and my development as a scientist. Thank you to Andy and Noah, whose patience and kindness provided a supportive environment for this Forestry undergraduate major to grapple with complex concepts in the Earth sciences. Michael, thank you for all the helpful conversations which helped me stay true to my ecology roots.

I would like to extend my sincerest thanks to the mentors that continue to inspire me. In particular, Dr. Jasper Oshun, who introduced me to the 'critical zone'

and field-based science. Thank you for challenging me to dig deeper - both beyond the shallow soil and to explore interdisciplinary scientific questions. Additionally, I have benefited immensely from the mentorship from Drs. Kerri Johnson, Mong-Han Huang, Russell Callahan, David Dralle, Jesse Hahm, Daniella Rempe, and Todd Dawson. I feel tremendously grateful to have a network of such kind, brilliant, talented, and fun people to do science with.

I am grateful to past and present members of the Watershed Hydrology Lab including but not limited to Chris Causbrook, Michael Wilshire, Nerissa Barling, Andi Greene, Emilio Grande, Adam Hayes, and Adam Price. Your technical support, guidance, good music and conversations during long car rides, and friendships kept me going. I am grateful to the community of people at Blue Oak Ranch Reserve, namely Zac Harlow and Zac Tuthill. I am also indebted to anyone who ever came to Arbor Creek Experimental Catchment to take a water sample, swing a hammer, or dig a hole. Apologies for not mentioning you by name but you know who you are and this dissertation would not have been completed with you.

I am the scientist and the person I am today because of the support from Katy Hall, Anna Nordstrom, Bailey Kline, Jenny Pensky, Kristin Dickerson, Maya Montalvo, and Lauren Giggy. A special thank you to my partner, Gavin Piccione. Thank you for being with me through the peaks and valleys of life and science. I would like to thank my family including but not limited to Scott, Angel and Gina, Vince, and Daniel, whose endless love has propelled my educational and personal achievements. Thank you for always loving me, for Me.

Finally, I am extremely grateful for the financial support that have enabled this research. This includes the National Science Foundation CAREER grant, the Mildred E. Mathias Graduate Student Research Grant, and funding from the Achievement Rewards for College Scientists Foundation. In addition, I am thankful for funding opportunities provided through the University of California, Santa Cruz including the Kathryn D. Sullivan Impact Award, Hammett Fellowship for Interdisciplinary Water Science, Eli Silver Opportunities Fund, Zhen and Wu Memorial Fund Award and the Office of the President's Pre-Professoriate Fellowship.

Chapter 1

Aspect Differences in Vegetation Type Drive Higher Evapotranspiration on a Pole-facing Slope in a California Oak Savanna

This chapter is based on a manuscript in-review within the Journal of Geophysical Research: Biogeosciences with the following coauthors: David Dralle, Nerissa Barling, Russell Callahan, Michael E. Loik and Margaret Zimmer.

Abstract

Quantifying evapotranspiration is critical to accurately predict vegetation health, groundwater recharge, and streamflow generation. Hillslope aspect, the direction a hillslope faces, results in variable incoming solar radiation and subsequent vegetation water use that influence the timing and magnitude of evapotranspiration. Previous work in forested landscapes has shown that equator-facing slopes have higher evapotranspiration due to more direct solar radiation and higher evaporative demand. However, it remains unclear how differences in vegetation type (i.e., grasses and trees) influence evapotranspiration and water partitioning between hillslopes with opposing aspects. Here, we quantified evapotranspiration and subsurface water storage deficits between a pole- and equator-facing hillslope with contrasting vegetation types within central coastal California. Our results suggest that cooler pole-facing slopes with oak trees have higher evapotranspiration than warmer equator-facing slopes with grasses, which is counter to previous work in landscapes with singular vegetation types. Our water storage deficit calculations indicate that the pole-facing slope has a higher subsurface storage deficit and a larger seasonal dry down than the equator-facing slope. This aspect difference in subsurface water storage deficits may influence subsequent deep groundwater recharge and streamflow generation. In addition, larger root-zone storage deficits on pole-facing slopes may reduce their ability to serve as hydrologic refugia for oaks during periods of extended drought. This research provides a novel integration of field-based and remotely-sensed estimates of evapotranspiration required to properly

quantify hillslope-scale water balances. These findings emphasize the importance of resolving hillslope-scale vegetation structure within Earth system models, especially in landscapes with diverse vegetation types.

1.1 Introduction

Differences in hillslope aspect, or the direction a hillslope faces, produce subcatchment-scale variability in the delivery of solar radiation to the land surface, which is one of the strongest controls on vegetation distribution and water partitioning within terrestrial landscapes (Chorover et al., 2011; Ying et al., 2019). Equator-facing slopes (EFS; south-facing in the northern hemisphere) with more direct solar radiation have higher air temperature, aridity, and evaporative demand compared to pole-facing slopes (PFS, north-facing in the northern hemisphere)(Smith and Bookhagen, 2021). Current conceptual frameworks depict warmer EFS with higher potential evapotranspiration and subsequently lower infiltration, groundwater recharge, and runoff (García-Gamero et al., 2021; Pelletier et al., 2018; Regmi et al., 2019; Webb et al., 2023). In contrast, cooler PFS are considered to have lower potential evapotranspiration and higher infiltration, groundwater recharge, and runoff (García-Gamero et al., 2021; Pelletier et al., 2018; Regmi et al., 2019; Webb et al., 2023). While this current conceptual model may provide insight into how differences in energy inputs drive hydrologic partitioning, it is unclear if the expected patterns are universal across diverse environments and vegetation types (Brooks et al., 2015; Ying et al., 2019; Zapata-Rios et al., 2016).

Understanding the compounding role of variable solar radiation and plant functional groups (e.g., grass, tree, shrub) is important for determining the transferability of current expectations of hydrologic partitioning between hillslopes with opposing aspects (Kumari et al., 2020). The current conceptual model of hydrologic partitioning within aspect-regulated landscapes is largely based on environments where potential differences in actual evapotranspiration (ET) due to variability in plant functional groups are not incorporated (Pelletier et al., 2018; Regmi et al., 2019). Studies in watersheds with similar plant functional groups (e.g., trees) have shown higher transpiration rates on EFS compared to PFS (Bilir et al., 2021; Burns et al., 2023; Holst et al., 2010). However, there is also documented diversity in the responses of different plant functional groups and species between aspects, which create complex patterns of vegetation water uptake (e.g. due to differences in rooting depth) and have lesser known consequences on subsurface water cycling (Armesto and Martinez, 1978; Gutiérrez-Jurado et al., 2013; Hassler et al., 2018). Given the importance of vegetation water uptake in driving subsurface hydrologic partitioning, understanding the role of vegetation type is required to accurately forecast water cycling patterns within Earth system models (Kumari et al., 2020; Marston et al., 2022; Ying et al., 2019).

Here, we address these knowledge gaps by quantifying hourly to monthly ET and shallow subsurface water storage between a grass-dominated EFS and an oak tree-dominated PFS in central California. We combined field-based measurements of soil moisture, oak and grass transpiration, tree survey-based scaling, and remotely-sensed normalized difference vegetation index (NDVI) and ET to determine how hydrologic

partitioning differs between hillslopes with opposing aspects and different plant community types.

1.2 Methods

1.2.1 Site description and instrumentation

The study site (Arbor Creek Experimental Catchment; 37.393, -121.723) ranges from 720 to 790 m above sea level and is located within the University of California Blue Oak Ranch Reserve (Figure 1.1). This reserve is located within the Mt. Diablo Range, 24 km northeast of San Jose, California, USA. The local climate is classified as Mediterranean, with hot, dry summers and cool, wet winters and an average 600 mm of precipitation mostly falling as rain between October - April (Donaldson et al., 2023). Soils are loamy and thin (50 cm) and the dominant rock types are sandstone and shale consistent with the Yolla Bolly Unit and the Great Valley Sequence (Donaldson et al., 2023).

We installed a weather station (ClimaVUE50, Campbell Scientific; Logan, Utah) at the ridge of the PFS to record precipitation at 10-min intervals from October 1, 2020 - September 30, 2021 (2021 water year). We excavated soil pits at each landscape position (e.g. toeslope, mid-slope, and shoulder) on the PFS and EFS (Figure 1). We monitored soil moisture (ECHO/EC-5, Decagon, Devices Inc. Washington, USA) every 10-min at 10 cm and 50 cm depths from winter 2020 through September 2021 (start date varied due to sensor installation).

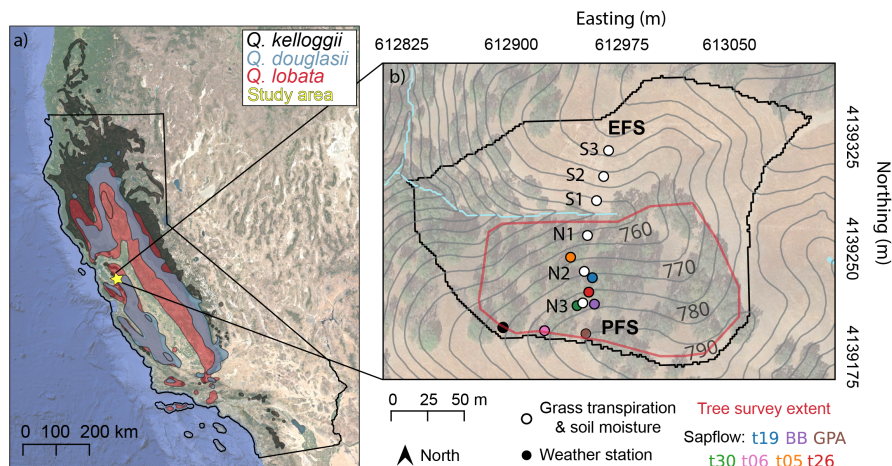


Figure 1.1: (a) Location of study area (yellow star) and approximate natural range of *Q. kelloggii* (black shaded region), *Q. lobata* (red shaded region), *Q. douglasii* (blue shaded region) (United States. Forest Service, 1971). Background is a Google Earth Imagery shaded relief of topography. (b) Study site with instrumentation nests of grass transpiration and soil moisture measurements (white), weather station (black), study trees with sap flow sensors (colors) and tree survey extent (red line). Stream channels are delineated in light blue; contour interval is 5 m and numbers refer to elevation in m above sea level.

The study site is characterized as a mixed-deciduous oak savanna composed of blue oak (*Quercus douglasii* Hook., Fagaceae), black oak (*Quercus kelloggii*, Newb.), and valley oak (*Quercus lobata*, Nee), with evidence of some extent of hybridization between species (Nixon, 2002). While oaks are largely on the PFS, grasses are across the study site and include species from both native and non-native genera, including *Avena*, *Bromus*, and *Elymus* (Pers. Comm. land steward Zachariah Tuthill).

1.2.2 Field-based transpiration measurements

We measured plot-scale, surface ET with an open-path, infrared gas analyzer (model LI-7500, LICOR, Lincoln, Nebraska) within a chamber (0.5 m x 0.5 m x 0.5 m) constructed of a PVC pipe frame, covered by Tefzel film with a fan placed inside for chamber mixing (Supplementary Figure 1; (Huxman et al., 2004)). This measurement included both evaporation from the ground surface and grass transpiration, however, we assume that the evaporative flux is negligible, thus we refer to this measurement as “grass transpiration” throughout the manuscript (Arnone and Obrist, 2003; Schlesinger and Jasechko, 2014). We collected measurements weekly at each instrument nest starting when the grass became active after the first rainfall (December 10, 2020) to when the grass senescence (June 10, 2021), which represented a full grass growing season. We averaged grass transpiration across landscape positions on the PFS and EFS to determine hillslope-averaged grass transpiration for each measurement period. To determine a weekly hillslope-averaged grass transpiration, we assumed each measurement to be representative of the week and multiplied by 7 (number of days in the week). To calculate total grass growing season transpiration (December - June), we summed each hillslope-averaged grass transpiration value.

To quantify oak water use, we installed heat pulse velocity sap flow probes (Edaphic Scientific; (Forster, 2019, 2020)) within seven mature oak trees at 1.4 m height above ground surface (e.g., breast height) along the PFS of Arbor Creek Experimental Catchment. We chose the instrumented oak trees to include a wide range of landscape

positions and sizes (Supplementary Table 1). We measured sap flux during the oak tree growing season at 10 mm (outer position) and 20 mm (inner position) within the xylem every 15-min from May - December 2021. To correct for probe misalignment during installation, we assumed zero flow after leaf off (late December 2021) and used a wound correction diameter of 0.2 mm (Burgess et al., 2001). To measure sapwood thickness, we extracted tree cores using an increment borer in August 2021 and identified a shift from translucence to opaqueness, which represented the sapwood to heartwood transition (Quiñonez-Piñón and Valeo, 2018). With these cores, we quantified wood water content and density, which we used to convert heat pulse velocity to sap flux (Burgess et al., 2001). We quantified the radial profile of sap flux in two ways and for the final calculations we assume a constant sap flux across the sapwood (see Supplementary Section 1.2 for details;(Link et al., 2014)). To calculate sap flow volumetrically, we multiplied the sap flux by the corresponding sapwood area of the tree.

To scale oak tree sap flow measurements to hillslope-scale transpiration, we performed cruising surveys of every oak on the pole-facing hillslope (red outline in Figure 1b). A total of 113 trees were surveyed within the 12,550 m² survey area, which were used to estimate total hillslope-scale oak transpiration. We recorded the species and diameter at breast height (DBH) for each tree (Supplementary Table 2). Trees that forked below breast height were recorded as two individual trees. We estimated the growing season total sap flow for the surveyed trees using a power law function relating tree diameter to the growing season total sap flow for the instrumented trees. We summed the total sap flow for all trees and divided it by the survey area to quantify

a hillslope-scale transpiration magnitude [mm].

1.2.3 Remotely-sensed NDVI and ET

To explore temporal variability in vegetation greenness, we used Google Earth Engine to extract weekly NDVI values from the mid-slope position on the PFS and EFS using images collected from January 2017 to December 2021 on the Copernicus Sentinel-2 mission (10-m spatial resolution). NDVI compares the intensity of reflectance in the visible red and near-infrared spectrum to quantify vegetation greenness (Acker et al., 2014).

We quantified ET at the mid-slope position of our study hillslopes, with remotely-sensed ET products using Python application programming interface to access models from OpenET (Melton et al., 2022). OpenET uses Landsat imagery to estimate monthly ET at 30 m resolution with a variety of approaches, including surface energy balance, Priestley-Taylor, and psychrometry (FAO, 2023)(see Supplementary 1.3 for details). A multi-model Ensemble ET estimate was calculated by OpenET based on the arithmetic average after removing outliers using the Median Absolute Deviation method (Leys et al., 2013; Volk et al., 2024). While we included the ET results from all models in the Supplementary information (Supplementary Figure 3), we used the Ensemble model for analyses in this study

1.2.4 Subsurface water storage deficit calculations

We calculated the hillslope-average soil water storage [mm] by integrating soil water content from the surface to the 50 cm depth. We calculated the soil water storage deficit by subtracting the volumetric water content at each timestep from the maximum recorded volumetric water content, assuming the maximum represents a maximum unsaturated water content at field capacity. In addition, we compare this to an estimated subsurface water storage deficit calculated by the total field-based ET measurements on the EFS and the PFS.

Previous studies have shown that oak tree roots can extend beneath the soil, into the weathered bedrock, to extract deeper water storage referred to as rock moisture (Hahm et al., 2020, 2022; McCormick et al., 2021). To estimate this deeper storage we calculated the total subsurface water storage deficit (i.e. soil and rock moisture) across multiple water years, we calculated the root-zone storage deficit from October 2017 to September 2021 using statistically interpolated precipitation data (Oregon State’s PRISM daily precipitation) and remotely-sensed ET (Ensemble model from OpenET; described above) following the method by (Wang-Erlandsson et al., 2016) and adapted by (Dralle et al., 2021). The method used a mass-balance approach to estimate a root-zone storage deficit as a running, integrated difference between fluxes entering and exiting the root zone, assumed to be precipitation and ET, respectively. Here, we estimated the root-zone storage deficit over subsequent water years (2017-2021), where the running deficit represents a lower-bound on the amount of ET supplied from the

root zone that has not been replenished by precipitation. Therefore, the root-zone storage deficit represents the minimum amount of vegetation water uptake that is not accounted for by precipitation (refer to Wang-Erlandsson et al., 2016; Dralle et al., 2021; and McCormick et al., 2021 for details).

1.3 Results

1.3.1 Field-based estimates of grass and oak transpiration

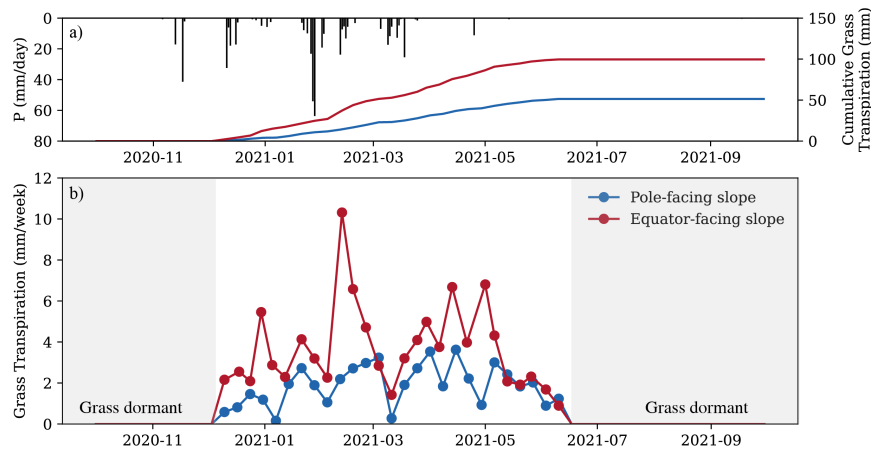


Figure 1.2: a) Daily precipitation (black) and cumulative grass transpiration for PFS (blue) and EFS (red) slopes, b) Slope-averaged weekly grass transpiration measurements for the PFS (blue) and EFS (red) slopes. Shaded regions are time periods with no measurements because grasses were dormant.

The EFS consistently had higher weekly grass transpiration than the PFS (Figure 1.2). The average grass transpiration on the EFS was 3.7 mm/week, while the average on the PFS was 1.9 mm/week. The total growing season grass transpiration

was 99 mm and 50 mm, on the EFS and PFS, respectively. Anecdotally, we observed higher grass density on the EFS compared to the PFS (Supplementary Figure 1.2).

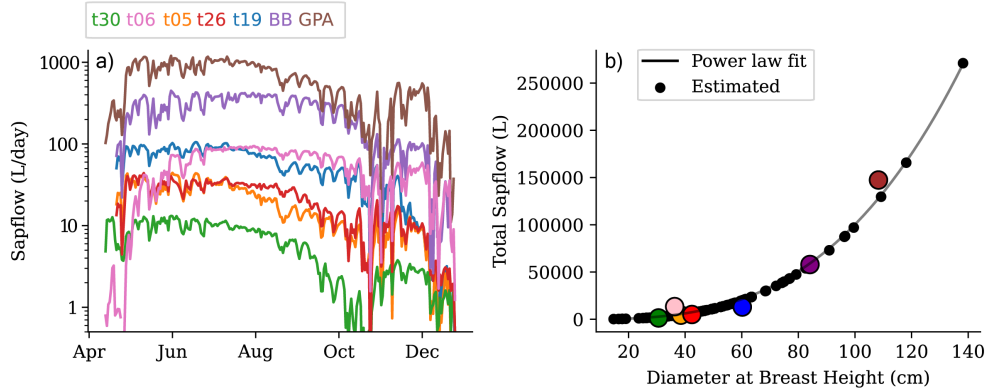


Figure 1.3: (a) Daily sap flow (L/day) on log-scale, (b) total sap flow (L) by DBH (cm) for each instrumented tree (colors) and surveyed trees fitted with a power-law function (black line).

Oak tree transpiration varied across the growing season (Figure 1.3a). Oak tree leaf development began in April (not entirely recorded due to sensor installation) and transpiration was generally low until a rapid increase in May. Transpiration reached a maximum in June and remained relatively constant until late August/September, when there was a decline. In October, there was an increase in transpiration that coincided with the first precipitation event of the fall, which lasted until December when the oak trees went dormant (Figure 1.3a).

Average volumetric oak tree transpiration (L/day) was positively correlated with DBH (Figure 3). For example, during oak tree peak water use (June), transpiration varied by DBH from approximately 12 L/day (T30; DBH: 30.6 cm) to 1100 L/day (GPA;

DBH: 108.3; Figure 1.3a). Consequently, total oak tree growing season transpiration generally varied with DBH (Figure 1.3b). From the smallest tree to the largest tree, the total growing season transpiration magnitude increased from 1427 L, 13433 L, 4373 L, 5078 L, 12988 L, 57962 L, and 147387 L (Figure 1.3b). The total hillslope-scale oak tree transpiration for the entire sap flow measurement period (May - December 2021) was 172 mm and 148 mm for the 2021 water year (May - September 2021).

1.3.2 Remotely-sensed NDVI and ET

There were annually consistent seasonal differences in NDVI values between the PFS and EFS (Figure 1.4a). During the winter season with only grasses actively transpiring (November - April), the EFS NDVI was on average 0.37, while the PFS NDVI was on average 0.32. During the oak tree growing season (April - October), the PFS had higher NDVI than the EFS with 0.39 and 0.28, respectively. During the 2021 water year, which coincided with our field-based measurement time period, the average NDVI values on the PFS and EFS were 0.33 and 0.28, respectively.

The remotely-sensed monthly ET was always higher on the PFS than the EFS (Figure 1.4b). During the winter, the average ET on the PFS was 41 mm/month, while the average ET on the EFS was 21 mm/month. During the oak tree growing season, the average ET on the PFS was 64 mm/month, while the average ET on the EFS was 29 mm/month. During the 2021 water year, the total ET on the PFS and EFS were 649 mm and 195 mm, respectively.

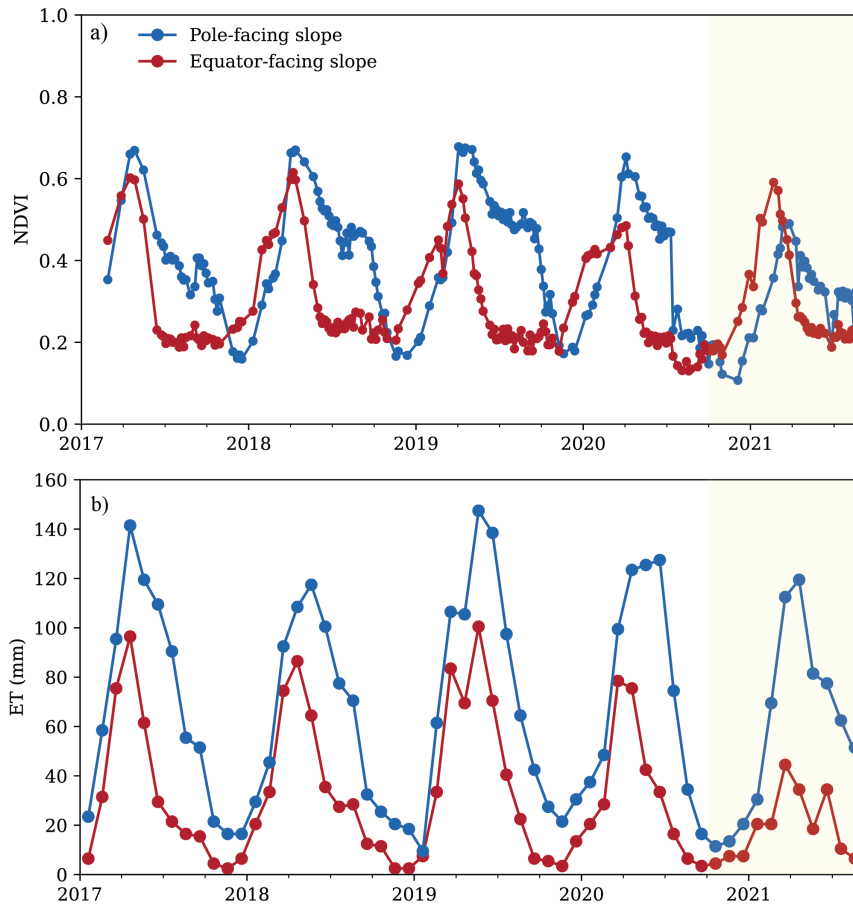


Figure 1.4: (a) Weekly NDVI on PFS (blue) and EFS (red) from January 2017 - September 2021. (b) Ensemble monthly ET on the PFS (blue) and EFS (red) for the same period. Timeframe of the field-based ET and soil moisture measurements are shaded in yellow.

1.3.3 Subsurface water storage deficit

During the 2021 water year, the timing and magnitude of field-calculated soil water storage depletion varied by season between hillslopes with opposing aspects (Figure 1.5b). There was higher subsurface water storage depletion on the EFS during the winter season, when grasses were active (January - April, Figure 2). In contrast, during the summer, the EFS had negligible soil water depletion, while there was considerable soil water storage depletion on the PFS with active oak trees (Figure 1.5b). At the end of the summer (September), there was a slightly lower cumulative soil water storage deficit on the EFS (94 mm) than the PFS (104 mm). In comparison, field-based ET measurements for the 2021 water year (October 2020 - September 2021) were used to calculate a subsurface storage deficit of 99 mm on the EFS (i.e. total grass transpiration) and 198 mm on the PFS (i.e. total grass and oak tree transpiration).

Across the 2017 - 2021 water years, the remotely-sensed root-zone storage deficits between the PFS and EFS showed contrasting behavior. Despite variability in precipitation magnitude, the root-zone storage deficit on the EFS (average 110 mm; standard deviation = 84 mm) was replenished each year (i.e. returned to zero; Figure 1.6). In contrast, on the PFS, the root-zone storage deficit was not annually replenished and increased from 534 mm at the end of water year 2017 to 1608 mm at the end of water year 2021.

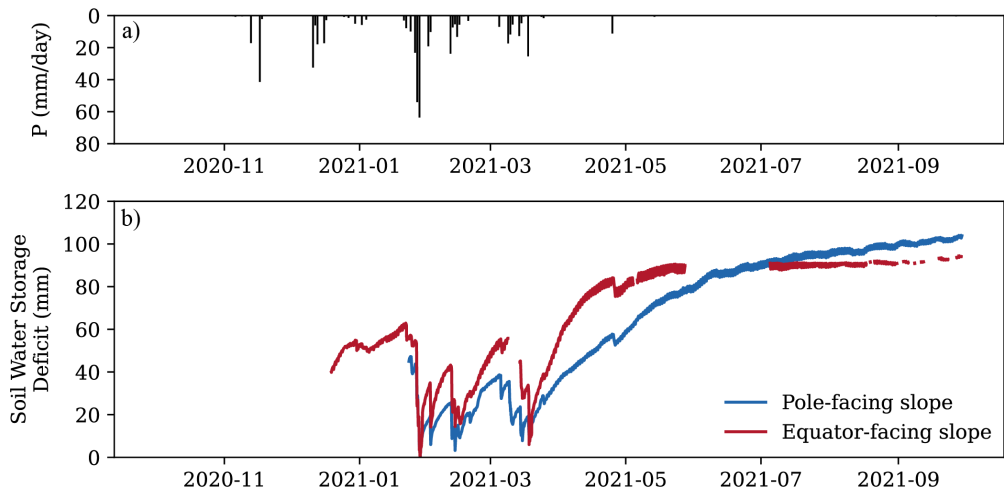


Figure 1.5: (a) Daily precipitation, (b) Field observations of slope-averaged soil water storage deficit within the top 50 cm from January - September 2021 on the PFS (blue) and EFS (red).

1.4 Discussion

1.4.1 Oak and grass transpiration in rain-dominated mediterranean climates

During water year 2021 (October 1 - September 30) the average ET within Arbor Creek Experimental Catchment ranged between 149 mm (field-based measurements) and 422 mm (remotely-sensed measurements). We interpret this range to represent a possible lower and upper bound on ET (see Section 1.4.3), which encompasses other reported ET values in California oak woodlands (Baldocchi et al., 2021; Lewis et al., 2000; Ma et al., 2020). Regardless of method, the majority of ET contributions were from the oak tree dominated PFS.

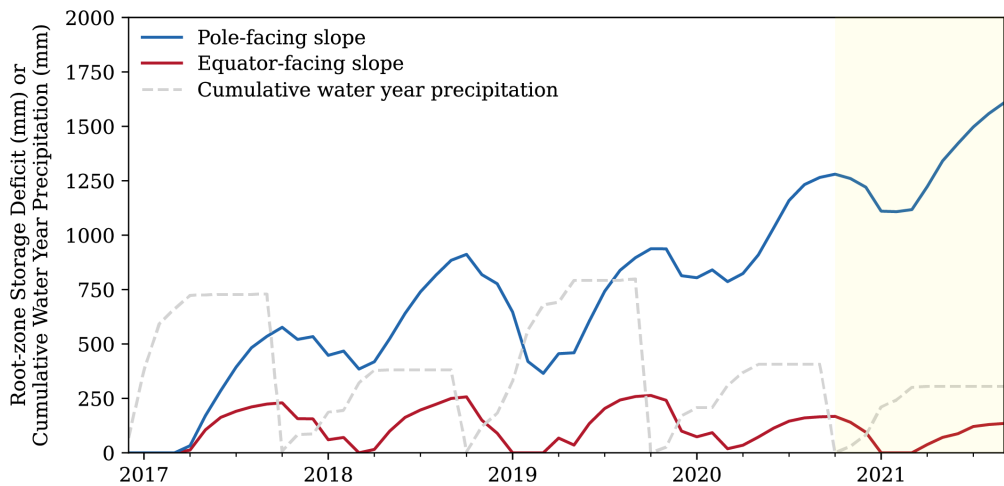


Figure 1.6: Monthly root-zone storage deficit for PFS (blue) and EFS (red) and cumulative water year precipitation (dashed gray) at the study site from remotely-sensed observations. The period of field-based ET and soil moisture measurements are shaded in yellow.

Extensive research quantifying and partitioning ET between oak and grass water use has been done within the Sierra Nevada, CA foothills dominated by blue oaks. For example, (Lewis et al., 2000) estimated an annual average ET of 364 mm over a 17 year period using a water balance approach. Over a similar time period, Baldocchi et al. (2021) used eddy flux towers to show that evaporative fluxes were higher within an oak savanna (420 ± 58.2 mm), compared to a nearby annual grassland (315 ± 37.7 mm). Within the same field site, Ma et al. (2020) combined nested eddy flux towers and partitioning models to determine that within the oak savanna, oak and grass transpiration contributed approximately 281 mm and 67 mm, respectively. These studies demonstrate the range of ET in oak savannas and highlight the need for more

research across different environmental conditions to identify the mechanistic controls on oak water use.

Outside of the Sierra foothills, there has been limited research quantifying oak woodland ET and the role of ET on subsurface water storage deficits. A notable exception includes work by (Hahm et al., 2022) that investigated blue oak transpiration and vadose zone storage dynamics within northern California. They reported that the mean annual ET at this site was 332 mm between 2001 and 2018 (Breathing Earth System Simulator; Ryu et al., 2011). By combining sapflow sensors and borehole hydrologic monitoring, they demonstrated that oak water use during the dry growing season was sustained by rock moisture below the soil (Hahm et al., 2022). However, while the authors describe the landscape as “aspect-regulated with negligible woody-vegetation on EFS,” the authors do not include information about the differences in oak and grass water uptake that drive subsurface water storage depletion.

In alignment with this study, our field-based and remotely-sensed estimates of ET suggest that soil water storage is insufficient to sustain oak tree transpiration during the summer. In addition, previous studies within Arbor Creek Experimental Catchment have shown that groundwater during the summer is depleted below 5 m (Donaldson et al., 2023), suggesting that oak transpiration is likely reliant on rock moisture on the PFS. Therefore, our research contributes to a growing body of literature that demonstrates the ecohydrologic importance of rock moisture for oak tree health.

1.4.2 Ecohydrologic implications for higher ET on PFS

The magnitude and timing of vegetation water uptake exerts a strong control on subsurface water storage and movement (Li et al., 2018; Sadayappan et al., 2023). In both the field-based estimates and remotely-sensed estimates of subsurface storage deficits, we observed higher subsurface water storage deficits on PFS compared to EFS. It is likely oak tree water uptake from rock moisture may limit groundwater recharge and streamflow generation on PFS (Dralle et al., 2023). Under these conditions, we hypothesize that groundwater recharge and streamflow contributions may be higher on EFS, which is contrary to existing conceptual models of water partitioning between hillslopes with opposing aspects (Pelletier et al., 2018; Regmi et al., 2019; Webb et al., 2023). Future field work utilizing deeper measurement tools, such as a neutron probe or other geophysical tools, will be used to validate the derived estimates of subsurface water storage and test this hypothesis.

In water-limited and rain-dominated landscapes, variability in root-zone storage deficit is a strong control on the spatial distribution of ecosystem resilience to disturbances, such as drought (Callahan et al., 2022). Our results suggest that multiple consecutive years of low precipitation inputs may exacerbate root-zone water storage deficits on PFS. During multi-year droughts, consistently high root-zone storage deficits on PFS may cause oak trees to be more susceptible to mortality (Ackerly et al., 2020; Brown et al., 2018; Kueppers et al., 2005). In comparison, even in relatively low precipitation years, subsurface water storage is replenished on the EFS. This finding highlights

an important question: why aren't there oaks on the EFS with a lower subsurface water storage deficit? We hypothesize that the absence of oak trees on EFS may be driven by higher air temperature, higher vapor pressure deficits, and lower shallow soil moisture that may limit oak seedling survival, despite potentially higher water availability below the soil (Nudurupati et al., 2023; Swiecki and Bernhardt, 1998). These findings highlight the importance of adequately representing plant functional group distributions and water uptake patterns through time to accurately refine water balances within aspect-regulated landscapes (Istanbulluoglu and Bras, 2005; Nudurupati et al., 2023; Ying et al., 2019; Zhou et al., 2013).

1.4.3 Multi-tool approaches to quantify oak savanna ET

An accurate quantification of hillslope-scale ET is essential for sustainable water resource management in the face of a changing climate, but it remains one of the biggest challenges within the ecohydrologic sciences (Brooks et al., n.d.; Marston et al., 2022; Ying et al., 2019). Through the advancement of field-based techniques and remote-sensing technology, the ecohydrology community is entering an exciting frontier where we can combine approaches and provide water resource managers with more accurate ET estimates (Volk et al., 2024). However, each method to quantify plant water uptake includes a suite of benefits and limitations that must be considered.

Field-based measurements using sap flow sensors can directly characterize biologically mediated plant-water uptake across diverse environmental conditions (Poyatos et al., 2021). In addition, sap flow sensors can provide high temporal resolution (e.g.,

minutes) data, which allows for a more robust characterization of transpiration patterns compared to remote sensing, which typically reports ET on daily to monthly time intervals (Melton et al., 2022; Link et al., 2014). However, sap flow measurements often produce a conservative estimate of ET and can be time consuming, expensive, limited in scope, and require substantial field expertise (Köstner et al., 1998). For example, re-installations early in the growing season due to probe misalignment hindered our ability to quantify transpiration in April 2021, which suggests our hillslope-scale transpiration values are underestimates. In addition, the relationship between DBH and sap flow may vary across stand structure (e.g. density, species, age) and the relationship between sapwood area and DBH may vary across the oak genus (Forrester et al., 2022; Schoppach et al., 2021, 2023). This highlights the importance of well-thought-out field-based studies to identify how stand structure influences sap flow to better constrain oak transpiration from the individual tree to hillslope-scale.

Remotely-sensed estimates of ET come with their own unique set of benefits and limitations (FAO, 2023). On the one hand, remotely-sensed ET data provides information at large spatial-scales, takes minimal time for a user to acquire, and is readily comparable between diverse landscapes and different ET models (Melton et al., 2022). On the other hand, individual ET models have known, difficult-to-resolve biases that inhibit their use within upland landscapes (Wang et al., 2022; Zhao and Li, 2015). For example, most remotely-sensed models within the OpenET ensemble do not include a correction for complex terrain (e.g., slope, aspect). The ET models' inability to correct for aspect-driven differences in solar radiation may contribute to the

unexpected higher ET during the winter on the PFS despite higher field-based ET on the EFS (<https://openetdata.org/known-issues/>; last accessed Jan 9, 2023). Therefore, we interpreted the ensemble ET to represent an upper bound of ET and highlight the need for more remotely-sensed ET models to incorporate corrections for variable terrain indices (e.g., slope, aspect) and vegetation phenology. Given that each approach has its limitations and produces a range of ET values, a more holistic and accurate approach to quantifying ET dynamics should include multiple methods in tandem.

1.5 Conclusion

A commonly used conceptual model of ET, hydrologic partitioning, and landscape evolution between hillslopes with opposing aspects is based on landscapes with similar plant functional groups (e.g., trees) (Pelletier et al., 2018; Riebe et al., 2017). This conceptual model assumes that a larger energy input on EFS will induce a higher evaporative demand, increase transpiration rates, and drive higher annual ET on EFS compared to PFS (Pelletier et al., 2018). However, these studies do not account for the potential confounding influence of distinct vegetation communities on hillslopes with opposing aspects. In the Arbor Creek Experimental Catchment, we observed that our PFS had higher annual ET due to oak tree water uptake, compared to the equator-facing hillslope with only grasses. Higher ET on PFS contributed to higher subsurface water storage deficits through time. Our work reveals the importance of accurately representing vegetation types and phenology at the scale of individual hillslopes to better

estimate ET and subsurface hydrologic partitioning.

1.6 References

- Acker, J., Williams, R., Chiu, L., Ardanuy, P., Miller, S., Schueler, C., Vachon, P. W., & Manore, M. (2014). *Remote sensing from satellites*. Reference Module in Earth Systems and Environmental Sciences. <https://cir.nii.ac.jp/crid/1360576123088102400>
- Ackerly, D. D., Kling, M. M., Clark, M. L., Papper, P., Oldfather, M. F., Flint, A. L., & Flint, L. E. (2020). *Topoclimates, refugia, and biotic responses to climate change*. *Frontiers in Ecology and the Environment*, 18(5), 288–297.
- Armesto, J. J., & Martinez, J. A. (1978). Relations Between Vegetation Structure and Slope Aspect in the Mediterranean Region of Chile. *The Journal of Ecology*, 66(3), 881–889.
- Arnone, J. A., & Obrist, D. (2003). A large daylight geodesic dome for quantification of whole-ecosystem CO₂ and water vapour fluxes in arid shrublands. *Journal of Arid Environments*, 55(4), 629–643.
- Baldocchi, D., Chen, Q., Chen, X., Ma, S., Miller, G., Ryu, Y., Xiao, J., Wenk, R., Battles, J., & Taylor, C. (2006). The dynamics of energy, water and carbon fluxes in a blue oak (*Quercus douglasii*) Savanna in California, USA. Retrieved January 8, 2024, from <https://nature.berkeley.edu/biometlab/pdf/Flux>
- Baldocchi, D., Ma, S., & Verfaillie, J. (2021). On the inter- and intra-annual variability of ecosystem evapotranspiration and water use efficiency of an oak savanna and annual grassland subjected to booms and busts in rainfall. *Global Change Biology*, 27(2), 359–375.

- Bilir, T. E., Fung, I., & Dawson, T. E. (2021). Slope-aspect induced climate differences influence how water is exchanged between the land and atmosphere. *Journal of Geophysical Research. Biogeosciences*, 126(5). <https://doi.org/10.1029/2020jg006027>
- Brooks, P. D., Chorover, J., & Fan, Y. (n.d.). Hydrological partitioning in the critical zone: Recent advances and opportunities for developing transferable understanding of water cycle dynamics. *Water Resources*. <https://doi.org/10.1002/2015WR017039>
- Brown, B. J., McLaughlin, B. C., Blakey, R. V., & Morueta-Holme, N. (2018). Future vulnerability mapping based on response to extreme climate events: Dieback thresholds in an endemic California oak. *Diversity & Distributions*, 24(9), 1186–1198.
- Burgess, S. S., Adams, M. A., Turner, N. C., Beverly, C. R., Ong, C. K., Khan, A. A., & Bleby, T. M. (2001). An improved heat pulse method to measure low and reverse rates of sap flow in woody plants. *Tree Physiology*, 21(9), 589–598.
- Burns, E. F., Rempe, D. M., Parsekian, A. D., Schmidt, L. M., Singha, K., & Barnard, H. R. (2023). Ecohydrologic dynamics of rock moisture in a Montane catchment of the Colorado front range. *Water Resources Research*, 59(6).
- Callahan, R. P., Riebe, C. S., Sklar, L. S., Pasquet, S., Ferrier, K. L., Hahm, W. J., Taylor, N. J., Grana, D., Flinchum, B. A., Hayes, J. L., & Holbrook, W. S. (2022). Forest vulnerability to drought controlled by bedrock composition. *Nature Geoscience*, 15(9), 714–719.
- Chorover, J., Troch, P. A., Rasmussen, C., Brooks, P. D., Pelletier, J. D., Breshears, D. D., Huxman, T. E., Kurc, S. A., Lohse, K. A., McIntosh, J. C., Meixner, T., Schaap, M. G., Litvak, M. E., Perdrial, J., Harpold, A., & Durcik, M. (2011). How

- water, carbon, and energy drive critical zone evolution: The jemez–Santa Catalina Critical Zone Observatory. *Vadose Zone Journal: VZJ*, 10(3), 884–899.
- Donaldson, A. M., Zimmer, M., Huang, M.-H., Johnson, K. N., Hudson-Rasmussen, B., Finnegan, N., Barling, N., & Callahan, R. P. (2023). Symmetry in hillslope steepness and saprolite thickness between hillslopes with opposing aspects. *Journal of Geophysical Research. Earth Surface*, 128(7). <https://doi.org/10.1029/2023jf007076>
- Dralle, D. N., Hahm, W. J., Chadwick, K. D., McCormick, E., & Rempe, D. M. (2021). Technical note: Accounting for snow in the estimation of root zone water storage capacity from precipitation and evapotranspiration fluxes. *Hydrology and Earth System Sciences*, 25(5), 2861–2867.
- Dralle, D. N., Hahm, W. J., & Rempe, D. M. (2023). Inferring hillslope groundwater recharge ratios from the storage-discharge relation. *Geophysical Research Letters*, 50(14). <https://doi.org/10.1029/2023gl104255>
- Fan, Y., Clark, M., Lawrence, D. M., Swenson, S., Band, L. E., Brantley, S. L., et al. (2019). Hillslope hydrology in global change research and Earth system modeling. *Water Resources Research*, 55, 1737–1772. <https://doi.org/10.1029/2018WR023903>
- FAO. (2023). Remote sensing determination of evapotranspiration – Algorithms, strengths, weaknesses, uncertainty and best fit-for-purpose.
- Forrester, D. I., Limousin, J.-M., & Pfautsch, S. (2022). The relationship between tree size and tree water-use: is competition for water size-symmetric or size-asymmetric? *Tree Physiology*, 42(10), 1916–1927.
- Forster, M. A. (2019). The Dual Method Approach (DMA) Resolves Measurement

- Range Limitations of Heat Pulse Velocity Sap Flow Sensors. *Forests, Trees and Livelihoods*, 10(1), 46. Forster, M. A. (2020). The importance of conduction versus convection in heat pulse sap flow methods. *Tree Physiology*, 40(5), 683–694.
- García-Gamero, V., Peña, A., Laguna, A. M., Giráldez, J. V., & Vanwallegem, T. (2021). Factors controlling the asymmetry of soil moisture and vegetation dynamics in a hilly Mediterranean catchment. *Journal of Hydrology*, 598, 126207.
- Gutiérrez-Jurado, H. A., Vivoni, E. R., Cikoski, C., Harrison, J. B. J., Bras, R. L., & Istanbulluoglu, E. (2013). On the observed ecohydrologic dynamics of a semiarid basin with aspect-delimited ecosystems. *Water Resources Research*, 49(12), 8263–8284.
- Hahm, W. J., Dralle, D. N., Sanders, M., Bryk, A. B., Fauria, K. E., Huang, M. H., Hudson-Rasmussen, B., Nelson, M. D., Pedrazas, M. A., Schmidt, L., Whiting, J., Dietrich, W. E., & Rempe, D. M. (2022). Bedrock vadose zone storage dynamics under extreme drought: Consequences for plant water availability, recharge, and runoff. *Water Resources Research*, 58(4). <https://doi.org/10.1029/2021wr031781>
- Hahm, W. J., Rempe, D. M., Dralle, D. N., Dawson, T. E., & Dietrich, W. E. (2020). Oak transpiration drawn from the weathered bedrock vadose zone in the summer dry season. *Water Resources Research*, 56(11). <https://doi.org/10.1029/2020wr027419>
- Hassler, S. K., Weiler, M., & Blume, T. (2018). Tree-, stand- and site-specific controls on landscape-scale patterns of transpiration. *Hydrology and Earth System Sciences*, 22(1), 13–30.
- Holst, J., Grote, R., Offermann, C., Ferrio, J. P., Gessler, A., Mayer, H., & Rennenberg, H. (2010). Water fluxes within beech stands in complex terrain. *International*

- Journal of Biometeorology, 54(1), 23–36.
- Huxman, T. E., Cable, J. M., Ignace, D. D., Eilts, J. A., English, N. B., Weltzin, J., & Williams, D. G. (2004). Response of net ecosystem gas exchange to a simulated precipitation pulse in a semi-arid grassland: the role of native versus non-native grasses and soil texture. *Oecologia*, 141(2), 295–305.
- Istanbulluoglu, E., & Bras, R. L. (2005). Vegetation-modulated landscape evolution: Effects of vegetation on landscape processes, drainage density, and topography. *Journal of Geophysical Research*, 110(F2). <https://doi.org/10.1029/2004jf000249>
- Köstner, B., Granier, A., & Cermák, J. (1998). Sapflow measurements in forest stands: methods and uncertainties. *Annales Des Sciences Forestières*, 55(1-2), 13–27.
- Kueppers, L. M., Snyder, M. A., Sloan, L. C., Zavaleta, E. S., & Fulfrost, B. (2005). Modeled regional climate change and California endemic oak ranges. *Proceedings of the National Academy of Sciences of the United States of America*, 102(45), 16281–16286.
- Kumari, N., Saco, P. M., Rodriguez, J. F., Johnstone, S. A., Srivastava, A., Chun, K. P., & Yetemen, O. (2020). The grass is not always greener on the other side: Seasonal reversal of vegetation greenness in aspect-driven semiarid ecosystems. *Geophysical Research Letters*, 47(15). <https://doi.org/10.1029/2020gl088918>
- Lewis, D., Singer, M. J., Dahlgren, R. A., & Tate, K. W. (2000). Hydrology in a California oak woodland watershed: a 17-year study. *Journal of Hydrology*, 240(1), 106–117.
- Leys, C., Ley, C., Klein, O., Bernard, P., & Licata, L. (2013). Detecting outliers: Do not

- use standard deviation around the mean, use absolute deviation around the median. *Journal of Experimental Social Psychology*, 49(4), 764–766.
- Li, H., Si, B., & Li, M. (2018). Rooting depth controls potential groundwater recharge on hillslopes. *Journal of Hydrology*, 564, 164–174.
- Marston, L. T., Abdallah, A. M., Bagstad, K. J., Dickson, K., Glynn, P., Larsen, S. G., Melton, F. S., Onda, K., Painter, J. A., Prairie, J., Ruddell, B. L., Rushforth, R. R., Senay, G. B., & Shaffer, K. (2022). Water-use data in the United States: Challenges and future directions. *Journal of the American Water Resources Association*, 58(4), 485–495.
- Ma, S., Eichelmann, E., Wolf, S., Rey-Sanchez, C., & Baldocchi, D. D. (2020). Transpiration and evaporation in a Californian oak-grass savanna: Field measurements and partitioning model results. *Agricultural and Forest Meteorology*, 295, 108204.
- McCormick, E. L., Dralle, D. N., Hahm, W. J., Tune, A. K., Schmidt, L. M., Chadwick, K. D., & Rempe, D. M. (2021). Widespread woody plant use of water stored in bedrock. *Nature*, 597(7875), 225–229.
- Melton, F. S., Huntington, J., Grimm, R., Herring, J., Hall, M., Rollison, D., Erickson, T., Allen, R., Anderson, M., Fisher, J. B., Kilic, A., Senay, G. B., Volk, J., Hain, C., Johnson, L., Ruhoff, A., Blankenau, P., Bromley, M., Carrara, W., . . . Anderson, R. G. (2022). OpenET: Filling a critical data gap in water management for the western United States. *Journal of the American Water Resources Association*, 58(6), 971–994.
- Nixon, K. C. (2002). The oak (*Quercus*) biodiversity of California and adjacent regions.

<https://www.researchgate.net/>

- Nudurupati, S. S., Istanbuluoglu, E., Tucker, G. E., Gasparini, N. M., Hobbey, D. E. J., Hutton, E. W. H., Barnhart, K. R., & Adams, J. M. (2023). On transient semi-arid ecosystem dynamics using Landlab: Vegetation shifts, topographic Refugia, and response to climate. *Water Resources Research*, 59(4).
<https://doi.org/10.1029/2021wr031179>
- Pelletier, J. D., Barron-Gafford, G. A., Gutiérrez-Jurado, H., Hinckley, E.-L. S., Istanbuluoglu, E., McGuire, L. A., Niu, G.-Y., Poulos, M. J., Rasmussen, C., Richardson, P., Swetnam, T. L., & Tucker, G. E. (2018). Which way do you lean? Using slope aspect variations to understand Critical Zone processes and feedbacks. *Earth Surface Processes and Landforms*, 43(5), 1133–1154.
- Percy L., Kevin S., Manns, H., Oshun J., Dawson T., Fung I. (2014). Species differences in the seasonality of evergreen tree transpiration in a Mediterranean climate: Analysis of multiyear, half-hourly sap flow observations. *Water Resources*.
<https://doi.org/10.1002/2013WR014023>
- Poyatos, R., Werner, C., & Martínez-Vilalta, J. (2021). Global Transpiration Data from Sap Flow Measurements: the SAPFLUXNET Database. *Universität*.
- Quiñonez-Piñón, M. R., & Valeo, C. (2018). Assessing the Translucence and Color-Change Methods for Estimating Sapwood Depth in Three Boreal Species. *Forests, Trees and Livelihoods*, 9(11), 686.
- Regmi, N. R., McDonald, E. V., & Rasmussen, C. (2019). Hillslope response under

- variable microclimate. *Earth Surface Processes and Landforms*, 44(13), 2615–2627.
- Riebe, C. S., Hahm, W. J., & Brantley, S. L. (2017). Controls on deep critical zone architecture: a historical review and four testable hypotheses. *Earth Surface Processes and Landforms*, 42(1), 128–156.
- Ryu, Y., Baldocchi, D. D., Kobayashi, H., van Ingen, C., Li, J., Black, T. A., Beringer, J., van Gorsel, E., Knohl, A., Law, B. E., & Roupsard, O. (2011). Integration of MODIS land and atmosphere products with a coupled-process model to estimate gross primary productivity and evapotranspiration from 1 km to global scales. *Global Biogeochemical Cycles*, 25(4). <https://doi.org/10.1029/2011gb004053>
- Sadayappan, K., Keen, R., Jarecke, K. M., Moreno, V., Nippert, J. B., Kirk, M. F., Sullivan, P. L., & Li, L. (2023). Drier streams despite a wetter climate in woody-encroached grasslands. *Journal of Hydrology*, 627, 130388.
- Schlesinger, W. H., & Jasechko, S. (2014). Transpiration in the global water cycle. *Agricultural and Forest Meteorology*, 189-190, 115–117.
- Schoppach, R., Chun, K. P., He, Q., Fabiani, G., & Klaus, J. (2021). Species-specific control of DBH and landscape characteristics on tree-to-tree variability of sap velocity. *Agricultural and Forest Meteorology*, 307, 108533.
- Schoppach, R., Chun, K. P., & Klaus, J. (2023). Allometric relations between DBH and sapwood area for predicting stand transpiration: lessons learned from the *Quercus* genus. *European Journal of Forest Research*, 142(4), 797–809.
- Smith, T., & Bookhagen, B. (2021). Climatic and biotic controls on topographic asymmetry at the global scale. *Journal of Geophysical Research. Earth Surface*, 126(1).

<https://doi.org/10.1029/2020jf005692>

- Swiecki, T. J., & Bernhardt, E. (1998). Understanding blue oak regeneration. *Fremon-
tia*, 26(1), 19–26.
- United States. Forest Service. (1971). Atlas of United States Trees: (no.1146). Conifers
and important hardwoods, by E.L. Little, Jr. U.S. Government Printing Office.
- Volk, J. M., Huntington, J. L., Melton, F. S., Allen, R., Anderson, M., Fisher, J. B.,
Kilic, A., Ruhoff, A., Senay, G. B., Minor, B., Morton, C., Ott, T., Johnson, L.,
Comini de Andrade, B., Carrara, W., Doherty, C. T., Dunkerly, C., Friedrichs, M.,
Guzman, A., ... Yang, Y. (2024). Assessing the accuracy of OpenET satellite-based
evapotranspiration data to support water resource and land management applica-
tions. *Nature Water*, 1–13.
- Wang-Erlandsson, L., Bastiaanssen, W. G. M., Gao, H., Jägermeyr, J., Senay, G. B.,
van Dijk, A. I. J. M., Guerschman, J. P., Keys, P. W., Gordon, L. J., & Savenije,
H. H. G. (2016). Global root zone storage capacity from satellite-based evaporation.
Hydrology and Earth System Sciences, 20(4), 1459–1481.
- Wang, L., Wu, B., Elnashar, A., Zhu, W., Yan, N., Ma, Z., Liu, S., & Niu, X. (2022).
Incorporation of Net Radiation Model Considering Complex Terrain in Evapotran-
spiration Determination with Sentinel-2 Data. *Remote Sensing*, 14(5), 1191.
- Webb, R. W., Litvak, M. E., & Brooks, P. D. (2023). The role of terrain-mediated
hydroclimate in vegetation recovery after wildfire. *Environmental Research Letters*
- Zapata-Rios, X., Brooks, P. D., Troch, P. A., McIntosh, J., & Guo, Q. (2016). Influence
of terrain aspect on water partitioning, vegetation structure and vegetation greening

in high-elevation catchments in northern New Mexico. *Ecohydrology*, 9(5), 782–795.

Zhao, W., & Li, A. (2015). A Review on Land Surface Processes Modelling over Complex Terrain. *Advances in Meteorology*, 2015. <https://doi.org/10.1155/2015/607181>

Zhou, X., Istanbuluoglu, E., Vivoni, E. R. (2013). Modeling the ecohydrological role of aspect-controlled radiation on tree-grass-shrub coexistence in a semiarid climate. *Water Resources Research*, 49(5), 2872–2895.

1.7 Supplementary Materials

1.7.1 Grass transpiration methods

We measured water fluxes with an open-path, infrared gas analyzer (model LI-7500, LI-COR Inc., Lincoln, Nebraska) within a chamber (0.5 m x 0.5 m x 0.5 m) constructed of a PVC pipe frame and covered by Tefzel film with a fan placed inside to maximize chamber mixing (Supplementary Figure 1.7) (Huxman et al., 2004). We started data collection approximately 30 seconds after the chamber was secured flat on the ground surface to ensure no leakage from the chamber; each measurement lasted for approximately 90 seconds. We determined water fluxes by plotting the 1-second water flux accumulation measurements over the 90-second period. The slope of the change in concentration (mg/m³/s) was converted into a flux (mmols/m²/s) by using the following equation:

$$\text{Flux}[\text{mmols}/\text{m}^2/\text{s}] = \frac{(\text{slope} \times \frac{\text{chamber volume}}{\text{chamber area}})}{\text{molecular weight of H}_2\text{O} \times 1000} \quad (1.1)$$

where the chamber volume was 0.125 m³, the surface area was 0.25 m², and the molecular weight of H₂O was 18 g/mol.

We assumed the surface plot-scale estimates of water fluxes represent only grass transpiration but we acknowledge that these measurements also include evaporative fluxes. We believe this assumption is reasonable because transpiration has been shown to be the largest component of ET (Schlesinger & Jasechko, 2014). However, the reported grass transpiration measurements likely represent an upper bound or may overestimate grass transpiration due to variability in grass density (Supplementary Figure 1.8).

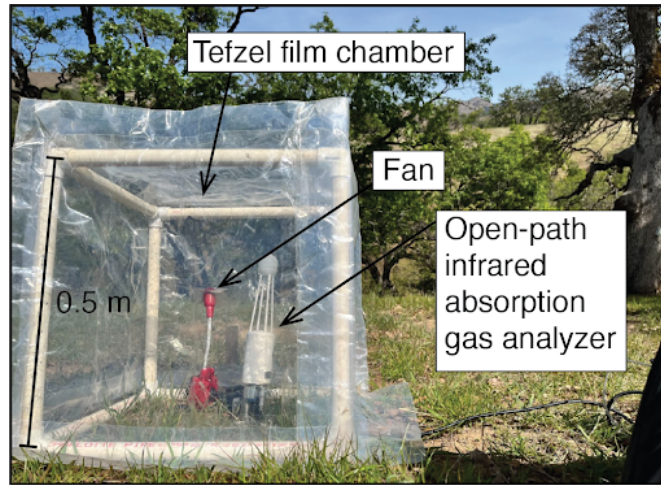


Figure 1.7: Annotated image of the constructed chamber to measure grass transpiration within Arbor Creek Experimental Catchment.

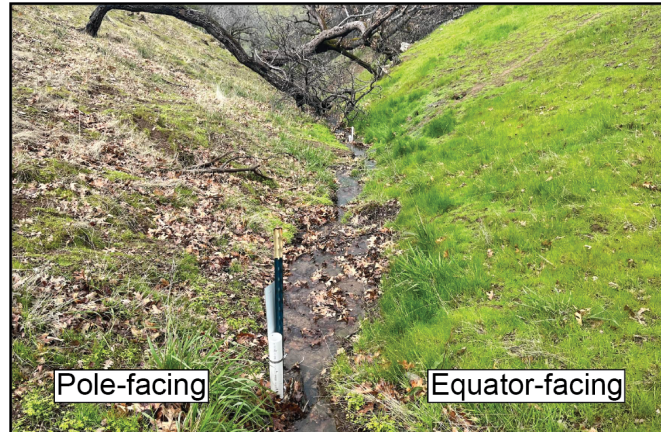


Figure 1.8: Image showing relatively higher grass density on the equator-facing slope compared to the pole-facing slope in March 2023.

1.7.2 Sapflow methods

Sap flux is known to vary radially through the sapwood but the radial profile is difficult to constrain. Here, we tested two possible radial flux profiles (1) constant sap flux across the sapwood based on the position with the maximum sap flux. The outer sapwood position typically had a much higher sap flux compared to the inner sap flux and was used to calculate volumetric sap flow (except T06 and T05). T06 had relatively similar sap flux between the inner and outer positions; therefore the outer position was used for the calculation for consistency. T05 had a higher inner position sap flux which was attributed to probe installation error. Specifically, the sap flow sensor may not have been installed deep enough beyond the bark. (2) Average sap flux between the outer and inner position which represents a linear decline in sap flux from the outer to inner position.

There are several limitations and assumptions made in converting heat-pulse measurements to hillslope-scale ET. Previous studies have noted that sap flow measurements can underestimate tree transpiration by as much as 35% (Steppe et al., 2010). Underestimates of transpiration may be due to wounding effects from sensor installation or probe misplacement in less functional xylem within the ring-porous oaks (Burgess et al., 2001; Burns et al., 2023; Miller, 1980). In addition, we had variable data coverage in April due to sensor installation, therefore the calculations of total tree sapflow begin on the earliest date with uniform data coverage (May 1st) which also contributes to an underestimate of total transpiration. By including two types of calculations, one

based on the maximum sap flux and another based on the average sap flux, we provide a possible range of sap flow.

Tree ID	DBH (cm)	Species	Sapwood thickness (cm)
T30	30.6	blue oak	4.9
T06	36.3	valley oak	6.6
T05	38.5	black oak	3.5
T26	42.5	black oak	4.5
T19	60.2	black oak	4.8
TBB	84.1	blue oak	5.8
TGPA	108.3	blue oak	5.8

Table S2. Hillslope-scale tree survey characteristics

Tree count	Species	DBH (cm)	Tree count (cont.)	Species (cont.)	DBH (cm, cont.)
1	blue oak	99.57	57	black oak	30.73
2	black oak	59.69	58	black oak	42.42
3	black oak	118.11	59	black oak	25.15
4	black oak	90.93	60	black oak	26.42
5	black oak	82.55	61	black oak	32.77
6	black oak	74.93	62	black oak	37.85
7	blue oak	42.42	63	black oak	33.02
8	blue oak	36.32	64	black oak	33.53
9	blue oak	44.70	65	black oak	33.78
10	blue oak	39.12	66	black oak	43.18
11	valley oak	138.18	67	black oak	61.21
12	black oak	49.53	68	black oak	35.56
13	black oak	72.14	69	black oak	44.20
14	black oak	68.58	70	blue oak	16.51
15	blue oak	46.99	71	blue oak	14.73
16	blue oak	46.74	72	blue oak	55.12
17	blue oak	54.61	73	blue oak	47.75
18	blue oak	30.48	74	blue oak	34.80
19	blue oak	63.50	75	blue oak	61.47
20	blue oak	29.21	76	blue oak	44.96
21	blue oak	60.71	77	blue oak	31.75
22	blue oak	60.20	78	blue oak	17.78
23	blue oak	50.55	79	blue oak	63.25
24	blue oak	76.96	80	blue oak	46.99
25	blue oak	68.33	81	blue oak	30.48
26	black oak	63.50	82	black oak	96.52
27	black oak	30.48	83	black oak	49.28
28	blue oak	52.58	84	black oak	61.21
29	blue oak	74.17	85	black oak	57.66
30	blue oak	50.55	86	black oak	46.23
31	blue oak	17.78	87	black oak	46.99
32	blue oak	19.05	88	black oak	35.56
33	blue oak	57.15	89	black oak	52.58
34	blue oak	109.22	90	black oak	83.06
35	blue oak	83.82	91	black oak	46.23
36	blue oak	79.25	92	black oak	56.39
37	black oak	43.18	93	black oak	33.78
38	black oak	26.16	94	blue oak	46.48
39	black oak	46.74	95	black oak	96.27
40	blue oak	53.34	96	black oak	63.25
41	black oak	50.04	97	blue oak	39.12
42	black oak	38.10	98	black oak	38.86
43	black oak	45.72	99	black oak	34.29
44	black oak	59.44	100	black oak	36.83
45	black oak	28.70	101	black oak	43.94
46	black oak	29.21	102	black oak	32.77
47	black oak	30.23	103	black oak	34.04
48	black oak	27.43	104	black oak	45.47
49	black oak	23.62	105	black oak	46.99
50	black oak	28.70	106	black oak	26.42
51	black oak	41.66	107	black oak	76.71
52	black oak	43.94	108	black oak	37.59
53	blue oak	31.75	109	black oak	49.78
54	blue oak	59.69	110	black oak	37.34
55	valley oak	36.32	111	black oak	49.28
56	black oak	31.75	112	black oak	44.96
			113	black oak	43.94

1.7.3 OpenET methods

The OpenET ensemble model includes five satellite-derived ET model inputs after the removal of outlier values (FAO, 2023). It should be noted that the SIMS model in OpenET (which is the only model that explicitly includes measurements of plant phenology through NDVI) is only developed for croplands, so it was not available within the OpenET ensemble for Arbor Creek Experimental Catchment (Volk et al., 2024). A detailed comparison of the differences, limitations and benefits of each model is outlined in literature developed by the Food and Agriculture Organization (FOA, 2023). Here, we provide a brief overview of model approaches.

Within the OpenET framework there are three ET models included based on a surface energy balance approach: geeSEBAL (Surface Energy Balance Algorithm for Land developed within the GEE environment; (Laipelt et al., 2021) DisALEXI (The Disaggregated Atmosphere – Land Exchange Inverse (Anderson et al., 2018) and eeMETRIC (Mapping ET at high Resolution with Internalized Calibration; (Allen Richard G. et al., 2007). The surface energy balance approach derives ET indirectly from the components of net radiation including the soil heat flux, latent heat flux and sensible heat flux.

In addition, there is one ET model based on the psychrometric approach, SSEBop (The Operational Simplified Surface Energy Balance; (Senay et al., 2017), and one model based on the Priestley-Taylor approach, PTJPL (The Priestley – Taylor ET (Fisher et al., 2008). The psychrometric approach differs from the surface energy

balance approach in that it does not solve for all components of the energy balance such as the sensible and soil heat flux. Instead this method uses a psychrometric constant for the air derived for the location and day of year that is adapted as a “surface” psychrometric constant (FOA, 2023). Lastly, the Priestley-Taylor approach determines actual ET from two primary components: setting an upper boundary of the ET flux and a set of eco-physiological constraining functions, reducing potential ET to actual ET (FOA, 2023).

1.7.4 Sapflow results

As expected, the total individual tree sap flow was lower when calculated based on the average sap flux compared to the assumed constant maximum sap flux across the sapwood (Supplementary Table 3). Therefore, the total hillslope-scale oak transpiration was 124 mm (average sap flux method) compared to 172 mm (maximum sap flux method). However, regardless of method, the relationship between DBH and total tree sap flow and the main conclusion of higher total ET on the pole-facing slope compared to the equator-facing slope remained true.

Tree ID	Total Average Sapflow (L)	Total Maximum Sapflow (L)
T05	3515	4273
T06	13728	13433
T19	9410	12988
T26	2935	5078
T30	864	1427
TGPA	13728	147387
TBB	97461	57962

1.7.5 Open ET results

Across all models (excluding eeMetric) the pole-facing slope has higher ET than the equator-facing slope (Supplementary Figure 1.9). Based on the timing and magnitude of ET reported by the eeMetric ET model, it is likely not accurate within Arbor Creek Experimental Catchment, may be flagged as an outlier within the filtering process and excluded from the Ensemble ET model calculation. However, at this time it is not possible to systematically extract which models are included within the Ensemble ET model with the OpenET API (Pers. Comm. Open ET developer team).

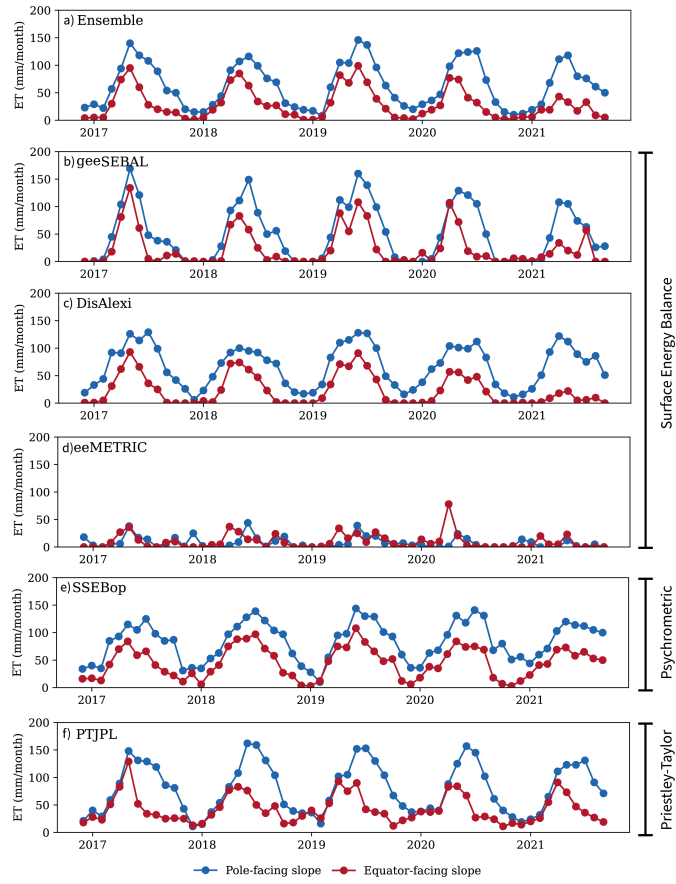


Figure 1.9: Remotely-sensed monthly ET from the OpenET based a) Ensemble model, b) geeSEBAL model, c) DisAlexi model, d) eeMETRIC model, e) SSEBop model, and f) PTJPL model.

1.7.6 Supplementary References

- Allen Richard G., Tasumi Masahiro, & Trezza Ricardo. (2007). Satellite-Based Energy Balance for Mapping Evapotranspiration with Internalized Calibration (METRIC)—Model. *Journal of Irrigation and Drainage Engineering*, 133(4), 380–394.
- Anderson, M., Gao, F., Knipper, K., Hain, C., Dulaney, W., Baldocchi, D., Eichelmann, E., Hemes, K., Yang, Y., Medellin-Azuara, J., & Kustas, W. (2018). Field-Scale Assessment of Land and Water Use Change over the California Delta Using Remote Sensing. *Remote Sensing*, 10(6), 889.
- Burgess, S. S., Adams, M. A., Turner, N. C., Beverly, C. R., Ong, C. K., Khan, A. A., & Bleby, T. M. (2001). An improved heat pulse method to measure low and reverse rates of sap flow in woody plants. *Tree Physiology*, 21(9), 589–598.
- Burns, E. F., Rempe, D. M., Parsekian, A. D., Schmidt, L. M., Singha, K., & Barnard, H. R. (2023). Ecohydrologic dynamics of rock moisture in a Montane catchment of the Colorado front range. *Water Resources Research*, 59(6).
- FAO. (2023). Remote sensing determination of evapotranspiration – Algorithms, strengths, weaknesses, uncertainty and best fit-for-purpose. FAO.
- Fisher, J. B., Tu, K. P., & Baldocchi, D. D. (2008). Global estimates of the land–atmosphere water flux based on monthly AVHRR and ISLSCP-II data, validated at 16 FLUXNET sites. *Remote Sensing of Environment*, 112(3), 901–919.
- Huxman, T. E., Cable, J. M., Ignace, D. D., Eilts, J. A., English, N. B., Weltzin, J., & Williams, D. G. (2004). Response of net ecosystem gas exchange to a simulated

- precipitation pulse in a semi-arid grassland: the role of native versus non-native grasses and soil texture. *Oecologia*, 141(2), 295–305.
- Laipelt, L., Henrique Bloedow Kayser, R., Santos Fleischmann, A., Ruhoff, A., Bastiaanssen, W., Erickson, T. A., & Melton, F. (2021). Long-term monitoring of evapotranspiration using the SEBAL algorithm and Google Earth Engine cloud computing. *ISPRS Journal of Photogrammetry and Remote Sensing*, 178, 81–96.
- Miller, D. H. (1980). Measurement of Sap Flow and Transpiration in Ring-porous Oaks Using a Heat Pulse Velocity Technique.
- Schlesinger, W. H., & Jasechko, S. (2014). Transpiration in the global water cycle. *Agricultural and Forest Meteorology*, 189-190, 115–117.
- Senay, G. B., Schauer, M., Friedrichs, M., Velpuri, N. M., & Singh, R. K. (2017). Satellite-based water use dynamics using historical Landsat data (1984–2014) in the southwestern United States. *Remote Sensing of Environment*, 202, 98–112.
- Steppe, K., De Pauw, D. J. W., Doody, T. M., & Teskey, R. O. (2010). A comparison of sap flux density using thermal dissipation, heat pulse velocity and heat field deformation methods. *Agricultural and Forest Meteorology*, 150(7), 1046–1056.
- Volk, J. M., Huntington, J. L., Melton, F. S., Allen, R., Anderson, M., Fisher, J. B., Kilic, A., Ruhoff, A., Senay, G. B., Minor, B., Morton, C., Ott, T., Johnson, L., Comini de Andrade, B., Carrara, W., Doherty, C. T., Dunkerly, C., Friedrichs, M., Guzman, A., . . . Yang, Y. (2024). Assessing the accuracy of OpenET satellite-based evapotranspiration data to support water resource and land management applications. *Nature Water*, 1–13.

Chapter 2

Subsurface Weathering and Vadose Zone Water Storage Between Hillslopes with Opposing Aspects

This chapter reflects a manuscript in-prep with the following coauthors:

Nerissa Barling, Russell Callahan, Daniella Rempe and Margaret Zimmer.

2.1 Abstract

Subsurface weathering mediates water cycling, slope stability, nutrient availability, and ecosystem productivity. However, relative to the shallow soil layer, the relationship between aboveground microclimates and vegetation patterns to subsurface bedrock weathering remains largely unknown. Here, we quantify subsurface weathering and vadose zone water cycling with a central coast California catchment with distinct incoming solar radiation and vegetation between aspects. We utilized deep drilling (6 - 40 m) and downhole hydrologic monitoring to characterize how the weathered profile relates to water storage and vegetation water uptake within a landscape dominated by sandstone. We observed a higher extent of weathering and a larger dynamic storage zone within the cooler pole-facing slope composed of oak trees relative to the warmer equator-facing slope with only grasses. Deep drilling observations and measurements of chemical weathering and matrix porosity suggest nested weathering fronts with the highest degree of weathering within the shallow subsurface due to the effect of biotic and hydrologic processes. The shallowest weathering front occurs at a sharp depletion of Na, Mg, P, and Mn within the saprolite. This zone aligns with the depth of high matrix porosity, low mechanical strength, and the dynamic storage zone. In addition, we observed evidence of weathering patterns likely due to past vegetation distributions with trees on either hillslope and elevated water table within the cooler and wetter Pleistocene. Our findings indicate clear evidence for the impact of both present-day and past microclimate and vegetation to mediate hillslope-scale weathering processes.

2.2 Introduction

The subsurface critical zone, which extends from the Earth's surface down to fresh bedrock, regulates the transport and storage of water, carbon, energy, and nutrients that are essential to sustain life (Maher and Chamberlain, 2014; Moravec and Chorover, 2020; Rasmussen, Troch, et al., 2011). The subsurface critical zone structure can be delineated by the soil, saprolite, weathered bedrock and fresh bedrock based on spatially heterogeneous properties including porosity and chemical composition (S. L. Brantley, Lebedeva, et al., 2017; S. L. Brantley and Lebedeva, 2021). Subsurface water storage and fluxes mediate the subsurface critical zone structure through chemical weathering (Lebedeva and Brantley, 2013, 2020; Rempe and Dietrich, 2014). As chemically reactive meteoric water travels through the subsurface it dissolves and precipitates minerals, thereby influencing subsurface porosity and permeability (Navarre-Sitchler et al., 2015). The resulting chemical dissolution and increased rock pore space may enable a faster rate of water movement and reduce the rock mechanical strength, making it more susceptible to additional subsurface weathering (Maher, 2010; Maher and Navarre-Sitchler, 2019). While the role of water fluxes is widely recognized as an important component of subsurface weathering, it remains unclear how contemporary hydrologic fluxes correspond to chemical weathering patterns that develop over geologic timescales (Wang, Chen, et al., 2021; White et al., 1998). This is largely driven by the challenges associated with the cost and maintenance of detailed subsurface critical zone studies. The scientific community's inability to understand the relationship

between water cycling and subsurface weathering hinders Earth's system models from accurately predicting how shifts in subsurface water fluxes will influence critical zone evolution and function (Li et al., 2021; Sullivan et al., 2020).

Conceptual and numerical models for the co-evolution of the weathered profile and water cycling have commonly been developed from study sites dominated by igneous or fine-grained sedimentary rocks such as granites and shales (Gu et al., 2020; Holbrook et al., 2014; Wang, Chen, et al., 2021). Within these systems, the slow drainage of chemically-equilibrated groundwater within hillslopes has been proposed as one hydrologic mechanism driving the lower bound of chemical weathering (i.e. the weathering front; (Rempe and Dietrich, 2014; Sullivan et al., 2016). Above the water table, the subsurface critical zone structure has been delineated by nested reaction fronts which are suggested to be driven by the chemical evolution of meteoric waters along hydrologic flowpaths (S. L. Brantley et al., 2013; Pedrazas et al., 2021). However, limited data exist to investigate how subsurface water storage and movement correspond to chemical weathering within coarse-grained sedimentary rocks such as sandstone, which is an important lithology for regional-scale water storage and geoengineering (Bjørlykke and Jahren, 2015; Rahman et al., 1995). A better understanding of the interplay between water cycling and chemical weathering is critically needed to assess the transferability of these models to landscapes with differing rock types, which is essential to better predict key Earth surface processes such as landscape evolution, biogeochemical cycling and ecosystem productivity (Li et al., 2021; Sullivan et al., 2020).

Quantifying the sensitivity of subsurface weathering patterns to water move-

ment and storage are essential to predicting how future changes in climate will affect feedbacks between geomorphic, biogeochemical, and hydrologic processes (Rasmussen, Brantley, et al., 2011; Raymond, 2017; White and Blum, 1995). Aspect, or the direction a hillslope faces, produces small-scale variability in incoming solar radiation, which provides a natural experiment to investigate the climatic controls on water cycling and subsurface weathering (Chorover et al., 2011; Regmi et al., 2019; Smith and Bookhagen, 2021). Specifically, on pole-facing slopes (north-facing slopes in the northern hemisphere), there is less direct solar radiation compared to equator-facing slopes (south-facing slopes in the northern hemisphere) which leads to denser vegetation, higher infiltration rates, and higher shallow soil water storage (Pelletier et al., 2018; Ying et al., 2019). Given the difficulty to obtain direct samples from the subsurface below the soil, studies that quantify how differences in aspect have impacted subsurface weathering patterns largely rely solely on geophysical methodologies (with some exception including Hall et al., 2005; Pedrazas et al., 2021). From these geophysical surveys, pole-facing slopes are often characterized as having a thicker weathering extent compared to equator-facing slopes (Befus et al., 2011; Nielson et al., 2021; Wang, Nyblade, et al., 2021). However, this is not always the case, where recent studies have shown a similar regolith thickness between aspects or even a thicker regolith on equator-facing slopes, which is opposite of expectations (A. M. Donaldson et al., 2023; Hudson Rasmussen et al., 2023; Leone et al., 2020). These deviations from expectations highlight the need for more direct sampling and quantification of subsurface weathering to better understand the mechanistic biogeochemical and ecohydrologic processes that are responsible

for variations in critical subsurface structure.

Here, we utilize a catchment where aspect drives differences in microclimates and vegetation to explore the relationship between subsurface water cycling and chemical weathering in central California hillslopes underlain by sandstone-dominated lithology. Specifically, using drilled boreholes, we combine bulk geochemistry and matrix porosity measurements of the weathered profile with neutron probe surveys of rock moisture to investigate how variability in vegetation and water cycling influence the subsurface critical zone structure.

2.3 Methods

2.3.1 Site description

Arbor Creek Experimental Catchment, here referred to as Arbor Creek catchment, is a small headwater catchment (0.04 km²) that contributes to a first-order intermittent stream within Blue Oak Ranch Reserve (University of California Natural Reserve System). Arbor Creek catchment is located in central coast California approximately 24 km east of San Jose, California, USA (Figure 1) and spans elevations from 720 to 790 m above sea level. Arbor Creek catchment and the greater Blue Oak Ranch reserve is situated on the ancestral unceded tribal lands of the present day Muwekma Ohlone Tribe of the San Francisco Bay Area.

This region experiences a Mediterranean climate characterized by warm dry summers and cool wet winters. The mean annual air temperature and annual precip-

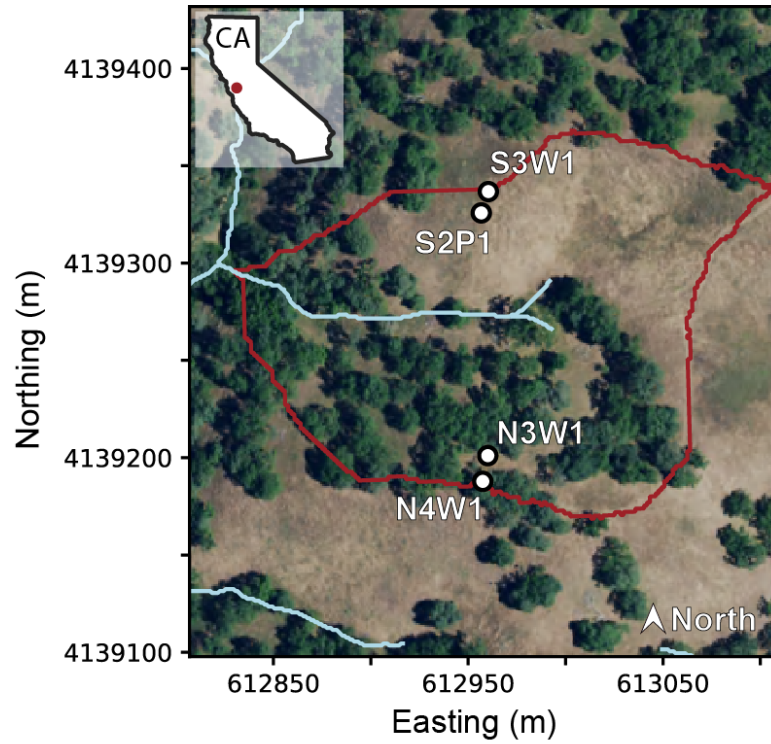


Figure 2.1: Arbor Creek Experimental Catchment delineated in red with stream channels delineated with light blue lines. The locations of boreholes on the pole-facing slope (N4W1 and N3W1) and equator-facing slope (S3W1 and S2P1) are delineated with white circles.

itation between 1981 and 2022 was 14.3 degrees C and 397 mm respectively (PRISM Climate Group, 2022). Arbor Creek catchment is classified as oak savannas with aspect-regulated vegetation distributions. Arbor Creek catchment is dominated by blue oak (*Quercus douglasii*), black oak (*Quercus kelloggii*) and valley oak (*Quercus lobata*) with other hardwood species including California bay laurel (*Umbellularia Californica*) and California buckeye (*Aesculus californica*) present at lower elevations. Potential evapotranspiration exceeds precipitation for most of the year with greatest actual evapotranspiration during the spring-early summer, which is determined by the seasonal phenology of the deciduous oak trees (Donaldson et al., in-review). Understory includes herbaceous ground cover with species from both native and non-native genera, including *Avena*, *Bromus*, and *Elymus*. Oak tree species dominate on the pole-facing slope with the herbaceous ground cover present on the pole- and equator-facing slopes.

Arbor Creek catchment's steep slopes (24°) are thinly mantled with soil (30-80 cm) and lack systematic differences (e.g., soil texture, depth) between the pole-facing and equator-facing slope (A. M. Donaldson et al., 2023). Geographically, Arbor Creek Catchment is situated within the Mt. Diablo Range. Based on localized outcrop observations, the catchment is underlain by the coarse-grained metagreywacke sandstone with interbeds of shale that is situated within the larger Franciscan complex. Based on previous geochemical studies, source rock includes volcanic and plutonic rocks from the southern Sierra Nevadas (Surpless, 2015).

2.3.2 Drilling, standard penetration tests and borehole completion

To relate the physical and chemical characteristics of the critical zone to vadose zone water storage, we drilled four boreholes within the study site (Figure 2.1). Borehole locations were limited to the near-ridge and ridge top locations to due drill rig constraints and were drilled using a combination of standard penetration testing (SPT), augering, split-spoon sampling, and diamond core rotary techniques.

On the ridge top positions of the pole-facing slope (N4W1) and equator-facing slope (S3W1), the drillers first used SPT, which is a measure of mechanical strength of the material, to advance through the weathered profile. The depth to SPT refusal indicates the depth to which drillers transition in drilling styles from SPT to coring because borehole collapse is no longer a risk; demonstrating a relatively high in-situ mechanical strength. After SPT, the drillers advanced through the material with a bullet bit to dry auger, set the grout casing to secure, and then used a diamond-bit to core and recover samples from deeper depths. Below the shallow grout casing, the small air gap between the borehole wall and the PVC was not filled. N4W1 was drilled to a depth of 40.8 m and S3W1 was drilled to a depth of 27.7 m.

The boreholes, at the near-ridge position of the pole-facing slope (N3W1) and equator-facing slope (S2P1) were completed using SPT and dry-augering only, therefore no core was recovered. N3W1 and S2P1 were drilled to 12 m and 6 m. Within N3W1, the small air gap between the borehole wall and the 3-inch PVC was not filled. However, within S2P1, a 2-inch PVC was used therefore the air gap was filled with

polyurethane foam which has previously been shown to not interfere with downhole geophysical methods (Personal Comm. Dr. Daniella Rempe). To prevent ponding, all borehole well heads were constructed with outward sloping concrete.

2.3.3 Core characterization, matrix porosity and geochemistry

Callahan et al. (in-review) used drilling observations and oxidation presence and fracture density of the retrieved core to identify four weathering interfaces within N4W1 and S3W1. Here, we build on those observations with detailed physical and geochemical analyses to investigate the relationship between vadose zone water cycling and the critical zone structure. Within N4W1 and S3W1, we sampled and then dried and stored at air temperature rock chips, cuttings and recovered core samples for detailed physical and geochemical analyses. Specifically, we analyzed rock samples for porosity, total elemental concentrations, sulfur concentrations, and mineral composition.

We quantified the rock matrix porosity for 16 samples within N4W1 and 17 samples with S3W1. We measured matrix porosity within competent rock chips or when bedrock core was recovered we broke off small pieces of the core for analyses. To measure the rock matrix porosity, we used a helium pycnometer (Micromeritics AccuPyc II 340 Gas Pycnometer) and an envelope density analyzer (Micromeritics GeoPyc 1360 Envelope Density Analyzer) to obtain skeletal and envelope volume, respectively. The skeletal volume, or “absolute” volume includes the solid portion of the sample but excludes the volume of the open pore spaces. The skeletal volume is measured by a helium gas displacement method using the volume-pressure relationship of Boyle’s Law.

In comparison, the envelope volume, or “bulk” volume includes the solid portion of the sample and all pore spaces (both open and closed). The GeoPyc Envelope Density Analyzer uses a quasi-fluid that does not fill the sample’s pore spaces nor does it get the sample wet. From these volume measurements, we calculated the absolute density and bulk density and then differentiated between the two densities to achieve porosity values.

We sent 55 samples from S3W1 and 84 samples from N4W1 for geochemical analyses to Actlabs (Canada). Samples were dried, crushed, then pulverized and passed through a 140-mesh sieve. Samples were heated to measure loss on ignition and then further analyzed rock samples for total elemental compositions using lithium-borate fusion inductively coupled plasma emission spectroscopy (instrument model: Spectro Ciros/Arcos). A subset of samples were analyzed for sulfur concentrations using a IR Carbon Sulfur Analyzer (detection limit = 0.01%). To assess the mineral composition of rock cores, we sampled from four depths within N4W1 and S3W1 and used a Rigaku SmartLab™ X-ray diffractometer (XRD) at a scanning rate of 0.75 deg/min at the University of California, Santa Cruz. To determine the primary minerals, we visually aligned major peaks of the XRD results to a publicly available database containing confirmed XRD data for minerals (The RRUFF™ Project).

To characterize chemical weathering patterns with depth, we tracked gains and losses of individual elements relative to the concentrations of chemically immobile elements (e.g. Zr, Ti) within the parent material, expressed as τ (tau) for individual elements (Brimhall et al., 1988). We defined the geochemistry of the parent material

from 6 unweathered bedrock sandstone samples deeper than 25 m within S3W1 and 4 unweathered bedrock sandstone samples deeper than 39 m within N4W1. We used Ti as the immobile reference element. Under the assumption that the parent material is representative of the weathered material, this “mass-transfer coefficient” expresses the fractional mass loss of an element relative to the amount that element was present in parent material (Equation 1). Where, X is the element of interest, I is the concentration of the immobile element, and the subscripts regolith and protolith refer to the type of material which elemental concentrations are measured in (Equation 1). For example, A τ_x value of -0.1 indicates a 10% decrease in an element relative to the initial concentration of that element in the parent material.

$$\tau_x = \frac{X_{\text{regolith}}I_{\text{protolith}}}{X_{\text{protolith}}I_{\text{regolith}}} - 1 \quad (2.1)$$

2.3.4 Vadose zone hydrologic monitoring

To quantify unsaturated zone water content, we measured neutron counts in 0.25 m intervals within N4W1, N3W1, S3W1 and S2P1 during the winter and summer in 2023 (Figure 2.1; Instrotek CPN 503 H320306484). Measured changes in neutron probe counts indicate temporal changes in subsurface volumetric water content above the water table (Long and French, 1967). Here, we report the magnitude of subsurface volumetric water content change during the 2023 water year by subtracting neutron counts from a dry survey (measurement date October 18, 2023) from neutron counts of a wet survey (measurement date March 24, 2023). At the time of the wet survey, 925

mm of the total 994 mm of precipitation had fallen for 2023 water year. At the time of the dry survey measurement, there had been 5 months with ≥ 2 mm of precipitation total. We define the dynamic storage by identifying the depth at which we saw no significant change in neutron counts (i.e. change is smaller than the standard deviation of neutron counts with the discretely fractured bedrock). We corrected for sensor drift based on the standard deviation from the mean between the depth range 20 to 25 m in which the change in volumetric water content is less than the neutron probe measurement uncertainty (i.e. no dynamic storage).

2.4 Results

2.4.1 Core description, standard penetration tests, matrix porosity

Using the SPT depth of refusal to represent the saprolite to weathered bedrock interface, the combined soil and saprolite thickness was 3 m at N4W1 and 5.2 m at S3W1 (Figure 2.2). Similarly, at the near-ridge positions, the combined soil and saprolite thickness was 3 m at N3W1 and 6.4 m at S2P1 (Supplementary Figure 2.2). Generally, the matrix porosity increases toward the surface (Figure 2.2). After removing the anomalous porosity value which was due to an interbed of shale at 27.4 m within N4W1, matrix porosity ranged from 0.07 to 34% within N4W1 and 2 to 19% within S3W1. There was large variability in the matrix porosity at depth, evidenced by the anomalously high matrix porosity at 27.4 m on the pole-facing slope and the high fracture density observed within the cores. Overall, the data indicate that N4W1 has slightly higher

matrix porosity than S3W1, especially within the soil and saprolite layer (Figure 2.2).

2.4.2 Bulk geochemistry and chemical depletion

Total sulfur concentrations (%) generally did not exceed the detection limit until 15 m below the surface within N4W1 and S3W1 (Figure 2.3). Within N4W1, sulfur concentrations were on average 0.015% (standard deviation (sd) = 0.012%) and the maximum sulfur concentration was 0.05%, which occurred at 22 m. In comparison, with S3W1, sulfur concentrations were on average 0.019% (sd = 0.015%), and the maximum sulfur concentration was 0.06% at 27 m.

On average, the absolute concentrations of the major rock forming elements were similar within the protolith of N4W1 and S3W1 (Supplementary Table 1). However, the weathered bedrock elemental concentrations varied across depths, between sandstone and shale samples, and between the pole-facing slope and the equator-facing slope (Figure 2.4). In general, the individual elemental concentrations had higher variability toward the surface than at depth for sandstone samples. However, within the shale samples at N4W1, there was markedly higher variability and distinct elemental concentrations relative to the sandstone samples except for P, Mn, and Zr (Figure 2.4, light blue circles). For the sandstone samples, P, Mg, Na and to a lesser extent Mn and K generally declined in concentrations toward the surface. However, Si, Al, Fe, Ca, and Zr did not show systematic patterns with depth. Within the top 15 m, there were generally higher Ca concentrations within N4W1 compared to S3W1, while there were slightly higher Al concentrations within S3W1 compared to N4W1. Beyond Ca and

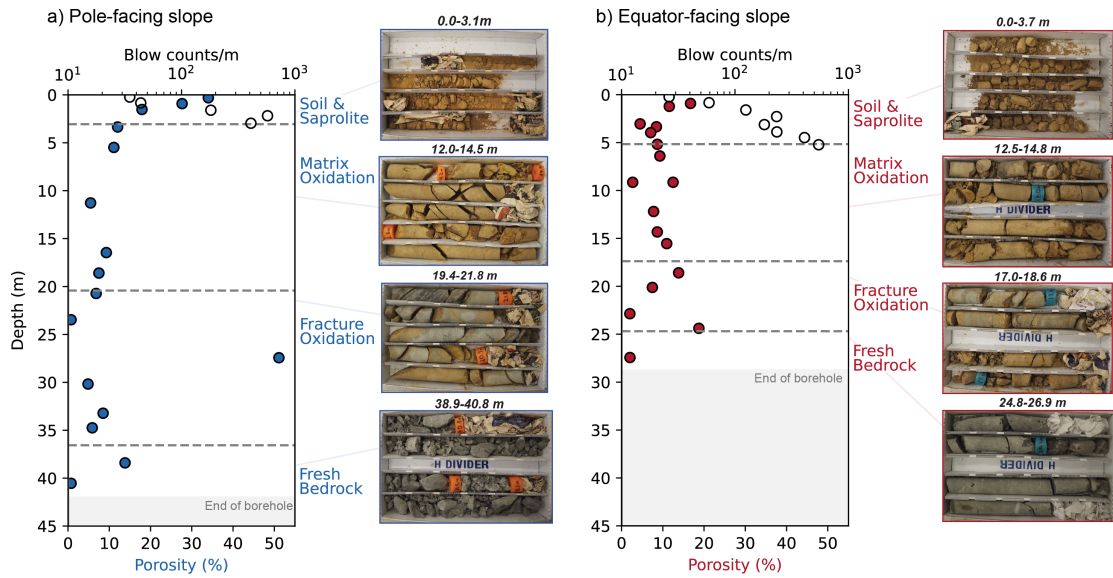


Figure 2.2: Depth profiles of matrix porosity and core images of recovered rock samples for the a) pole-facing slope (blue) and b) equator-facing slope (red). White circles indicate the standard penetration blow counts for each borehole, respectively. Shaded gray region indicates the end of the borehole. Dashed lines represent the reported weathering interfaces based on physical rock core observations (Callahan et al., in-review). Shaded blue and red bars indicate the average matrix porosity within the weathering interface for the pole-facing and equator-facing slope, respectively.

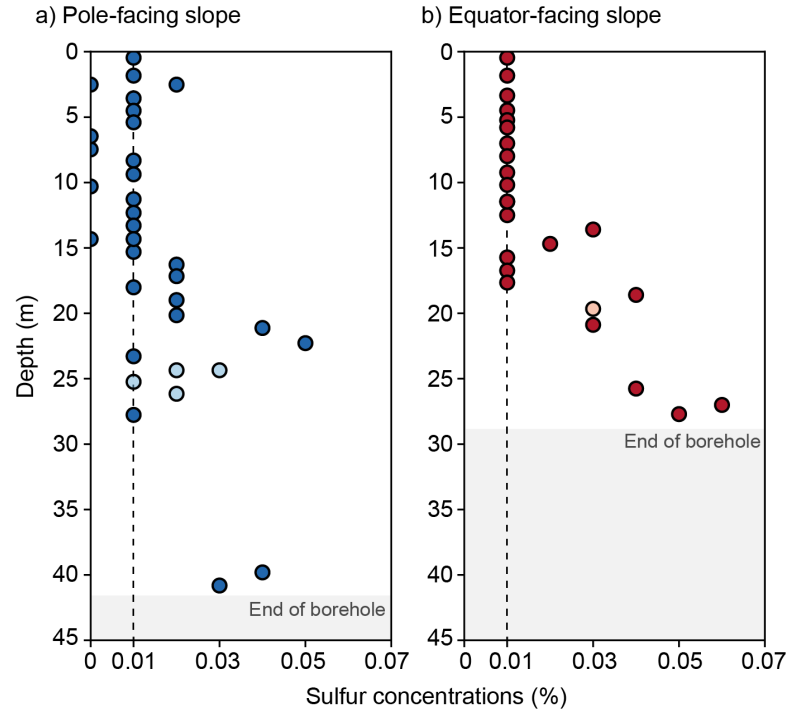


Figure 2.3: Sulfur concentrations (%) for the a) pole-facing slope and b) equator-facing slope. Dark blues and reds indicate sandstone samples while light blues and reds indicate shale samples. Dashed line at 0.01% indicates the instrument detection limit. Depths shaded gray delineate beyond the borehole extent.

Al, no other individual elemental concentrations showed systematic differences between aspects.

The $\tau\text{Ti},x$ depth profile patterns varied between the relatively mobile and immobile elements (Figure 2.5). The $\tau\text{Ti},x$ values were more depleted within the top 5 m for Mg, Na, P, Mn, and to a lesser extent K relative to the parent material (Figure 2.5). However, there was significant scatter without any clear patterns for Ca, which is typically considered a relatively mobile element. In comparison, there was much less scatter about zero, but no clear depth pattern for relatively immobile elements: Si, Fe, Al, and Zr. Several elemental $\tau\text{Ti},x$ values showed a systematic difference between N4W1 and S3W1, including Ca, Mg, Na, and Mn. For example, toward the surface Ca became generally more depleted within S3W1 but became more enriched within N4W1. Throughout the entire depth profile, Mg was more depleted relative to the parent material within N4W1 compared to S3W1. In comparison, Na was more depleted within the first few meters of S3W1 relative to N4W1 but Na became more depleted below 5 m. Lastly below 10 m, Mn $\tau\text{Ti},x$ values were generally more depleted within N4W1 than S3W1 but became more similarly depleted toward the surface.

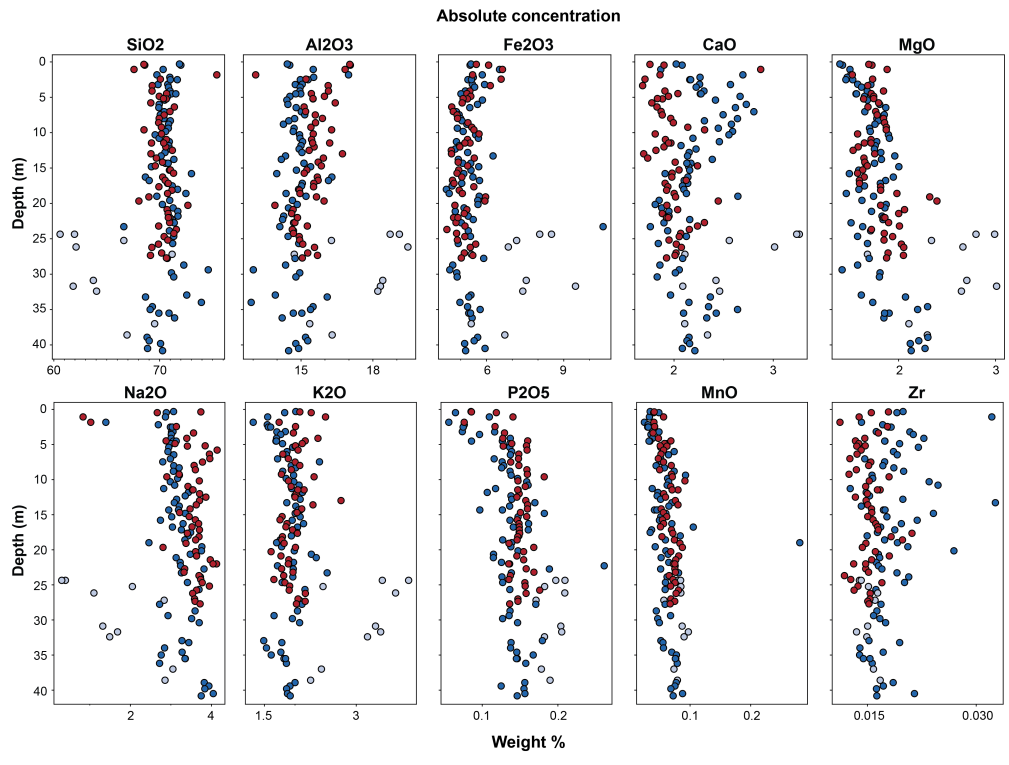


Figure 2.4: Absolute geochemical compositions of rock samples from N4W1 (blue circles) and S3W1 (red circles). Light blue circles represent N4W1 samples that were visually identified to be shale. All other samples were visually identified to be sandstone. Note distinct abscissa axis scales across elements.

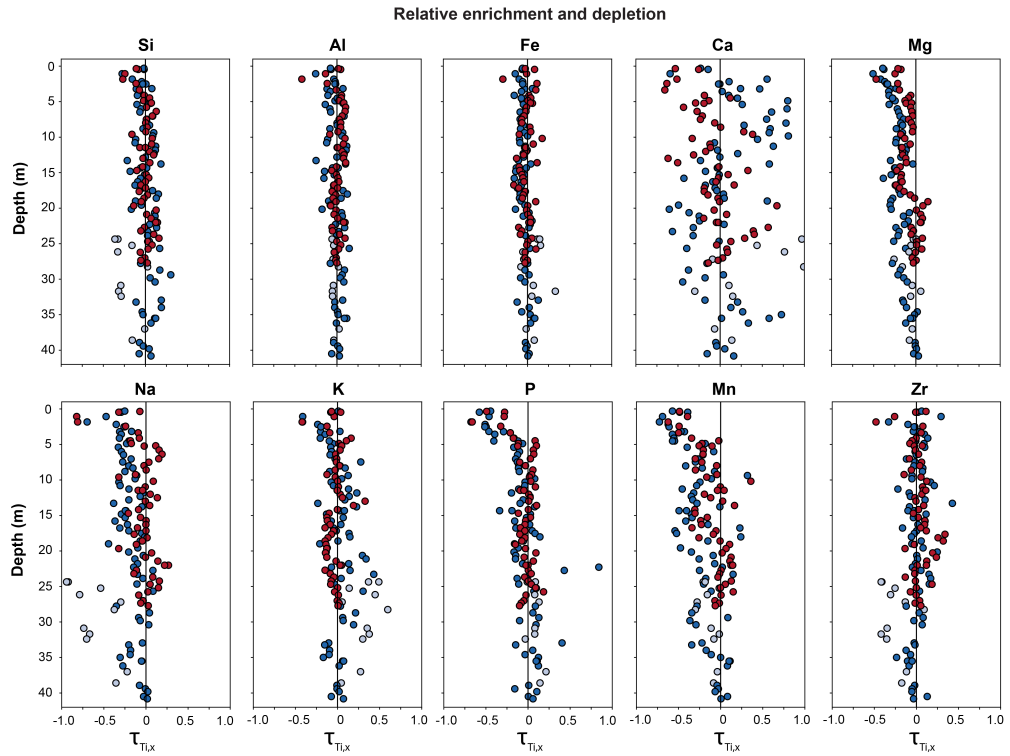


Figure 2.5: Chemical depletion (negative values) and enrichment (positive values) plots of individual elements, expressed as τ (tau) of rock samples from N4W1 (blue circles) and S3W1 (red circles). Light blue circles represent samples that were visually identified to be shale. All other samples were visually identified to be sandstone.

2.4.3 Mineral assemblages and evolution

While the XRD analyses suggest that the mineral assemblages are similar between N4W1 and S3W1, there are several indications that there is a higher degree of weathering within N4W1. Specifically, the XRD analyses of the unweathered sandstone within N4W1 (39.4 m) and S3W1 (27.0 m) suggest they have similar mineral assemblages containing quartz and plagioclase feldspar, and an intensity peak at $2\theta = 12.5^\circ$ that is characteristic of kaolinite and/or chlorite. Previous studies have documented that it is challenging to distinguish whether kaolinite or chlorite (or both minerals) are present because they have similar d-values (Kinoshita et al. 2011); Supplementary Fig 2). While several methods have been proposed to distinguish between kaolinite and chlorite, it was beyond the scope of the present study to discern (see Starkey et al. 1984 for more details). The XRD patterns toward the surface show a minimal change in quartz peak intensities but a significant decrease in the peak intensities for plagioclase feldspar upon weathering (Figure 2.6). Within N4W1, the plagioclase peak intensities decreased from 395 counts at 39.4 m (unweathered bedrock) to 51 counts at 1.8 m (saprolite; Figure 2.6). In comparison, the plagioclase peak intensities decreased from 242 counts at 27.0 m (unweathered bedrock) to 96 counts at 4.1 m (saprolite; Figure 2.6). Additionally, the kaolinite and/or chlorite that was present in the unweathered material was no longer detectable by 30.4 m within the N4W1 borehole and at 9.6 m within the S3W1 borehole.

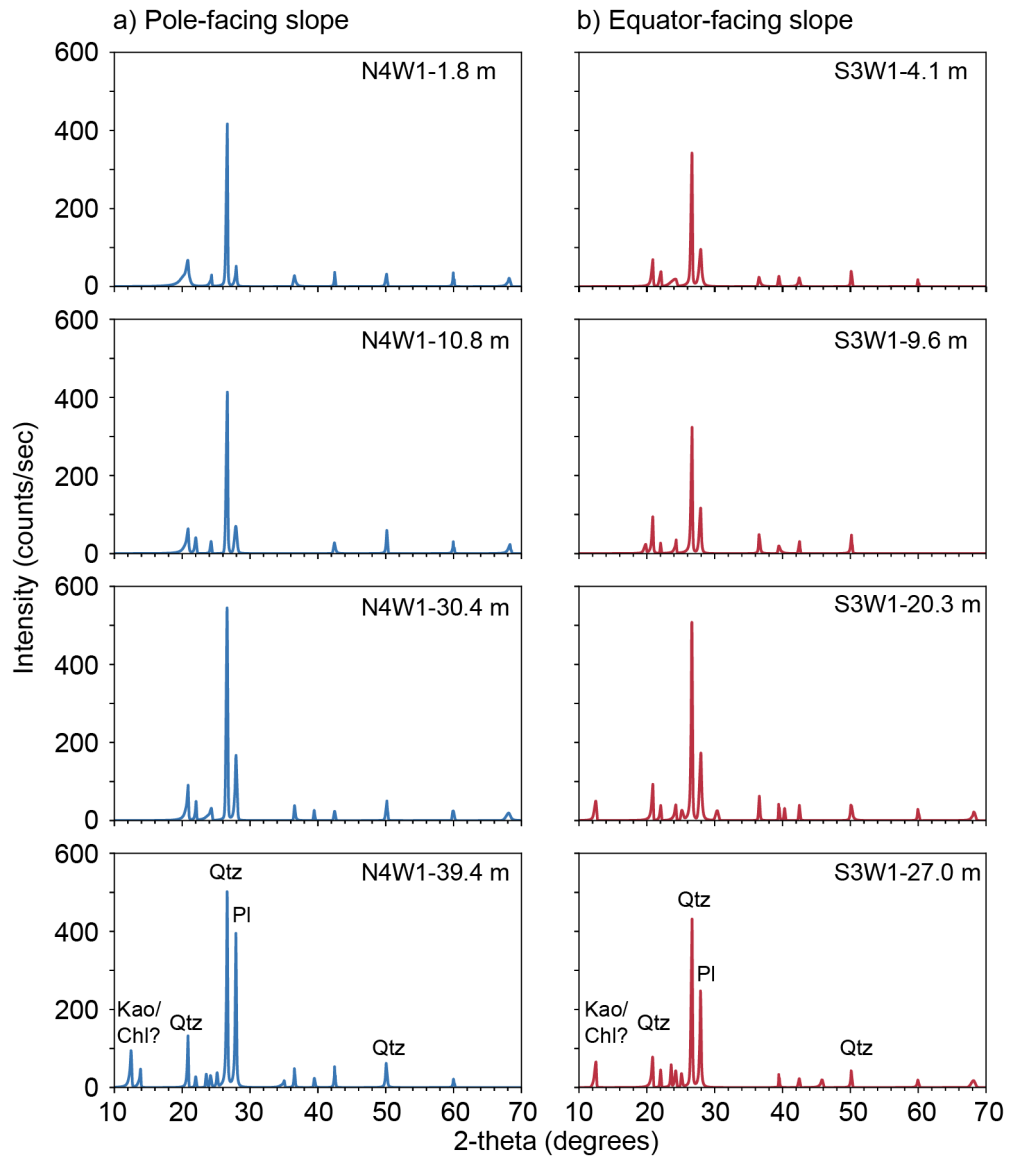


Figure 2.6: XRD analyses for the a) N4W1 (pole-facing slope; blue) and b) S3W1 (equator-facing slope; red) at indicated depths. Identified mineral peak intensities are delineated in unweathered bedrock (Qtz = Quartz, Pl = Plagioclase feldspar, Kao = Kaolinite, Chl = Chlorite).

2.4.4 Water storage in the weathered bedrock

The largest seasonal change in neutron counts occurred toward the surface and decreased with depth (Figure 2.7). On the equator-facing slope (Figure 2.7b), the dynamic storage was largely confined to the top 5 m and a significant portion of the deeper vadose zone did not exhibit a measurable change in water content below 5 m. In comparison, within the pole-facing slope (Figure 2.7a), the depth of dynamic storage extended down to 10 m. Additionally, from 15-18 m there was a measurable decrease in subsurface water content on the pole-facing slope, which corresponded to a location with pervasive fractured sandstone. Within N4W1, there was a measured increase in neutron counts (negative change) between the wet and dry surveys between 30-35 m, which is the approximate depth to the water table (Callahan et al., in-review.).

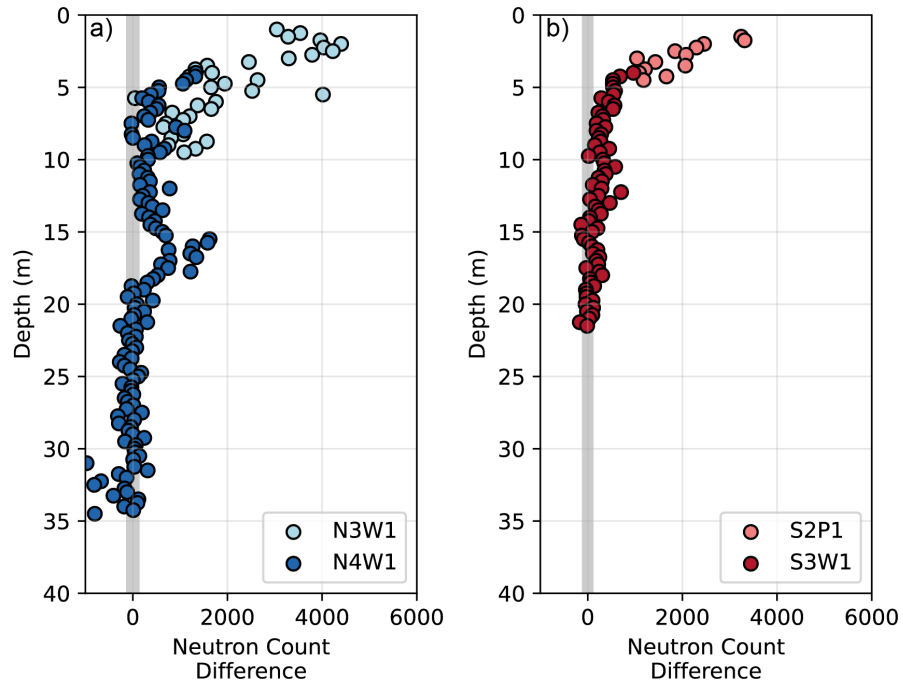


Figure 2.7: Depth profiles of neutron count difference within N4W1 (dark blue circle), N3W1 (light blue circle), S3W1 (dark red circles) and S2P1 (light red circles). Neutron count difference shows seasonal change from March 24, 2023 (wet measurement date) and October 18, 2023 (dry measurement date) in neutron counts, a proxy for unsaturated zone water content. Gray bars represent the standard deviation of the neutron count difference between 25 m to 30 m within the N4W1 and 15 m to 20 m within S3W1. Measurement coverage varies across boreholes due to differences in borehole depth and completion techniques used.

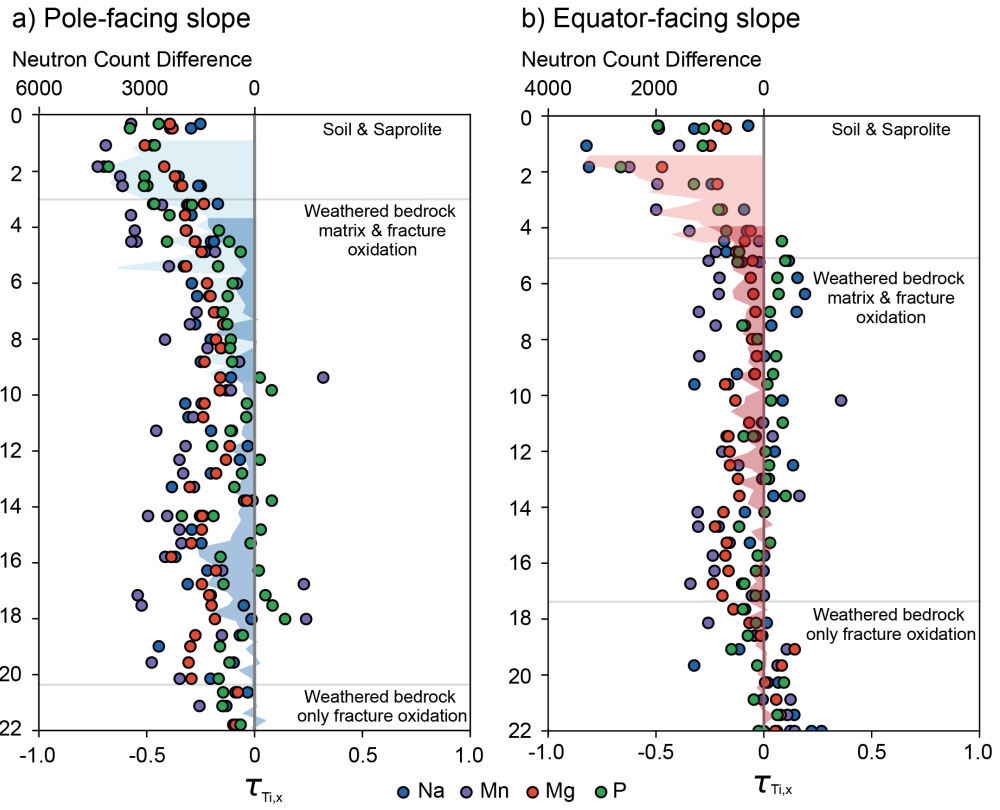


Figure 2.8: Depth profile comparisons between changes in neutron counts for pole-facing boreholes (shaded blues) and equator-facing boreholes (shaded reds) overlaid by the measured chemical depletion of Na (blue circles), Mn (purple circles), Mg (orange circles), and P (green circles).

2.5 Discussion

2.5.1 Subsurface chemical weathering and water storage patterns within Arbor Creek catchment

Subsurface critical zone structure is defined by the chemical and physical evolution of the parent material as it is uplifted toward the surface (Riebe et al., 2017). The transformation of the mineralogy, chemistry, and porosity of the parent material provide key evidence that is used to delineate the weathering interfaces within the subsurface (Goodfellow et al., 2016). Within Arbor Creek catchment, the geochemical and matrix porosity observations reported here align with the delineated weathering interfaces based solely on visual inspection of the rock cores (Callahan et al., in-review).

The deepest chemical weathering front corresponds to the transition between fractured bedrock with no oxidation to weathered bedrock with oxidation along fracture planes. The weathered bedrock with oxidation along fracture planes shows the initiation of Na, Mg and Mn depletion. The depletion of Na and Mg within the weathered profile may be associated with plagioclase weathering (e.g. albite) and chlorite dissolution as indicated by the decline in the associated XRD intensity peaks. In addition, across this interface there is measurable depletion in Mn. The second deepest chemical weathering front occurs between the weathered bedrock with oxidation along fracture planes to weathered bedrock with both matrix and fracture oxidation. Within this zone Na, Mg, and Mn were consistently depleted relative to the parent material, the XRD intensity peaks suggested the transformation of clays, and there was an increase in matrix poros-

ity. Within the weathered bedrock with matrix and fracture oxidation, we observed measurable (albeit small) changes in rock moisture dynamics likely from water drainage from pores and fractures indicative of deep water delivery into the bedrock.

The shallowest chemical weathering front detectable from the rock cores is the transition between weathered bedrock with matrix oxidation to saprolite. This boundary was marked by a relatively sharp and intense depletion in Na, Mg, and Mn. In addition, there was a pronounced loss in P with signs of K depletion at the near surface. This chemical reaction front coincided with a significant increase in matrix porosity, reduction of mechanical strength, and the highest change in subsurface rock moisture. While we were unable to identify the presence of phosphates within the samples using XRD, previous studies within the Great Valley Sequence have reported the presence of phosphate nodules within the sandstone-dominant regions (Graymer and Langenheim, 2021). Therefore, we assume the depletion of P within the saprolite to represent the weathering of a P-bearing mineral (e.g., predominantly albite). The release of P from primary minerals may be leached into solution, taken up by plants and microorganisms which suggests that this zone has higher hydrologic and biologic activity (Bünemann et al., 2010; Lajtha and Schlesinger, 1988).

2.5.2 Controls on weathering and water cycling between hillslopes with opposing aspects

There are several lines of evidence to suggest that there is a higher degree of weathering within the pole-facing slope compared to the equator-facing slope. For

example, there was a relatively larger decrease in XRD intensity counts for plagioclase feldspar content throughout the pole-facing weathered profile. In addition, there was generally a higher depletion of Na, Mg, and Mn as well as a higher saprolite matrix porosity on the pole-facing slope relative to the equator-facing slope. The evidence for a higher degree of chemical and physical weathering within the pole-facing slope corresponded with the observed higher magnitude and deeper extent of seasonally dynamic storage. These findings align with previous aspect studies that have demonstrated that increased woody-vegetation on pole-facing slopes may enhance subsurface weathering through biogenic and hydrologic processes (Befus et al., 2011; Burns et al., 2023; García-Gamero et al., 2021; Pedrazas et al., 2021).

Trees can enhance chemical and physical weathering on the pole-facing slope both indirectly by altering hydrologic storage and flowpaths and directly through root-level interactions (Brantley, et al., 2017; Brantley et al., 2011). For example, previous studies have demonstrated that oak trees rely on more and deeper water sources than grasses (A. Donaldson et al., n.d.; Hahm et al., 2020; Ma et al., 2020). Therefore, a more pronounced wetting and drying cycle on the pole-facing slope due to oak water uptake during the summer season may lead to more water passing through the subsurface and interacting with mineral surfaces during the subsequent winter, rainy season (Brantley et al., 2007; Hua et al., 2017). In addition, roots contribute directly to subsurface weathering through the production of root exudates, root wedging along fractures, and elevating subsurface CO₂ through root respiration (Hasenmueller et al., 2017; Roque-Malo et al., 2022). While there is a clear relationship between the depths at which the

greatest chemical weathering, matrix porosity, and dynamic storage occur it remains difficult to determine how present-day rooting depths relate to the weathered profile due to limited tools to map in-situ deep root architecture (Maeght et al., 2013).

Interestingly, there was no observable difference between the tau values between aspects for P. Previous studies have shown a relationship between the amount of above-ground biomass and P leaching from bedrock (Dzombak and Sheldon, 2020; Lajtha and Schlesinger, 1988). We hypothesized that there would be a higher amount of P depletion on the oak-dominated pole-facing slope compared to the grass-dominant equator-facing slope. However, we did not observe a difference in the depth nor degree of P depletion between aspects. One explanation for the lack of difference in P depletion between aspects may be because the chemical weathering patterns that we observe today partially reflect the weathering during the cooler, wetter Pleistocene, when Arbor Creek catchment was likely not a precipitation-limited ecosystem (Adam and West, 1983). During this climate regime, the weathering profile may have been impacted by the presence of woody-vegetation on either aspect and the observed differences in vegetation type (e.g. grass versus tree) may be a relatively recent (11-13 Ka) phenomenon (Cole, 1983; Donaldson et al., 2023).

In addition to the “top-down” processes addressed above (e.g. vegetation and water cycling), previous research within the field site has demonstrated a higher fracture density within the unweathered bedrock on the pole-facing slope compared to the equator-facing slope (Callahan et al., in-review). Inherent rock damage during bedrock formation and fracture spacing has been suggested to play a role in the rate

of oxidation within the critical zone (Langston et al., 2015; Reis and Brantley, 2017). Therefore, both top-down hydrologic and biogenic weathering agents combined with bottom-up differences in rock fracturing may also influence the observed contrasts in chemical weathering (Flinchum et al., 2018; Riebe et al., 2001).

2.5.3 Weathering across sites underlain by clastic sedimentary rocks

The focus of sedimentary rock chemical weathering has previously been on fine-grained sedimentary rocks such as shales, mudstones and greywackes (Anderson et al., 2002; Chigira, 1990; Chigira and Oyama, 2000; Gu et al., 2020; Jin et al., 2011; Pedrazas et al., 2021; Sullivan et al., 2016). A key observation across rock types including clastic sedimentary systems is that chemical weathering patterns and subsurface water cycling are commonly co-located (Brantley, Lebedeva, et al., 2017). For example, pyrite oxidation fronts (defined here as the transition between undetectable to detectable sulfur) have been shown to align with the depth of the water table (Chigira, 1990; Sullivan et al., 2016). However, within Arbor Creek catchment, the pyrite dissolution front was above the observed water table. Pedrazas et al. (2021) speculated that within the Great Valley sequence of central California, the pyrite oxidation front may be more shallow than the water table due to low fracture density and sufficiently low infiltration of chemically reactive meteoric water at depth (Lebedeva and Brantley, 2020). Within Arbor Creek catchment we observed highly fractured bedrock, likely due to the close proximity to the Caldarez fault, therefore we don't suspect that pyrite oxidation is limited at depth (Callahan et al., in-review). Alternatively, we suspect that the relatively

shallow pyrite dissolution front relative to the location of the present-day water table is an indication of the location of the paleo-water table within the wetter and cooler Pleistocene (Hudson Rasmussen et al., 2023).

Within fine-grained sedimentary rocks, the significant depletion of Ca, Na, and Mg is commonly reported within the saprolite and associated with the dissolution of carbonates (e.g. calcite), feldspars (e.g. albite), and clays (e.g. chlorite). Within Arbor Creek catchment, we were unable to discern a clear carbonate reaction front, owing to the relatively low Ca concentrations and lack of systematic variability in Ca losses or gains with depth. Previous studies have noted the difficulty of identifying carbonate weathering fronts due to the “cyclic dissolution and reprecipitation of calcite” as shown by the depleted and enriched Ca τ values (Pedrazas et al., 2021; Wan et al., 2019). Within Arbor Creek catchment we observed pronounced Na at the soil-saprolite boundary and Mg depletion which aligned with the saprolite to weathered bedrock boundary. Previous studies have noted a grain-size dependence on the reaction mechanisms driving chemical weathering, especially for the chlorite (Worden et al., 2020). However, further work at the site is required to quantitatively characterize the mineralogy and grain sizes with depth to identify the dominant chemical reactions driving critical zone development.

Within Arbor Creek catchment, we find that evidence of both top-down and bottom-up controls on weathering could be operating in tandem similar to other clastic sedimentary systems (Lebedeva and Brantley, 2013; Rempe and Dietrich, 2014). However, Arbor Creek catchment is rather unique in that the present-day weathering profile

may still retain a relict weathering signal from past vegetation distribution dynamics which has previously been largely underrepresented in models of subsurface weathering and climate change due to the differences in operating timescales (Gurung et al., 2024). Additionally, the fresh bedrock within Arbor Creek remains highly fractured which is distinct from other sites which have reported relatively intact and pristine fresh bedrock (Gu et al., 2020; Pedrazas et al., 2021). Further research is required to investigate how fracture density influences the chemical evolution of the critical zone in sedimentary rocks.

2.5.4 Nuances and limitations of study

Overall there are observable chemical depletion patterns with depth and between aspects, especially at the saprolite to weathered bedrock transition. The variability observed is likely a product of the parent material composition and the assumed immobile reference element, Ti. The assumed parent material within N4W1 and S3W1 were all sandstone samples and are likely not a representative source rock for the shale samples within the weathered profile, but are included for reference. Therefore, we observed a pronounced difference between the chemical depletion and enrichment between sandstone and shale samples across individual elements. Additionally, we assume that Ti was the ideal immobile element to calculate relative enrichment and depletion of individual elements within the weathered profile. While the Ti had less variability relative to Zr, future research is required to better refine how parent material samples are identified and the variability due to the immobile element chosen (Price and Velbel,

2003).

We used significant changes in neutron counts (defined as a change greater than the standard deviation between a zone expected to have no vegetation uptake) to delineate the extent of the dynamic storage zone. Interestingly, there was an observed change in neutron counts between 15 to 18 m within the subsurface, which extends beyond the deepest observed oak rooting depths during drilling (12 m; Supplementary Figure 5) and well beyond average reported oak rooting depths (5.2 m; (Fan et al., 2017). These anomalous neutron count changes are aligned with a section of pervasive fracturing in a zone with otherwise discretely fractured (Callahan et al., in-review). Therefore, we hypothesize that this pervasively fractured zone may store and drain water more than the surrounding rock.

2.6 Conclusion

Quantifying the depth and extent of subsurface weathering is critical to understanding how interactions between vegetation distribution and microclimates regulate ecosystem form and functions. Here, we used two hillslopes with opposing aspects as a natural experiment to determine how differences in incoming solar radiation and vegetation type (trees vs. grass) mediate rock-water interactions within the vadose zone. Common to other sedimentary systems, we observed a deep weathering front (tens of meters) within the subsurface which suggests the deep cycling and storage of chemical reactive meteoric water. Additionally, we identified a sharp reaction front within the

near-surface (5-10 m) within the subsurface of both study hillslopes that aligned with the extent of dynamic storage. While these shallow and deep similarities persisted across slopes with opposing aspects, we observed higher magnitudes of chemical weathering on the cooler pole-facing slope with oak trees compared to the warmer equator-facing slope with grasses. In addition, the dynamic storage zone was nearly double the depth on the pole-facing slope. These findings provide strong evidence for the importance of woody vegetation with deep roots to mediate subsurface weathering through root-water uptake and root-rock interactions, enhancing subsurface water cycling and reaction potential. However, a lack of difference between the weathering extent and magnitude of phosphorus and the observation that the pyrite oxidation front above the deep water table may be a relic fingerprint of past dominant hydrologic, vegetative, and weathering processes within a cooler and wetter Pleistocene. These findings provide insights into the fundamental relationship between landscape evolution, water storage, and vegetation distributions. A better understanding of these relationships are critical to predicting how changes in climate may alter terrestrial water cycling, storage capacity, and material export.

2.7 References

- Adam, D. P., and West, G. J. (1983). Temperature and precipitation estimates through the last glacial cycle from clear lake, california, pollen data. *Science*, 219(4581), 168–170. <https://doi.org/10.1126/science.219.4581.168>
- Anderson, S. P., Dietrich, W. E., and Brimhall, G. H., Jr. (2002). Weathering profiles, mass-balance analysis, and rates of solute loss: Linkages between weathering and erosion in a small, steep catchment. *Geological Society of America Bulletin*, 114(9), 1143–1158. [https://doi.org/10.1130/0016-7606\(2002\)114j1143:wpmbaa;2.0.co;2](https://doi.org/10.1130/0016-7606(2002)114j1143:wpmbaa;2.0.co;2)
- Befus, K. M., Sheehan, A. F., Leopold, M., Anderson, S. P., and Anderson, R. S. (2011). Seismic constraints on critical zone architecture, Boulder Creek watershed, Front Range, Colorado. *Vadose Zone Journal: VZJ*, 10(3), 915–927. <https://doi.org/10.2136/vzj2010.0108>
- Bjørlykke, K., and Jahren, J. (2015). Sandstones and Sandstone Reservoirs. In K. Bjørlykke (Ed.), *Petroleum Geoscience: From Sedimentary Environments to Rock Physics* (pp. 119–149). Springer Berlin Heidelberg.
- Brantley, S., Kubicki, J., and White, A. (2007). *Kinetics of Water-Rock Interaction*. Springer Science and Business Media.
- Brantley, S. L., Eissenstat, D. M., Marshall, J. A., Godsey, S. E., Balogh-Brunstad, Z., Karwan, D. L., Papuga, S. A., Roering, J., Dawson, T. E., Evaristo, J., Chadwick, O., McDonnell, J. J., and Weathers, K. C. (2017). Reviews and syntheses: On the roles trees play in building and plumbing the Critical Zone. *Biogeosciences*

- Discussions , 1–41. <https://doi.org/10.5194/bg-2017-61>
- Brantley, S. L., Holleran, M. E., Jin, L., and Bazilevskaya, E. (2013). Probing deep weathering in the Shale Hills Critical Zone Observatory, Pennsylvania (USA): the hypothesis of nested chemical reaction fronts in the subsurface. *Earth Surface Processes and Landforms*, 38(11), 1280–1298. <https://doi.org/10.1002/esp.3415>
- Brantley, S. L., and Lebedeva, M. I. (2021). Relating land surface, water table, and weathering fronts with a conceptual valve model for headwater catchments. *Hydrological Processes*, 35(2). <https://doi.org/10.1002/hyp.14010>
- Brantley, S. L., Lebedeva, M. I., Balashov, V. N., Singha, K., Sullivan, P. L., and Stinchcomb, G. (2017). Toward a conceptual model relating chemical reaction fronts to water flow paths in hills. *Geomorphology* , 277, 100–117. <https://doi.org/10.1016/j.geomorph.2016.09.027>
- Brantley, S. L., Megonigal, J. P., Scatena, F. N., Balogh-Brunstad, Z., Barnes, R. T., Bruns, M. A., Van Cappellen, P., Dontsova, K., Hartnett, H. E., Hartshorn, A. S., Heimsath, A., Herndon, E., Jin, L., Keller, C. K., Leake, J. R., McDowell, W. H., Meinzer, F. C., Mozdzer, T. J., Petsch, S., . . . Yoo, K. (2011). Twelve testable hypotheses on the geobiology of weathering. *Geobiology*, 9(2), 140–165. <https://doi.org/10.1111/j.1472-4669.2010.00264.x>
- Brimhall, G. H., Lewis, C. J., Ague, J. J., Dietrich, W. E., Hampel, J., Teague, T., and Rix, P. (1988). Metal enrichment in bauxites by deposition of chemically mature aeolian dust. *Nature*, 333(6176), 819–824. <https://doi.org/10.1038/333819a0>
- Bünemann, E. K., Oberson, A., and Frossard, E. (2010). Phosphorus in Action:

Biological Processes in Soil Phosphorus Cycling. Springer Science and Business Media.

Burns, E. F., Rempe, D. M., Parsekian, A. D., Schmidt, L. M., Singha, K., and Barnard, H. R. (2023). Ecohydrologic dynamics of rock moisture in a Montane catchment of the Colorado front range. *Water Resources Research*, 59(6). <https://doi.org/10.1029/2022wr034117>

Callahan, R., Huang, M.-H., Donaldson, A., Hudson-Rasmussen, B., and Zimmer, M. (in-review). Pervasive rock fracturing drives deep weathering and water flow in the central California Coast Range. *Geophysical Research Letters*.

Chigira, M. (1990). A mechanism of chemical weathering of mudstone in a mountainous area. *Engineering Geology*, 29(2), 119–138. [https://doi.org/10.1016/0013-7952\(90\)90002-I](https://doi.org/10.1016/0013-7952(90)90002-I)

Chigira, M., and Oyama, T. (2000). Mechanism and effect of chemical weathering of sedimentary rocks. *Engineering Geology*, 55(1), 3–14. [https://doi.org/10.1016/S0013-7952\(99\)00102-7](https://doi.org/10.1016/S0013-7952(99)00102-7)

Chorover, J., Troch, P. A., Rasmussen, C., Brooks, P. D., Pelletier, J. D., Breshears, D. D., Huxman, T. E., Kurc, S. A., Lohse, K. A., McIntosh, J. C., Meixner, T., Schaap, M. G., Litvak, M. E., Perdrial, J., Harpold, A., and Durcik, M. (2011). How water, carbon, and energy drive critical zone evolution: The jemez–Santa Catalina Critical Zone Observatory. *Vadose Zone Journal: VZJ*, 10(3), 884–899. <https://doi.org/10.2136/vzj2010.0132>

Cole, K. (1983). Late Pleistocene Vegetation of Kings Canyon, Sierra Nevada, Califor-

nia. *Quaternary Research*, 19(1), 117–129. [https://doi.org/10.1016/0033-5894\(83\)90031-](https://doi.org/10.1016/0033-5894(83)90031-5)

5

Donaldson, A., Dralle, D., Barling, N., Callahan, R., Loik, M., and Zimmer, M. (in-review). Aspect differences in vegetation type drive higher evapotranspiration on pole-facing slope in a California Oak Savanna. *Journal of Geophysics: Biogeosciences*.

Donaldson, A. M., Zimmer, M., Huang, M.-H., Johnson, K. N., Hudson-Rasmussen, B., Finnegan, N., Barling, N., and Callahan, R. P. (2023). Symmetry in hillslope steepness and saprolite thickness between hillslopes with opposing aspects. *Journal of Geophysical Research. Earth Surface*, 128(7). <https://doi.org/10.1029/2023jf007076>

Dzombak, R. M., and Sheldon, N. D. (2020). Weathering Intensity and Presence of Vegetation Are Key Controls on Soil Phosphorus Concentrations: Implications for Past and Future Terrestrial Ecosystems. *Soil Systems*, 4(4), 73.

Fan, Y., Miguez-Macho, G., Jobbágy, E. G., Jackson, R. B., and Otero-Casal, C. (2017). Hydrologic regulation of plant rooting depth. *Proceedings of the National Academy of Sciences of the United States of America*, 114(40), 10572–10577. <https://doi.org/10.1073/pnas.1712381114>

Flinchum, B. A., Steven Holbrook, W., Rempe, D., Moon, S., Riebe, C. S., Carr, B. J., Hayes, J. L., St. Clair, J., and Peters, M. P. (2018). Critical zone structure under a granite ridge inferred from drilling and three-dimensional seismic refraction data. *Journal of Geophysical Research. Earth Surface*, 123(6), 1317–1343. <https://doi.org/10.1029/2017jf004280>

- García-Gamero, V., Peña, A., Laguna, A. M., Giráldez, J. V., and Vanwallegem, T. (2021). Factors controlling the asymmetry of soil moisture and vegetation dynamics in a hilly Mediterranean catchment. *Journal of Hydrology*, 598, 126207. <https://doi.org/10.1016/j.jhydrol.2021.126207>
- Goodfellow, B. W., Hilley, G. E., Webb, S. M., Sklar, L. S., Moon, S., and Olson, C. A. (2016). The chemical, mechanical, and hydrological evolution of weathering granitoid. *J. Geophys. Res. Earth Surf.* <https://doi.org/10.1002/2016JF003822>
- Graymer, R. W., and Langenheim, V. E. (2021). Geologic framework of Mount Diablo, California. *Regional Geology of Mount Diablo, California: Its Tectonic Evolution on the North America Plate Boundary: Geological Society of America Memoir 217.* [https://doi.org/10.1130/2021.1217\(01\)](https://doi.org/10.1130/2021.1217(01))
- Gurung, K., Field, K. J., Batterman, S. A., Poulton, S. W., and Mills, B. J. W. (2024). Geographic range of plants drives long-term climate change. *Nature Communications*, 15(1), 1805. <https://doi.org/10.1038/s41467-024-46105-1>
- Gu, X., Rempe, D. M., Dietrich, W. E., West, A. J., Lin, T.-C., Jin, L., and Brantley, S. L. (2020). Chemical reactions, porosity, and microfracturing in shale during weathering: The effect of erosion rate. *Geochimica et Cosmochimica Acta*, 269, 63–100. <https://doi.org/10.1016/j.gca.2019.09.044>
- Hahm, W. J., Rempe, D. M., Dralle, D. N., Dawson, T. E., and Dietrich, W. E. (2020). Oak transpiration drawn from the weathered bedrock vadose zone in the summer dry season. *Water Resources Research*, 56(11). <https://doi.org/10.1029/2020wr027419>
- Hasenmueller, E. A., Gu, X., Weitzman, J. N., Adams, T. S., Stinchcomb, G. E.,

- Eissenstat, D. M., Drohan, P. J., Brantley, S. L., and Kaye, J. P. (2017). Weathering of rock to regolith: The activity of deep roots in bedrock fractures. *Geoderma*, 300, 11–31. <https://doi.org/10.1016/j.geoderma.2017.03.020>
- Holbrook, W. S., Riebe, C. S., Elwaseif, M., L. Hayes, J., Basler-Reeder, K., L. Harry, D., Malazian, A., Dosseto, A., C. Hartsough, P., and W. Hopmans, J. (2014). Geophysical constraints on deep weathering and water storage potential in the Southern Sierra Critical Zone Observatory. *Earth Surface Processes and Landforms*, 39(3), 366–380. <https://doi.org/10.1002/esp.3502>
- Hua, W., Dong, S., Peng, F., Li, K., and Wang, Q. (2017). Experimental investigation on the effect of wetting-drying cycles on mixed mode fracture toughness of sandstone. *International Journal of Rock Mechanics and Mining Sciences*, 93, 242–249. <https://doi.org/10.1016/j.ijrmms.2017.01.017>
- Hudson Rasmussen, B. M., Huang, M.-H., Hahm, W. J., Rempe, D. M., Dralle, D., and Nelson, M. D. (2023). Mapping variations in bedrock weathering with slope aspect under a sedimentary Ridge-Valley system using near-surface geophysics and drilling. *Journal of Geophysical Research. Earth Surface*, 128(7).
- Jin, L., Andrews, D. M., Holmes, G. H., Lin, H., and Brantley, S. L. (2011). Opening the “black box”: Water chemistry reveals hydrological controls on weathering in the Susquehanna Shale Hills Critical Zone Observatory. *Vadose Zone Journal: VZJ*, 10(3), 928–942. <https://doi.org/10.2136/vzj2010.0133>
- Kinoshita, M., Tobin, H., Ashi, J., Kimura, G., Lallemand, S., Screamon, E. J., and Curewitz, D. (2011). Data report: refined method for calculating percentages of

- kaolinite and chlorite from X-ray diffraction data, with application to the Nankai margin of southwest Japan. *Proc. IODP— Volume*, 314, 2.
- Lajtha, K., and Schlesinger, W. H. (1988). The biogeochemistry of phosphorus cycling and phosphorus availability along a desert soil chronosequence. *Ecology*, 69(1), 24–39. <https://doi.org/10.2307/1943157>
- Langston, A. L., Tucker, G. E., Anderson, R. S., and Anderson, S. P. (2015). Evidence for climatic and hillslope-aspect controls on vadose zone hydrology and implications for saprolite weathering. *Earth Surface Processes and Landforms*, 40(9), 1254–1269. <https://doi.org/10.1002/esp.3718>
- Lebedeva, M. I., and Brantley, S. L. (2013). Exploring geochemical controls on weathering and erosion of convex hillslopes: beyond the empirical regolith production function. *Earth Surface Processes and Landforms*, 38(15), 1793–1807.
- Lebedeva, M. I., and Brantley, S. L. (2020). Relating the depth of the water table to the depth of weathering. *Earth Surface Processes and Landforms*, 45(9), 2167–2178. <https://doi.org/10.1002/esp.4873>
- Leone, J. D., Holbrook, W. S., Riebe, C. S., Chorover, J., Ferré, T. P. A., Carr, B. J., and Callahan, R. P. (2020). Strong slope-aspect control of regolith thickness by bedrock foliation. *Earth Surface Processes and Landforms*, 45(12), 2998–3010. <https://doi.org/10.1002/esp.4947>
- Li, L., Sullivan, P. L., Benettin, P., Cirpka, O. A., Bishop, K., Brantley, S. L., Knapp, J. L. A., van Meerveld, I., Rinaldo, A., Seibert, J., Wen, H., and Kirchner, J. W. (2021). Toward catchment hydro-biogeochemical theories. *WIREs. Water*, 8(1).

<https://doi.org/10.1002/wat2.1495>

Long, I. F., and French, B. K. (1967). Measurement of soil moisture in the field by neutron moderation. *Journal of Soil Science*, 18(1), 149–166.

Maeght, J.-L., Rewald, B., and Pierret, A. (2013). How to study deep roots—and why it matters. *Frontiers in Plant Science*, 4.

Maher, K. (2010). The dependence of chemical weathering rates on fluid residence time. *Earth and Planetary Science Letters*, 294(1) 101–110.
<https://doi.org/10.1016/j.epsl.2010.03.010>

Maher, K., and Chamberlain, C. P. (2014). Hydrologic regulation of chemical weathering and the geologic carbon cycle. *Science*, 343(6178), 1502–1504.

Maher, K., and Navarre-Sitchler, A. (2019). Reactive Transport Processes that Drive Chemical Weathering: From Making Space for Water to Dismantling Continents. *Reviews in Mineralogy and Geochemistry*, 85(1), 349–380.
<https://doi.org/10.2138/rmg.2018.85.12>

Ma, S., Eichelmann, E., Wolf, S., Rey-Sanchez, C., and Baldocchi, D. D. (2020). Transpiration and evaporation in a Californian oak-grass savanna: Field measurements and partitioning model results. *Agricultural and Forest Meteorology*, 295, 108204.
<https://doi.org/10.1016/j.agrformet.2020.108204>

Moravec, B., and Chorover, J. (2020). Critical zone biogeochemistry. In *Biogeochemical Cycles* (pp. 131–149). John Wiley and Sons, Inc.
<https://doi.org/10.1002/9781119413332.ch6>

Navarre-Sitchler, A., Brantley, S. L., and Rother, G. (2015). How Porosity Increases

- During Incipient Weathering of Crystalline Silicate Rocks. *Reviews in Mineralogy and Geochemistry*, 80(1), 331–354. <https://doi.org/10.2138/rmg.2015.80.10>
- Nielson, T., Bradford, J., Holbrook, W. S., and Seyfried, M. (2021). The effect of aspect and elevation on critical zone architecture in the Reynolds Creek Critical Zone Observatory: A seismic refraction study. *Frontiers in Water*, 3. <https://doi.org/10.3389/frwa.2021.670524>
- Pedrazas, M. A., Hahm, W. J., Huang, M.-H., Dralle, D., Nelson, M. D., Breunig, R. E., Fauria, K. E., Bryk, A. B., Dietrich, W. E., and Rempe, D. M. (2021). The relationship between topography, bedrock weathering, and water storage across a sequence of ridges and valleys. *Journal of Geophysical Research. Earth Surface*, 126(4). <https://doi.org/10.1029/2020jf005848>
- Pelletier, J. D., Barron-Gafford, G. A., Gutiérrez-Jurado, H., Hinckley, E.-L. S., Istanbuloglu, E., McGuire, L. A., Niu, G.-Y., Poulos, M. J., Rasmussen, C., Richardson, P., Swetnam, T. L., and Tucker, G. E. (2018). Which way do you lean? Using slope aspect variations to understand Critical Zone processes and feedbacks. *Earth Surface Processes and Landforms*, 43(5), 1133–1154. <https://doi.org/10.1002/esp.4306>
- Price, J. R., and Velbel, M. A. (2003). Chemical weathering indices applied to weathering profiles developed on heterogeneous felsic metamorphic parent rocks. *Chemical Geology*, 202(3), 397–416. <https://doi.org/10.1016/j.chemgeo.2002.11.001>
- PRISM Climate Group. (2022). PRISM Rainfall Dataset.
- Rahman, S. S., Rahman, M. M., and Khan, F. A. (1995). Response of low-permeability, illitic sandstone to drilling and completion fluids. *Journal of Petroleum Science and*

- Engineering, 12(4), 309–322. [https://doi.org/10.1016/0920-4105\(94\)00052-6](https://doi.org/10.1016/0920-4105(94)00052-6)
- Rasmussen, C., Brantley, S., Richter, D. D., Blum, A., Dixon, J., and White, A. F. (2011). Strong climate and tectonic control on plagioclase weathering in granitic terrain. *Earth and Planetary Science Letters*, 301(3), 521–530. <https://doi.org/10.1016/j.epsl.2010.11.037>
- Rasmussen, C., Troch, P. A., Chorover, J., Brooks, P., Pelletier, J., and Huxman, T. E. (2011). An open system framework for integrating critical zone structure and function. *Biogeochemistry*, 102(1), 15–29. <https://doi.org/10.1007/s10533-010-9476-8>
- Raymond, P. A. (2017). Temperature versus hydrologic controls of chemical weathering fluxes from United States forests. *Chemical Geology*, 458, 1–13. <https://doi.org/10.1016/j.chemgeo.2017.02.025>
- Regmi, N. R., McDonald, E. V., and Rasmussen, C. (2019). Hillslope response under variable microclimate. *Earth Surface Processes and Landforms*, 44(13), 2615–2627. <https://doi.org/10.1002/esp.4686>
- Reis, F. D. A. A., and Brantley, S. L. (2017). Models of transport and reaction describing weathering of fractured rock with mobile and immobile water. *J. Geophys. Res. Earth Surf.* <https://doi.org/10.1002/2016JF004118>.
- Rempe, D. M., and Dietrich, W. E. (2014). A bottom-up control on fresh-bedrock topography under landscapes. *Proceedings of the National Academy of Sciences of the United States of America*, 111(18), 6576–6581. <https://doi.org/10.1073/pnas.1404763111>

- Riebe, C. S., Hahm, W. J., and Brantley, S. L. (2017). Controls on deep critical zone architecture: a historical review and four testable hypotheses. *Earth Surface Processes and Landforms*, 42(1), 128–156. <https://doi.org/10.1002/esp.4052>
- Riebe, C. S., Kirchner, J. W., Granger, D. E., and Finkel, R. C. (2001). Strong tectonic and weak climatic control of long-term chemical weathering rates. *Geology*, 29(6), 511–514. [https://doi.org/10.1130/0091-7613\(2001\)029;0511:STAWCC;2.0.CO;2](https://doi.org/10.1130/0091-7613(2001)029;0511:STAWCC;2.0.CO;2)
- Roque-Malo, S., Druhan, J. L., and Kumar, P. (2022). REWTCrunch: A modeling framework for vegetation induced reactive zone processes in the critical zone. *Journal of Geophysical Research. Biogeosciences*, 127(2). <https://doi.org/10.1029/2021jg006562>
- Smith, T., and Bookhagen, B. (2021). Climatic and biotic controls on topographic asymmetry at the global scale. *Journal of Geophysical Research. Earth Surface*, 126(1). <https://doi.org/10.1029/2020jf005692>
- Starkey, H. C., Blackmon, P. D., and Hauff, P. L. (1984). *The Routine Mineralogical Analysis of Clay-bearing Samples*. U.S. Government Printing Office.
- Sullivan, P. L., Hynek, S. A., Gu, X., Singha, K., White, T., West, N., Kim, H., Clarke, B., Kirby, E., Duffy, C., and Brantley, S. L. (2016). Oxidative dissolution under the channel leads geomorphological evolution at the Shale Hills catchment. *American Journal of Science*, 316(10), 981–1026. <https://doi.org/10.2475/10.2016.02>
- Sullivan, P. L., Li, L., Godd eris, Y., and Brantley, S. L. (2020). Poised to hindcast and earthcast the effect of climate on the critical zone. In *Biogeochemical Cycles* (pp. 207–222). John Wiley and Sons, Inc. <https://doi.org/10.1002/9781119413332.ch10>
- Surpless, K. D. (2015). *Geochemistry of the Great Valley Group: an integrated prove-*

- nance record. *International Geology Review*, 57(5-8), 747–766.
<https://doi.org/10.1080/00206814.2014.923347>
- Wang, W., Chen, P., Dueker, K., Zhang, Y., Lee, E.-J., Mu, D., Keifer, I., and Jiao, J. (2021). Coevolution of weathering front and water table. *Geophysical Research Letters*, 48(20). <https://doi.org/10.1029/2021gl092916>
- Wang, W., Nyblade, A., Mount, G., Moon, S., Chen, P., Accardo, N., Gu, X., Forsythe, B., and Brantley, S. L. (2021). 3D seismic anatomy of a watershed reveals climate-topography coupling that drives water flowpaths and bedrock weathering. *Journal of Geophysical Research. Earth Surface*, 126(12). <https://doi.org/10.1029/2021jf006281>
- Wan, J., Tokunaga, T. K., Williams, K. H., Dong, W., Brown, W., Henderson, A. N., Newman, A. W., and Hubbard, S. S. (2019). Predicting sedimentary bedrock subsurface weathering fronts and weathering rates. *Scientific Reports*, 9(1), 17198. <https://doi.org/10.1038/s41598-019-53205-2>
- White, A. F., and Blum, A. E. (1995). Effects of climate on chemical weathering in watersheds. *Geochimica et Cosmochimica Acta*, 59(9), 1729–1747. [https://doi.org/10.1016/0016-7037\(95\)00078-E](https://doi.org/10.1016/0016-7037(95)00078-E)
- White, A. F., Blum, A. E., Schulz, M. S., Vivit, D. V., Stonestrom, D. A., Larsen, M., Murphy, S. F., and Eberl, D. (1998). Chemical Weathering in a Tropical Watershed, Luquillo Mountains, Puerto Rico: I. Long-Term Versus Short-Term Weathering Fluxes. *Geochimica et Cosmochimica Acta*, 62(2), 209–226. [https://doi.org/10.1016/S0016-7037\(97\)00335-9](https://doi.org/10.1016/S0016-7037(97)00335-9)
- Worden, R. H., Griffiths, J., Wooldridge, L. J., Utley, J. E. P., Lawan, A. Y., Muhammed,

D. D., Simon, N., and Armitage, P. J. (2020). Chlorite in sandstones. *Earth-Science Reviews*, 204, 103105. <https://doi.org/10.1016/j.earscirev.2020.103105>

Ying, F., Martyn, C., David M., L., Sean, S., L. E., B., Brantley, S. L., Brooks, P. D., Dietrich, W. E., Flores, A., Grant, G., Kirchner, J. W.,... (2019). Hillslope hydrology in global change research and earth system modeling. *Water Resources Research*. <https://agupubs.onlinelibrary.wiley.com/doi/abs/10.1029/2018wr023903>

2.8 Supplementary Materials

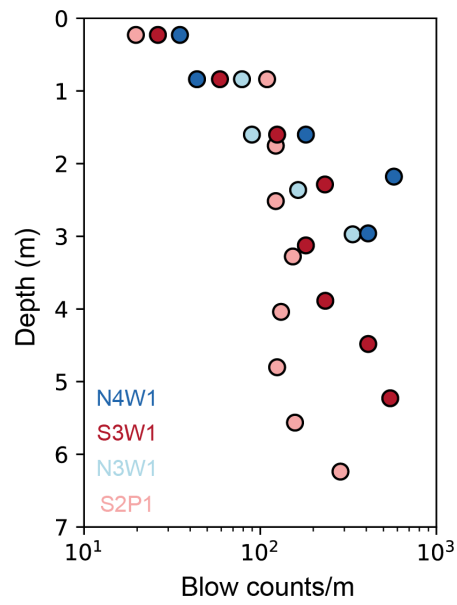


Figure 2.9: Standard penetration tests on the pole-facing slope (blues) and equator-facing slope (reds). Measurement depth extent indicates the depth to refusal.

Supplementary Table 1. Protolith percent average geochemistry for N4W1 and S3W1 with standard deviation.

Borehole	Element	Average %	Standard Deviation
S3W1	SiO ₂	69.980	0.685
N4W1	SiO ₂	69.556	0.726
S3W1	Al ₂ O ₃	15.266	0.301
N4W1	Al ₂ O ₃	14.861	0.330
S3W1	Fe ₂ O ₃	5.241	0.275
N4W1	Fe ₂ O ₃	5.451	0.367
S3W1	MnO	0.069	0.006
N4W1	MnO	0.073	0.008
S3W1	MgO	1.958	0.095
N4W1	MgO	2.183	0.072
S3W1	CaO	1.000	0.109
N4W1	CaO	1.290	0.105
S3W1	Na ₂ O	3.670	0.150
N4W1	Na ₂ O	3.892	0.128
S3W1	K ₂ O	2.037	0.116
N4W1	K ₂ O	1.894	0.029
S3W1	P ₂ O ₅	0.154	0.014
N4W1	P ₂ O ₅	0.146	0.015
S3W1	Zr	0.015	0.001
N4W1	Zr	0.018	0.002
S3W1	TiO ₂	0.623	0.028
N4W1	TiO ₂	0.642	0.036

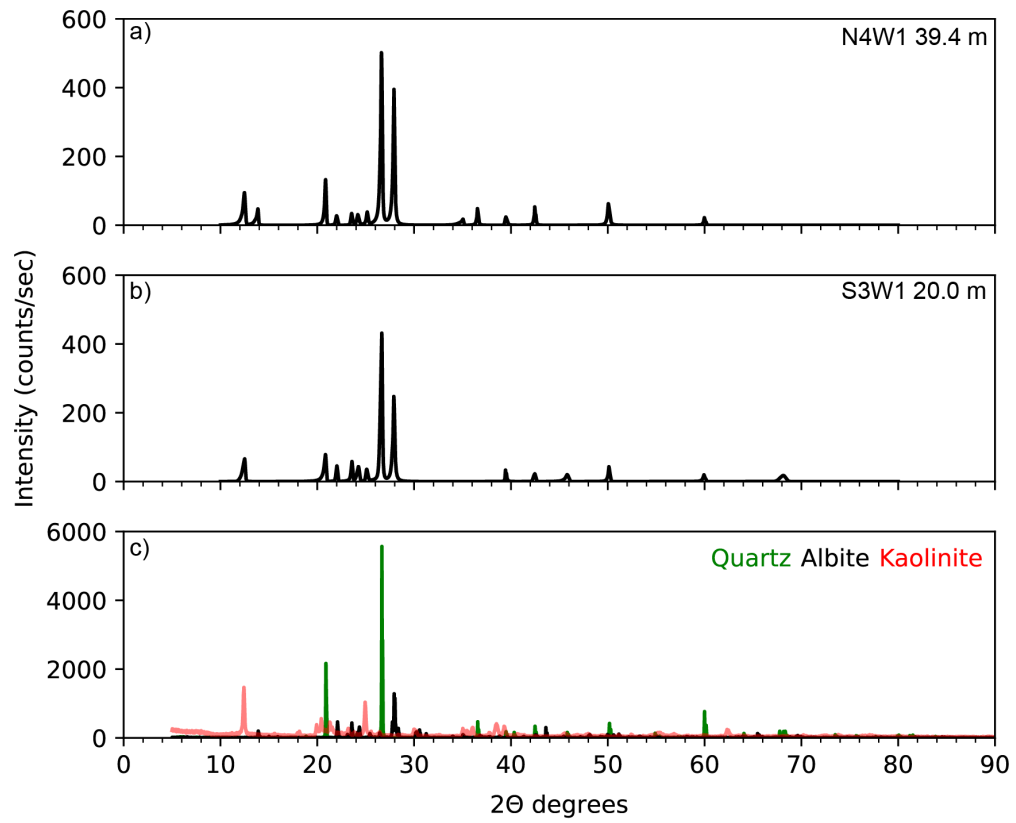


Figure 2.10: Comparison between the unweathered sample on the a) pole-facing slope, b) equator-facing slope and a composite of publicly available XRD intensity peaks for confirmed minerals.

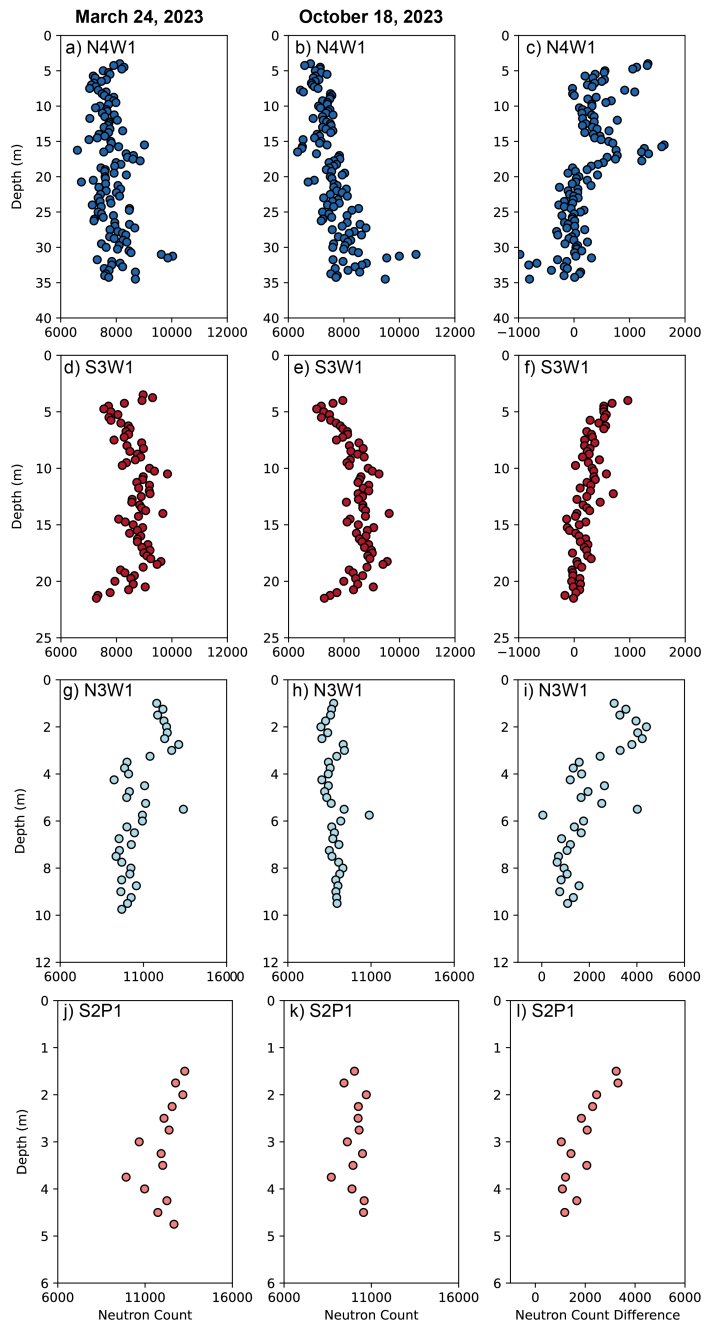


Figure 2.11: Individual neutron probe surveys for the winter measurement period (March 24, 2024) and the summer measurement period (October 18, 2023) and the difference between counts for N4W1 (a-c), S3W1 (d-f), N3W1 (g-i), and S2P1 (j-l)

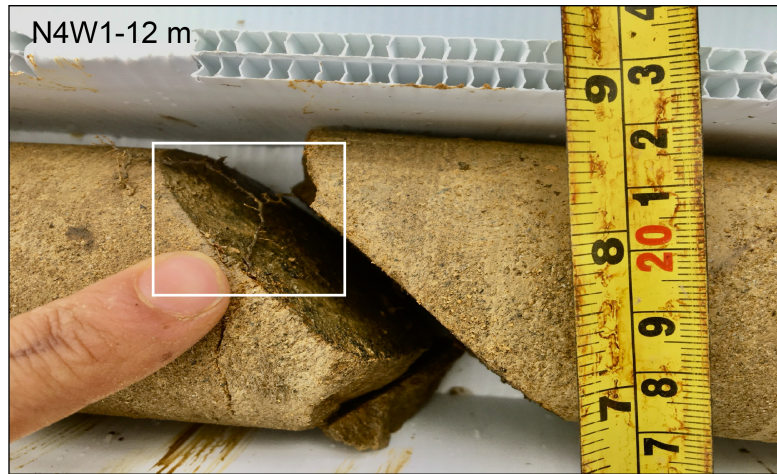


Figure 2.12: Image of rock core section extracted from N4W1 at 12 m with fine woody root present within discrete fracture

Chapter 3

Symmetry in Hillslope Steepness and Saprolite Thickness Between Hillslopes with Opposing Aspects

Reprinted from:

Donaldson, A. M., Zimmer, M., Huang, M.-H., Johnson, K. N., Hudson-Rasmussen, B., Finnegan, N., N. Barling, R. P. Callahan (2023). "Symmetry in hillslope steepness and saprolite thickness between hillslopes with opposing aspects," *Journal of Geophysical Research: Earth Surface* 128, e2023JF007076. <https://doi.org/10.1029/2023JF007076>

JGR Earth Surface

RESEARCH ARTICLE

10.1029/2023JF007076

Symmetry in Hillslope Steepness and Saprolite Thickness Between Hillslopes With Opposing Aspects

A. M. Donaldson¹, M. Zimmer¹, M.-H. Huang², K. N. Johnson^{1,3}, B. Hudson-Rasmussen², N. Finnegan¹, N. Barling¹, and R. P. Callahan¹¹Department of Earth and Planetary Sciences, University of California, Santa Cruz, CA, USA, ²Department of Geology, University of Maryland, College Park, MD, USA, ³Department of Integrative Biology, University of California, Berkeley, CA, USA

Key Points:

- Aspect-dependent microclimatic and vegetative differences do not correspond to physical structure between hillslopes
- Similar physical structure between hillslopes may be driven by various aspect-dependent processes leading to similar material loss and production
- A more comprehensive understanding of critical zone development requires integration of past and present biotic and climatic processes

Supporting Information:

Supporting Information may be found in the online version of this article.

Correspondence to:

A. M. Donaldson and M. Zimmer, andonald@ucsc.edu; margaret.zimmer@ucsc.edu

Citation:

Donaldson, A. M., Zimmer, M., Huang, M.-H., Johnson, K. N., Hudson-Rasmussen, B., Finnegan, N., et al. (2023). Symmetry in hillslope steepness and saprolite thickness between hillslopes with opposing aspects. *Journal of Geophysical Research: Earth Surface*, 128, e2023JF007076. <https://doi.org/10.1029/2023JF007076>

Received 19 JAN 2023

Accepted 24 MAY 2023

Author Contributions:

Conceptualization: A. M. Donaldson, M. Zimmer, M.-H. Huang, K. N. Johnson, N. Finnegan**Data curation:** A. M. Donaldson, M.-H. Huang, K. N. Johnson, B. Hudson-Rasmussen, N. Barling**Formal analysis:** A. M. Donaldson, M.-H. Huang, K. N. Johnson, R. P. Callahan**Funding acquisition:** A. M. Donaldson, M. Zimmer, K. N. Johnson

© 2023. The Authors.

This is an open access article under the terms of the [Creative Commons Attribution License](https://creativecommons.org/licenses/by/4.0/), which permits use, distribution and reproduction in any medium, provided the original work is properly cited.

Abstract The structure of the critical zone (CZ) is a product of feedbacks among hydrologic, climatic, biotic, and chemical processes. Past research within snow-dominated systems has shown that aspect-dependent solar radiation inputs can produce striking differences in vegetation composition, topography, and soil depth between opposing hillslopes. However, far fewer studies have evaluated the role of microclimates on CZ development within rain-dominated systems, especially below the soil and into weathered bedrock. To address this need, we characterized the CZ of a north-facing and south-facing slope within a first-order headwater catchment located in central coast California. We combined terrain analysis of vegetation distribution and topography with soil pit characterization, geophysical surveys and hydrologic measurements between slope-aspects. We documented denser vegetation and higher shallow soil moisture on north facing slopes, which matched previously documented observations in snow-dominated sites. However, average topographic gradients were 24° and saprolite thickness was approximately 6 m across both hillslopes, which did not match common observations from the literature that showed widespread asymmetry in snow-dominated systems. These results suggest that dominant processes for CZ evolution are not necessarily transferable across regions. Thus, there is a continued need to expand CZ research, especially in rain-dominated and water-limited systems. Here, we present two non-exclusive mechanistic hypotheses that may explain these unexpected similarities in slope and saprolite thickness between hillslopes with opposing aspects.

Plain Language Summary Small differences in solar radiation and water availability between hillslopes facing opposite directions may lead to distinct vegetation and hillslope structures. However, more research is needed to understand the controls and extent of structural differences in the subsurface, especially in rain-dominated landscapes. To investigate the physical and ecohydrologic characteristics between hillslopes that face opposite directions, we combined terrain analysis, soil pit characterization, geophysical surveys and hydrologic measurements taken from two hillslopes facing opposite directions. We found that the hillslope that faced north had higher oak tree density, and higher soil moisture than the hillslope that faced south. These observations match other published studies from a range of landscapes and climates in the northern hemisphere. However, contrary to expectations based on other studies, we found that the surface slope and weathered bedrock thickness were similar between the two hillslopes. Similarities in soil water at 50 cm and increased perched groundwater response on the hillslope that faces south suggest that how water moves within the hillslope and what water is available to plants may alter how rock breaks down. In addition, historic climate and water availability may be important to understand the present-day hillslope structure.

1. Introduction

The diversity of landforms on Earth's surface is intrinsically linked to the spatial distribution of the major components of climate: precipitation and air temperature (Perron, 2017; Sharp, 1982). Studies of the development of the critical zone (CZ), which extends from the top of vegetation to fresh bedrock, investigate the feedbacks among climatic conditions, hydrologic and ecological processes, underlying geology and tectonic stresses at time scales from individual precipitation events (Sólyom & Tucker, 2004) to millions of years (Lebedeva & Brantley, 2020). Differences in subsurface CZ structure (e.g., permeability, porosity, thickness) have been attributed to climate (Anderson et al., 2013, 2019), underlying lithology (Buss et al., 2017; Callahan et al., 2022; Hahm et al., 2019), subsurface water movement (Lebedeva & Brantley, 2013, 2018; Rempe & Dietrich, 2014) and regional tectonics (Ma et al., 2021; Moon et al., 2017; Riebe et al., 2001; St. Clair et al., 2015). However, the ability to identify

Investigation: A. M. Donaldson, M.-H. Huang, B. Hudson-Rasmussen, N. Barling
Methodology: A. M. Donaldson, M. Zimmer, M.-H. Huang, K. N. Johnson, B. Hudson-Rasmussen
Project Administration: A. M. Donaldson, M. Zimmer
Resources: A. M. Donaldson
Software: M.-H. Huang, B. Hudson-Rasmussen
Supervision: M. Zimmer
Validation: A. M. Donaldson
Visualization: A. M. Donaldson, M.-H. Huang, K. N. Johnson
Writing – original draft: A. M. Donaldson, M. Zimmer
Writing – review & editing: A. M. Donaldson, M. Zimmer, M.-H. Huang, K. N. Johnson, B. Hudson-Rasmussen, N. Finnegan, N. Barling, R. P. Callahan

the above and belowground causal mechanisms on CZ development and function across diverse landscapes is currently lacking. A better understanding of the relationship between climate and CZ development is essential to disentangle dominant drivers, improve process-based Earth Systems models (Fan, Clark, et al., 2019; Fan, Grant, & Anderson, 2019), predict environmental responses to climate change (Ferdowsi et al., 2021; Maxwell & Shobe, 2022), and manage water resources (Fan, Clark, et al., 2019; Fan, Grant, & Anderson, 2019).

Hillslopes with opposing aspects, or facing opposite directions, provide natural experiments to investigate how small-scale climatic differences control CZ development (Anderson et al., 2014; Chorover et al., 2011). For example, in the northern hemisphere, higher solar radiation inputs on south-facing slopes (SFS) generate hotter and drier conditions compared to north-facing slopes (NFS), which receive less solar radiation per unit area (Pelletier et al., 2017; Poulos et al., 2012; Yetemen et al., 2015). NFS remains cooler and wetter, which promotes the establishment of mesic species and denser vegetation structure (Armento & Martinez, 1978; Desta et al., 2004; Zapata-Rios et al., 2016). These aspect-dependent differences in vegetation have been shown to be key factors contributing to physical CZ asymmetries in water-limited ecosystems (Pelletier et al., 2017; Smith & Bookhagen, 2020).

Researchers have used these small spatial scale differences in solar radiation and vegetation to develop a set of common expectations of aspect-dependent hillslope-scale CZ characteristics (Pelletier et al., 2017; Regmi et al., 2019). Specifically, a common expectation is that lower vegetation densities on SFS will reduce soil surface infiltration capacity, enhancing surface runoff and the promotion of sediment transport (Gutierrez-Jurado et al., 2006; Yetemen et al., 2015). The result of these feedbacks may be the development of less steep SFS slopes compared to densely vegetated NFS with lower sediment transport efficiency (Inbar et al., 2018; Istanbuluoglu et al., 2008). That said, this is not universally true; case studies have shown that colluvial sediment transport processes (e.g., animal burrowing and floral-bioturbation) may dominate soil-mantled hillslopes (McGuire et al., 2014; Roering et al., 2002). In these places, hillslope asymmetry may deviate from our current expectations (Pelletier et al., 2017). For example, colluvial sediment transport can increase with vegetation density (Hughes et al., 2009; McGuire et al., 2014), which may enhance erosion on NFS and make them less steep than SFS. Therefore, despite the expectation that SFS will be less steep than NFS, competition exists between sediment transport processes across landscapes, making universal expectations challenging to identify.

Another common expectation is that aspect-dependent differences in vegetation density contribute to differences in hydrologic flowpaths, and thus, the degree of subsurface chemical weathering (Chorover et al., 2011). Specifically, more vegetation on NFS can increase organic matter and contribute to finer soil texture, which increases soil water retention capacity and promotes soil development (Anderson et al., 2014; Gutierrez-Jurado et al., 2006). Below the soil, higher soil water content may allow for deeper recharge into the saprolite, which contributes to thicker, more weathered saprolite on NFS (Garcia-Gamero et al., 2021; Langston et al., 2015). However, these expectations are largely based on snow-dominated catchments where other processes, such as freeze-thaw cycles and snowmelt, can compound the role of vegetation across aspect (Anderson et al., 2013; Befus et al., 2011; Nielson et al., 2021; West et al., 2019). Therefore, despite the expectation that NFS will have a deeper subsurface CZ, this common expectation must be tested in rain-dominated catchments to confirm its transferability across landscapes.

Recent aspect-based studies in rain-dominated catchments have suggested that the role of microclimates on CZ structure is more complex than previously documented in snow-dominated studies (Inbar et al., 2018; Kumari et al., 2020). Hudson-Rasmussen et al. (2023) combined seismic refraction geophysical surveys with geochemistry data from Pedrazas et al. (2021) to investigate subsurface weathering between opposing slopes within a rain-dominated oak woodland underlain by sedimentary rocks. While they observed slope-aspect differences in vegetation, hillslope steepness, and soil depth, there were no clear aspect-dependent differences in saprolite thicknesses. They suggested that the observed symmetry in saprolite thickness is a relic of past wetter climatic conditions and additional time is required to produce saprolite asymmetry.

Here, we test the current expectation that NFS are wetter, steeper, and have thicker soil and saprolite compared to SFS within a rain-dominated catchment underlain by sedimentary rocks. To do so, we identified a sedimentary catchment with end-member vegetation assemblages (i.e., grasses vs. trees) in the central California Coast Range and coupled topographic, hydrologic, pedologic, and geophysical data from two adjacent hillslopes with opposing aspects. Based on our observations, we introduce testable hypotheses that represent exciting frontiers within the ecohydrologic and CZ science communities.

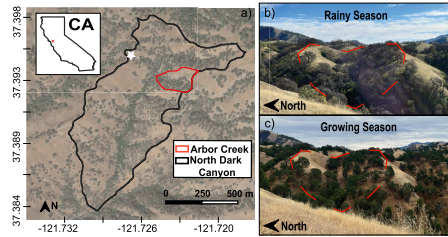


Figure 1. (a) Arbor Creek Experimental Catchment area delineated (red) within the larger North Dark Canyon Watershed (NDC, black) and inset map of California. (b) Arbor Creek Experimental Catchment during the rainy season (February 2022) and (c) Arbor Creek Experimental Catchment during the growing season (June 2022). White star in panel (a) indicates where the rainy season and growing season photos of Arbor Creek Experimental Catchment were taken.

2. Site Description

The study site is a small (0.04 km²) headwater catchment with an ephemeral stream that drains to the west, referred to as “Arbor Creek” (37.393, -121.723) within the North Dark Canyon Watershed (0.77 km²). Arbor Creek Experimental Catchment is located within the University of California Blue Oak Ranch Reserve (BORR; Figure 1) from 720 to 790 m above sea level. This reserve is located within the Mt. Diablo Range, ~24 km northeast of San Jose, California, USA.

2.1. Geologic and Tectonic Setting

The overall geologic setting of the study site is a recently uplifted coastal range with relatively low relief uplands (600–800 m above sea level) that are dissected by deep canyons (up to ~500 m) where large landslides are common (Page, 1999). The study site has no recorded Pleistocene glaciation or peri-glaciation (Marshall et al., 2021). The underlying geology of the study site has been mapped differently depending on the scale and purpose of investigation from local lithotectonic units observable in an outcrop (Raymond, 2014) to regional tectonic, deformation, and accretion studies that

prefer to use the Berkland et al. (1972) belt terminology (Bolhar & Ring, 2001; Ernst, 2011; Raymond, 2018). At the highest resolution of geologic mapping of 1:24,000, Dibblee and Minch (2005) characterized the area as Franciscan Assemblage comprised of massive to bedded metagraywacke sandstone, moderately to pervasively sheared shale and melange units (Crawford, 1975), bedded chert, greenstone, and blueschist. In its most general form, the surrounding region has been mapped broadly as “Franciscan complex undifferentiated.” Great Valley Sequence, and the controversial extension of the Eastern Belt/Yolla Bolly Unit with major rock types described as semi-schistose metawacke, meta-mudrock, metachert, and metabasite (Raymond, 2018; Wentworth et al., 1999). Our observations from outcrops within the study site suggest that locally, the dominant rock types are sequences of metagraywacke sandstone, shale, slaty shale with no evidence of chert, blueschist, or melanges, which is best described by the characteristics of the Yolla Bolly Unit and the Great Valley Sequence.

2.2. Climate and Vegetation

Blue Oak Ranch Reserve has a Mediterranean climate characterized by cool, wet winters and warm, dry summers. The average annual rainfall is 600 mm (standard deviation (SD) = 200 mm) from 2012 to 2021 and average air temperature of 8°C in January and 25°C in August (<http://www.wrcc.dri.edu/weather/ucbo.html>). Nearly all precipitation falls as rain between November and April, and the oak tree growing season extends from April to November.

This study area is characterized as a mixed oak savanna-woodland, where vegetation composition throughout the reserve is generally aspect-dependent (Figure 1). Within Arbor Creek Experimental Catchment, the NFS is a deciduous oak woodland dominated by blue oak (*Quercus douglasii*) and California black oak (*Quercus kelloggii*), with California bay laurel (*Umbellularia californica*) and California buckeye (*Aesculus californica*) present in the lower riparian area. The SFS is predominantly a perennial grassland (i.e., *Bromus diandrus* and *Elymus glaucus*) with sparse blue oak present at lower portions in the catchment that have a southeast slope angle.

3. Methods

The principal study transect within Arbor Creek Experimental Catchment covers two hillslopes, one NFS and one SFS, that drain to the ephemeral stream channel. On the transect, we established six instrumented stations across different landscape positions: near-stream, mid-slope, and near-ridge (Figure 2).

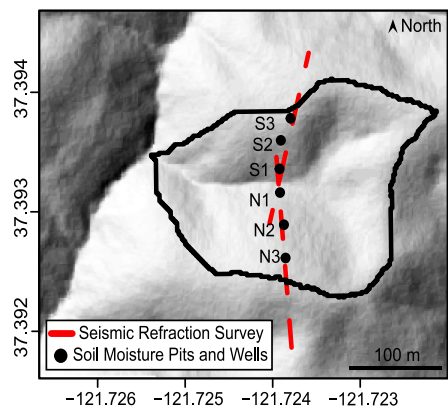


Figure 2. Hillshade of Arbor Creek Experimental Catchment showing instrumentation stations with the location of soil moisture sensors, groundwater wells (black circles; S3, S2, S1, N1, N2, N3) and seismic refraction transects (red dashed lines).

3.1. Terrain Analysis

We explored relationships between insolation, hillslope gradient, and vegetation using 1-m resolution 2020 LiDAR data collected for Santa Clara County (U.S. Geological Survey, 2020). We downloaded a bare-earth raster model of these data produced by the U.S. Geological Survey, and a raster of unfiltered first-return (vegetation top) data, both from opentopography.org. The first-return data were reprojected and resampled to align with the bare-earth data. Vegetation height was calculated by subtracting the bare-earth data from the first-return (vegetation top) data. A binary tree/no tree layer was generated with a 2-m vegetation height threshold after experimenting and spot checking this threshold against field knowledge. Chaparral is not very common in these areas, but where present is included in the “no tree” category. Insolation was modeled for the bare-earth data in ArcGIS Desktop using the Area Solar Radiation tool as direct radiation, diffuse radiation, and duration of radiation for the solstices, equinox, and annual totals. In addition, slope, aspect, and degrees from south were calculated from the bare-earth data. We compared the distributions of these terrain features in Arbor Creek Experimental Catchment to other watersheds in the same local region of the Diablo Range with similar lithology and geomorphic context to assess if the terrain features observed at our study site were representative of the larger region. We excluded infilled and fault-influenced valleys along the San Andreas Fault and excluded areas to the north within the Arroyo Hondo watershed that have much faster incision rates and hence steeper terrain.

3.2. Precipitation Measurements, Soil Characterization and Moisture

At the ridge of the NFS, we installed a weather station (ClimaVUE50, Campbell Scientific; Logan, Utah) to record precipitation inputs at 10-min intervals from 1 October 2020 to 30 September 2021 (2021 water year). We excavated soil to refusal (~1 m) and characterized the soil and top of saprolite at the near-stream, mid-slope, and near-ridge positions. We delineated soil horizons, depth to saprolite, and characterized parent material within the vertical pit faces. We define the soil as the organic or unconsolidated material that extends from the ground surface to the top of the “C” horizon. The measurement accuracy of the EC-5 sensors is 0.025 m³/m³ and 0.045 m³/m³ for sandy loam and silty loam soil, respectively (Kanso et al., 2020). We recorded soil VWC (cm³/cm³) at 10-min intervals from 1 October 2020 to 30 September 2021 (2021 water year).

We compared soil moisture across landscape positions within storm events, between storm events, and over the dry summer period. Storm events were defined with an event separation method that relied on two thresholds: minimum precipitation amount and minimum period without precipitation inputs (Wiekenkamp et al., 2016). A minimum precipitation amount of 1 mm was chosen because it was within the scope of precipitation sensor error and reduced the likelihood of analyzing precipitation inputs caused by fog that would not produce soil moisture response. A minimum period without precipitation of 12 hr was chosen because durations less than 12 hr did not fully capture soil moisture responses to incoming precipitation and durations of 24 hr led to lengthy events (>20 days) that were not representative of observed on-site storm lengths. We began the analyses on 21 January 2021 once all the soil moisture probes were operational, and a total of 13 precipitation events were delineated. The beginning of the summer period began on 25 April 2021, which was the date of the last precipitation input for that water year.

3.3. Saprolite Lithology and Perched Groundwater Measurements

We characterized the dominant saprolite lithology and the presence of a shallow, perched, and transient groundwater response at the saprolite-weathered bedrock interface by drilling boreholes and installing wells. Notably, the deeper, persistent water table is below the depth of observations that are pertinent to this work. Adjacent to soil pits, we hand-augered 2-inch boreholes to refusal (~1 m) and then drilled with a gas-powered backpack drill (Shaw Tool Ltd., Yamhill, Oregon) to 3–5 m, constrained by the drill's ability to advance through the material. On the NFS, the well depths were 3.33, 3.96, 3.80 m at the near-stream, mid-slope, and near-ridge landscape positions, respectively. On the SFS, the well depths were 3.10, 4.20, 4.67 m at the near-stream, mid-slope, and near-ridge, respectively. We characterized exhumed borehole samples by lithology type (i.e., shale vs. sandstone; Table S2 in Supporting Information S1).

Within each borehole, we installed wells to measure perched groundwater levels every 10-min using pressure transducers (± 0.1 mm resolution; Solinst, California). We screened the wells from the bottom of the adjacent soil pit (~1 m) to the bottom of the borehole to isolate hydrologic responses between the soil and underlying saprolite.

Table 1
Geometric Information for the Seven Seismic Refraction Surveys

Line #	Line name	Date collected	Geophone spacing (m)	Shot spacing (m)	Stack #	Seismic line length (m)
1	SFS_deep	10 August 2021	3	8	8	144
2	SFS_shallow1	10 August 2021	1	1	2	48
3	SFS_shallow2	10 August 2021	1	1	2	48
4	NFS_deep	11 August 2021	4	8	8	192
5	NFS_shallow1	11 August 2021	1	1	2	48
6	NFS_shallow2	11 August 2021	1	1	2	48
7	NFS_shallow3	11 August 2021	1	1	2	48

Due to the long screen intervals, it should be noted that we cannot definitely state which depth perched groundwater response originates. However, we believe that the depth to the refusal of the drill represents a transition from more friable to less friable material (thus a strong contrast in permeability) that may contribute to transient saturated conditions. We quantified the duration of perched groundwater response for each well as the percent of time that perched groundwater was present (i.e., sensor readings were ≥ 0.1 m) from 27 January 2021 to 25 April 2021. This date range presents the period from when all water level sensors were installed to the date of the last precipitation input for that water year.

3.4. Seismic Refraction

In August 2021, we conducted an active source seismic refraction campaign to investigate subsurface weathering patterns within the CZ. We completed seven surveys along the study transect, with four on the NFS and three on the SFS. We used two 24-channel Geode seismographs (Geometrics; San Jose, California). We generated the seismic source by swinging a sledgehammer onto an aluminum plate with 2–8 stacked shots adjacent to the survey lines. For the surveys, we used geophone spacing that ranged from 1 to 4 m and shot intervals that ranged from 1 to 8 m (Table 1). It should be noted that the seismic refraction surveys cannot be used to determine soil depth because the source frequency of hammer shots (~ 30 Hz) was not high enough to sufficiently resolve the seismic velocity of material less than 1 m depth range. We determined the topographic geometry for the seismic model from a 1.5 m spatial resolution Digital Elevation Model collected from an airborne LiDAR mission in 2006.

For each survey, we used the software *Pickwin* (Geometric Inc.) to pick the first P-wave (primary wave from the active seismic source) arrival time to each geophone location. Prior to the inversion, the travel-time data from the NFS and SFS were combined to create a single set of inputs for the inversion on each hillslope. We then performed a Transdimensional, Hierarchical, Bayesian inversion approach with reverse-jump Markov Chain Monte Carlo (THB rjMCMC) from Huang et al. (2021). The initial velocity model was proposed by interpolation of 40 model cells that are randomly distributed in the model domain, and the velocity was ranged from 300 m/s at the surface to 5,000 m/s at the bottom of the model. We randomly iterated the velocity model to create, delete, or move a model cell. We also allowed a random model cell to vary its velocity within the range of 300 and 5,000 m/s. As the measurement uncertainty is not known, it is inferred by the noise hyperparameter. The THB rjMCMC method randomly accepts or rejects the proposed model based on the algorithm proposed by Metropolis et al. (1953). This method calculates a mean model distribution from an ensemble of posterior velocity models after burn-in that can fit the measured P-wave travel time equally well. With this approach, we can reliably estimate measurement uncertainty as well as model resolving power at depth. After $\sim 6 \times 10^5$ iterations of this inversion approach, we used the estimated mean velocity of the ensemble posterior distribution to create a two-dimensional cross section of the best-fit subsurface seismic velocity structure. The interpreted transitional depths in subsurface structure are an approximation due to model structure and limitations (i.e., ray path coverage, smoothing factors, and cell size), but combined with ground-truthed observations of boreholes excavated materials provide a useful approach to identify seismically significant shifts in CZ structure. For more details on post-processing of the seismic velocity model, refer to Huang et al. (2021).

From our resulting velocity models described above, we calculated the vertical velocity gradient, defined as the change of P-wave seismic velocity with depth. Maxima in vertical velocity gradients have been shown to correlate with a transition from highly disaggregated or weathered material to more pristine, low porosity bedrock (Flinchum et al., 2022). Thus, we used vertical velocity gradient profiles across our study transect to identify potential transitions in CZ structure (i.e., porosity, lithology). We calculated the thickness of the saprolite along the survey transect by subtracting the land surface elevations from the average depth of the highest vertical velocity gradient and the corresponding seismic velocity contour, which has previously been shown to represent a transition to saprolite (Flinchum et al., 2018; Hudson-Rasmussen et al., 2023). We then binned the data into 5 m intervals (horizontal resolution of seismic data) and compared the difference in the calculated saprolite thickness between the max velocity gradient method and corresponding contour method between hillslope aspect. We used the Shapiro-Wilk Normality Test to test for normality across the different data sets, which determines whether data are normally (parametric) or not normally (non-parametric) distributed (Yazici & Yolacan, 2007). We determined whether the differences between slope-aspects across landscape positions are statistically significant using *t*-tests for parametric data and the Mann-Whitney U tests for non-parametric data (McKnight & Najab, 2010).

4. Results

4.1. Terrain Characteristics

Insolation has the greatest influence on tree presence in our study area. Above about 2,500 WH/m², we see a decrease in the ratio of hillslope pixels classified as trees (Figure S1 in Supporting Information S1, dashed line). This pattern can be observed qualitatively on the landscape most readily when looking at the vegetation contrast between adjacent NFS and SFS, which average around 1,500 WH/m² (~60% tree pixels) and 3,500 WH/m² (~20% tree pixels), respectively, in this local region (e.g., Figure 2; Figure S2 in Supporting Information S1). Within Arbor Creek Catchment, hillslope pixels oriented within 45° of North and South have similar distributions of slope angles (mean slope of 23.7° on NFS and 24.4° on SFS) (Figure 3a). Despite variability in hillslope orientation due to stream network shape, when comparing pixels across the larger region, NFS and SFS also have similar slope angles (mean slope of 24.7° on NFS and 23.2° on SFS).

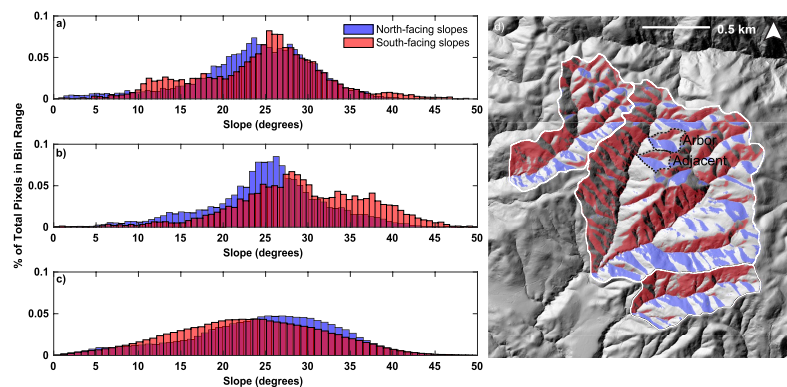


Figure 3. Slope distributions (a) for Arbor Creek Experimental Catchment (delineated in black (d)), for an (b) adjacent catchment to the south with similar solar orientation (delineated in black (d)), and for a (c) broader sample of catchments in the local region with similar geomorphology and lithology (delineated in white (d)). NFS's are shaded with blue and SFS's are shaded with red.

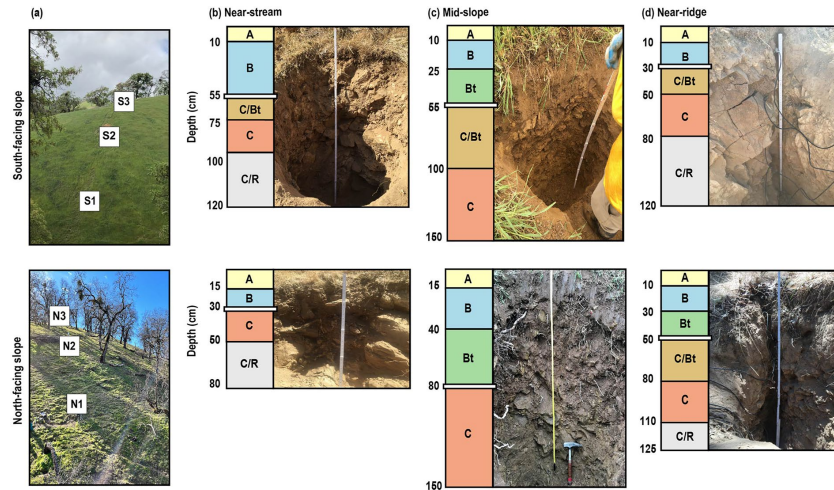


Figure 4. (a) Images of Arbor Creek Experimental Catchment's south-facing slopes and north-facing slopes. Soil pit images with soil horizons delineated at the (b) near-stream, (c) mid-slope and (d) near-ridge landscape positions. White line on the illustrated monolith represents the transition between soil to saprolite.

4.2. Soil Characteristics

Across the six soil pits, the soil depth ranged from 30 to 80 cm, with a mean depth of 51 cm (Table S1 in Supporting Information S1). On the NFS, soil depth varied by landscape position, with the shallowest soil depth occurring at the near-stream position (30 cm), the deepest soil depth at the mid-slope (80 cm) and intermediate depth (50 cm) at the near-ridge position. On the SFS, the soil depth was more uniform relative to the NFS; the near-stream and mid-slope both had 55 cm soil depths, while the near-ridge soil depth was only 30 cm (Figure 4).

4.3. Saprolite Characteristics

The seismic refraction mean velocity, vertical velocity gradient, and coefficient of variation are shown in Figure 5, showcasing the similarity in saprolite thickness between slope-aspects. The max vertical velocity gradient best corresponds to the depth at which the seismic velocity ranges from 1,200 to 1,400 m/s (Figure S3 in Supporting Information S1). This range is similar to velocities used to distinguish the saprolite-weathered bedrock transition in sandstones and mudstones (1,300 m/s; Hudson-Rasmussen et al., 2023) and granitic gneiss (1,400 m/s; Flinchum et al., 2019). We therefore inferred that the transition between the saprolite and weathered bedrock occurred within the range of the max velocity gradient, the depth to the 1,200 and 1,400 m/s seismic velocity contour. We observed the thickness of the saprolite to generally decrease from the ridge to the stream channel (Figure 6). These geophysical observations indicate that the saprolite thickness is similar between hillslopes with opposing aspects (Figure 6). Though the maximum vertical velocity gradient is systematically higher on the NFS (686 m/s/m) compared to the SFS (277 m/s/m). Based on the depth to the maximum gradient, the average saprolite depth was 6.6 ± 0.31 m and 5.7 ± 0.32 m on the NFS and SFS, respectively, and not statistically significant between slope-aspects ($t = 1.89$, p -value = 0.07). Based on the depth to the 1,200 m/s contour, the average saprolite depth was 6.1 ± 0.42 m and 5.6 ± 0.27 m for the NFS and SFS, respectively, which were not statistically different ($t = 0.95$, p -value = 0.34). Finally, using the 1,400 m/s velocity contour, the saprolite depth, 7.5 ± 0.64 m and 7.3 ± 0.49 m for the NFS and SFS, respectively, was also not statistically different ($W = 145.5$, p -value = 0.72). The root-mean-square error misfit evolution, mean misfit, a SD of the misfit in the mean velocity model, modeled travel time and observed travel time and raypath density of the mean velocity model are provided in Supporting Information S1 for the NFS and SFS (Figures S4 and S5 in Supporting Information S1, respectively).

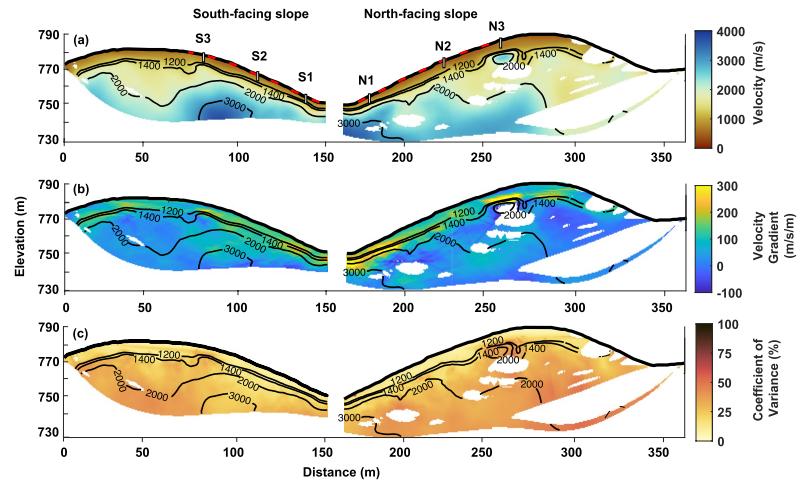


Figure 5. (a) Mean seismic refraction velocity model, (b) mean vertical velocity gradient, and (c) coefficient of variation for velocity model (inferred as model uncertainty) with 1,200, 1,400, 2,000, and 3,000 m/s velocity contours. Dashed red lines in panel (a) represent the hillslope length further analyzed for saprolite thickness. Vertical white bars in panel (a) represent the well locations and extent.

Below the maximum vertical velocity gradient, the seismic velocity increased from ~1,300 to 3,000 m/s on average at 26 m (SD 10 m) and 49 m (SD 11 m) below the ground surface on the SFS and NFS, respectively. The increase in the seismic velocity could be due to a gradually decreasing porosity (Figure 5; Flinchum et al., 2022; Gu et al., 2020). This transition most likely represents the transition from weathered bedrock (more competent than the saprolite above) to more pristine, low porosity material. The P-wave velocity of pristine (not chemically altered) sandstone with <20% porosity has been shown to be >3,800 m/s (Geldart & Sheriff, 2004). However, based solely on the seismic velocity data, we are unable to distinguish between weathered bedrock with low fracture density and fresh bedrock with high fracture density.

4.4. Soil Moisture and Perched, Transient Groundwater Responses

During the 13 delineated storm events, the soil VWC was similar between slope-aspects except at the 10 cm mid-slope position (Figure 7). At the near-stream position, the average 10 cm soil VWC was 0.16 and 0.18 on the SFS and NFS, respectively. At the mid-slope position, the 10 cm soil VWC was on average 0.19 and 0.28 on the SFS and NFS, respectively. At the near-ridge position, the 10 cm soil VWC was on average 0.22 and 0.25 on the SFS and NFS, respectively. Deeper within the soil, at the near-stream position, the 50 cm soil VWC was on average 0.16 and 0.18 on the SFS and NFS, respectively. At the mid-slope position, the 50 cm soil VWC was on average 0.25 on both the NFS and the SFS. At the near-ridge position, the 50 cm soil VWC was on average 0.24 and 0.27 on the SFS and NFS, respectively. Notably, at the near-ridge position, the SFS 50 cm soil VWC had flashy responses that increased the soil VWC above the NFS 50 cm soil VWC (Figure 7).

Between storm events, the soil VWC on the SFS was generally drier than the NFS (Figure 7). Specifically, between storm events, the 10 cm soil VWC on the SFS was on average 0.13, 0.17, and 0.22 at the near-stream, mid-slope, and near-ridge positions, respectively. The NFS 10 cm soil VWC was 0.16,

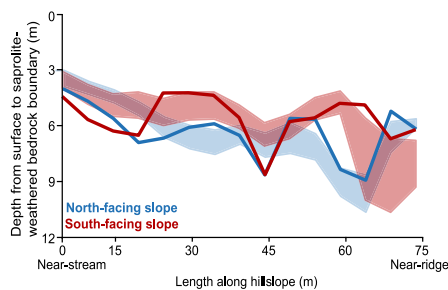


Figure 6. Average saprolite depth based on the depth to the 1,200 m/s velocity contour and 1,400 m/s velocity contour (top and bottom of shaded region, respectively) and the max velocity gradient (bold lines) for the north-facing slopes (blue) and south-facing slopes (red) within Arbor Creek Experimental Catchment.

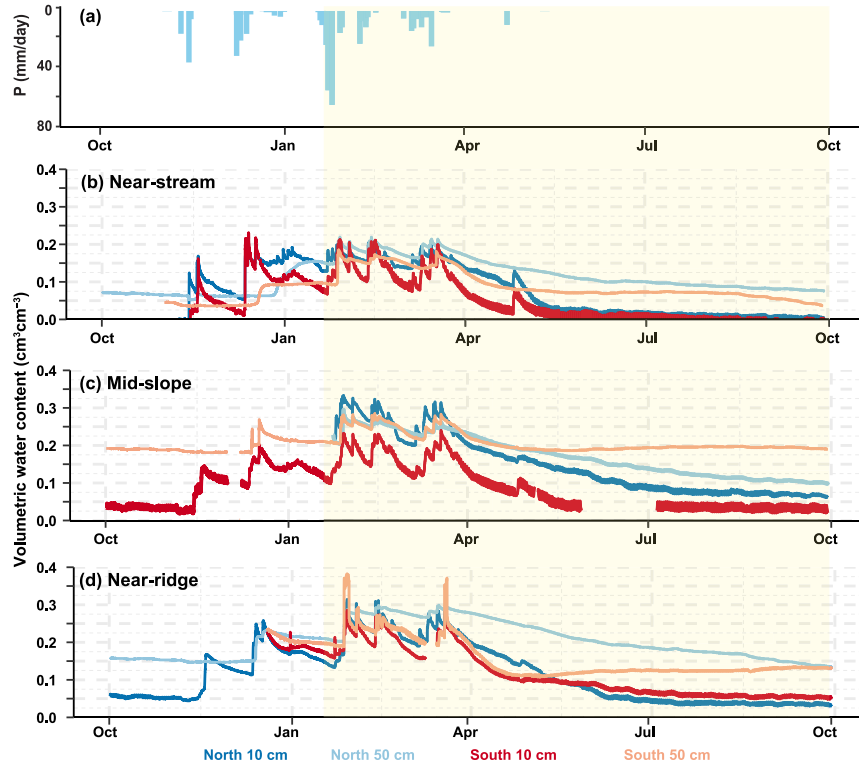


Figure 7. (a) Precipitation time series; Soil moisture at the (b) near-stream, (c) mid-slope, and (d) near-ridge landscape positions. At each landscape position, 10 cm (light) and 50 cm (dark) depths are shown for north-facing slopes (blues) and south-facing slopes (reds). Missing data are due to sensor malfunction. The yellow shaded region indicates the time period when soil moisture was compared in this study (21 January 2021–30 September 2021).

0.26, and 0.22 at the near-stream, mid-slope, and near-ridge positions, respectively (Figure 7). Deeper within the soil, at the near-stream position, the 50 cm soil VWC was on average 0.16 on the SFS and 0.18 on the NFS. At the mid-slope position, the 50 cm soil VWC was 0.24 on both the SFS and NFS. At the near-ridge position, the 50 cm soil VWC was 0.24 on the SFS and 0.27 on the NFS (Figure 7).

At the start of the summer 2021, the soil VWC was higher on the NFS compared to the SFS, except at the 50 cm depth mid-slope position where the soil VWC was similarly 0.19 (Figure 7). From April to May, the SFS dried down more than the NFS across all landscape positions and depths. By July, the 10 cm soil VWC dried down below 0.06 on both the NFS and SFS. At the 50 cm depth, the SFS soil VWC drying had plateaued in June while the NFS continued to dry down until September (Figure 7). At the end of the growing season (October), the soil VWC was similar between slope-aspects across all landscape positions and depths, except at the mid-slope position, 50 cm depth, where the NFS was 0.09 drier than the SFS.

Observed water levels in boreholes indicated higher perched groundwater response on SFS compared to NFS at the mid-slope and near-ridge landscape positions (Figure 8). During the period of observation for transient, perched groundwater (27 January 2021–25 April 2021), water levels responded to incoming precipitation events

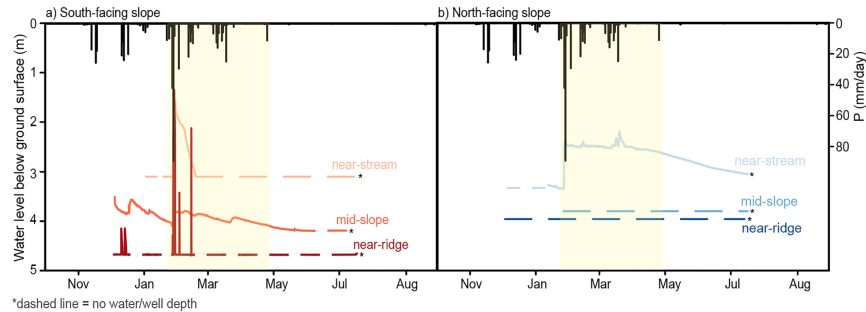


Figure 8. (a) South-facing slopes groundwater time series and (b) north-facing slopes groundwater time series during the 2021 water year for the near-stream, mid-slope and near-ridge landscape positions. Missing data at the beginning of the water year were due to delayed sensor installation and dashed lines represent no water present at the bottom of the well. The yellow shaded region indicates the time period when perched groundwater duration was quantified for this study (27 January 2021–25 April 2021).

across all landscape positions on the SFS, but only responded at the near-stream position on the NFS. Here, the dominant lithology is shale, which differs from the other sandstone-dominated landscape positions. On the NFS, perched groundwater was measurable 99%, 0%, and 0% of the observation period for the near-stream, mid-slope, and near-ridge positions, respectively. On the SFS, perched groundwater was measurable 21%, 98%, and 2% for the near-stream, mid-slope, and near-ridge positions, respectively. While the perched groundwater level at the SFS mid-slope was sustained throughout the observation period, perched groundwater levels at the near-stream and near-ridge positions only responded directly to precipitation events.

5. Discussion: Frameworks to Explain the Unexpected Symmetry in Hillslope Steepness and Saprolite Thickness Between Hillslopes With Opposing Aspects

A key goal of CZ science is to understand the relationship between the observed hillslope form and the past and present dominant geomorphic and hydrologic processes operating within the hillslope (Anderson et al., 2021; West et al., 2019). In the case of Arbor Creek Experimental Catchment, we observed similarities in the physical form (e.g., slope, average soil depth, and saprolite thickness) between hillslope aspects, despite distinct differences in microclimates and vegetation. These observations deviate from current common expectations borne out of extensive work in snow-dominated landscapes that suggest cooler, densely vegetated NFS will have steeper slopes, thicker soil, and thicker saprolite compared to warmer, sparsely vegetated SFS (Pelletier et al., 2017). Here, we contextualize our physical observations based on topographic analysis, soil pits, and geophysical measurements with relevant literature and in situ hydrologic measurements (e.g., soil moisture and perched groundwater) to provide potential explanations for the observed hillslope symmetry between aspects. Lastly, we discuss how the observed physical and ecohydrologic characteristics of Arbor Creek Experimental Catchment compare to current slope-aspect conceptual models. Our work highlights the importance of investigating CZ development between slope-aspects in rain-dominated climates.

We introduce two frameworks with non-exclusive mechanisms that may explain the symmetry in slope, and average soil depth and saprolite thickness between hillslopes with opposing aspects (Figure 9). The first framework explores how contemporary environmental conditions promote processes that can contribute to the similarities in the physical CZ of the NFS and SFS within Arbor Creek Experimental Catchment. The second framework considers how past climate and vegetation distributions could contribute to the present-day hillslopes form. Here, we argue that we must consider both frameworks in tandem to fully understand the development of the CZ we see today.

5.1. Contemporary Framework: Present-Day Similarities in Saprolite Weathering and Sediment Fluxes Between Hillslopes With Opposing Aspects

The Contemporary Framework explores present-day mechanisms that may contribute to the observed similarities in average saprolite thickness, soil thickness and slope between hillslopes with opposing aspects. These observed

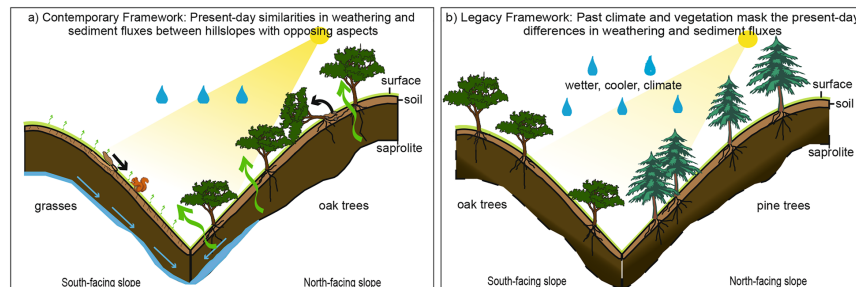


Figure 9. Two frameworks to explain similar hillslope steepness and/or saprolite thickness between hillslopes with opposing aspects. (a) Contemporary Framework: Present-day similarities in saprolite weathering and sediment fluxes between hillslopes with opposing aspects, despite aspect-dependent mechanisms. Similarities in sediment fluxes may be due to a balance between animal burrowing on the south-facing slopes (SFS) and wind-throw on the north-facing slopes (NFS). Similarities in saprolite weathering may be due to a balance between hydrologic dominated weathering on the SFS and hydrologic and biotic weathering on the NFS. (b) Legacy Framework: Past climate and vegetation effects on sediment fluxes and weathering may mask the present-day differences in weathering and sediment fluxes. There may have been similar sediment fluxes and saprolite weathering on the SFS and NFS because of the presence of woody vegetation on both slopes. Alternatively, material loss and production rates may have varied over geologic time, resulting in observed symmetry today. More time may be required under the current vegetative and climatic conditions to produce the expected critical zone asymmetries between aspects due to variable rates over geologic time. The gradient and dashed saprolite-weathered bedrock boundary represent the uncertainty in the past saprolite thickness between hillslope aspects.

similarities suggest that there is a uniform rate of saprolite weathering, soil production, and sediment transport across both slopes. However, we argue that the specific mechanisms driving these similarities vary by aspect.

5.1.1. Saprolite Weathering

One explanation for similar saprolite thickness between hillslopes with opposing aspects is that total saprolite weathering from both chemical and biological processes is uniform between slope-aspects. Within Arbor Creek, we observed more persistent perched shallow groundwater at the saprolite-weathered bedrock interface on the SFS, except at the NFS near-stream position, which is dominated by a different lithology than the rest of the study site (shale instead of sandstone; Figure 8). We hypothesize this perched groundwater presence enhances lateral flow, which accelerates chemical weathering on the SFS (Rempe & Dietrich, 2014; Wang et al., 2021). In contrast, lateral flow toward the stream on NFS may be lower due to limited saturated conditions in the saprolite from oak tree water uptake during the growing season. At the same time, deeply rooted oak trees on NFS may enhance biologically-driven weathering. Therefore, we hypothesize that the cumulative effects of reduced chemical weathering by limited lateral flow and enhanced biological weathering from vegetation on the NFS balance the heightened chemical weathering on SFS and may explain the observed symmetry in saprolite thickness across slopes.

Lateral flow toward the stream channel can occur at a portion of the subsurface where there is a sharp decrease in permeability with depth (Brantley et al., 2017). This perched, lateral drainage of fluids and subsequent replenishment with meteoric fluids is a process that has been proposed to dictate the extent of subsurface chemical weathering (Rempe & Dietrich, 2014). Since our geophysical results show uniform saprolite thickness across slopes, it suggests that if this specific weathering process acted in isolation, it would require lateral flow to be uniform across slopes. However, we observed a more persistent perched groundwater response on the SFS compared to the NFS, suggesting that the SFS may have a higher occurrence of lateral flow.

As stated above, one possible explanation for why we observe symmetry in saprolite thickness between hillslopes with opposing aspects may be due to the deeply rooted oak trees on NFS. Several mechanisms allow plant roots to directly and indirectly promote subsurface weathering processes (Brantley et al., 2017; Pawlik et al., 2016). For example, strain-induced porosity production due to root-wedging between existing fractures may contribute significantly to subsurface weathering (Hayes et al., 2019). Abiotic chemical weathering is strongly influenced by plant water uptake and redistribution, which can alter weathering pathways (Lucas, 2001). As deeply rooted oaks utilize water stored within the saprolite for transpiration (Hahm et al., 2020, 2022), depletion in water content

within the saprolite during the growing season could slow water residence times and increase the production of solutes.

Our observation of similar saprolite thickness across slope-aspects despite differences in vegetation and perched groundwater responses suggest that Arbor Creek Experimental Catchment may serve as an interesting site to investigate the relative importance of saprolite weathering via chemical loss (chemical weathering) and volumetric strain (physical weathering) (*sensu* Hayes et al., 2019; Riebe et al., 2021). To better understand the controls on subsurface weathering, future research should pair the seismic refraction surveys presented in this study with rock sample bulk geochemistry (e.g., ratios of immobile elements), physical properties analyses (e.g., bulk density, porosity) and a rock physics model (following Hayes et al., 2019). While this approach can not directly discern biotic-induced chemical weathering from water-driven chemical weathering, it can help disentangle the saprolite weathering driven by chemical loss (chemical weathering) and strain-induced porosity production (e.g., root-wedging).

5.1.2. Soil Production and Sediment Transport

Although we did not explicitly investigate erosion or soil production rates within this study, we provide a related hypothesis and justification for a potential driver of symmetry in hillslope steepness and soil thickness between slope-aspects. Based on the observed similarities in average soil thickness and hillslope steepness between aspects, we hypothesize that the soil production and sediment transport are similar despite variations in the dominant erosional and soil production processes operating. Specifically, we hypothesize that the balance between root-induced hillslope stabilization and sediment transport via wind-thrown trees may contribute to a net downslope sediment flux equivalent to the sediment flux on SFS from animal burrowing (Figure S6 in Supporting Information S1).

Small mammal burrowing is potentially a significant mode of sediment transport and soil production in steeply sloped and soil-mantled hillslopes (Black & Montgomery, 1991; Gabet et al., 2003). Although knowledge on the role of animal burrowing on sediment transport is limited to a few species and ecoregions, previous studies have identified a relationship between animal burrows and incoming solar radiation (Hall & Lamont, 2003; Übernickel et al., 2021). For example, Übernickel et al. (2021) conducted an inventory of burrowing animal entrances between NFS and SFS across four study sites with a hydroclimatic gradient in Chile. Their inventory revealed that the majority of small-animal entrances were located on the NFS, which have higher incoming solar radiation in the southern hemisphere (Poulos et al., 2012). They hypothesized that although more food and shelter may be present on the densely vegetated SFS, warmer temperatures on the NFS during the winter months may be favorable habitat for burrowing animals long-term.

Increased woody vegetation on a landscape can also have important implications for sediment transport and soil production due to higher rates of bioturbation (e.g., root decay, and wind-throw) (Gabet & Mudd, 2010). Although little research exists to the authors' knowledge on the causes, effects, and prevalence of wind-throw in oak woodlands, there are several studies investigating the effects of forest regeneration after wind disturbance in mixed-deciduous forests that include oaks (Götmark & Kiffer, 2014; Szwagrzyk et al., 2018). These studies suggest that wind-throw may be an important component of forested disturbance regimes (Cannon et al., 2017), which has unknown consequences for sediment transport and soil production. Therefore, more research is needed to have a better understanding of the potential for wind-throw to promote sediment transport on tree-dominated NFS, compared to grass-dominated SFS.

Similarities in average soil thickness and slope across our study hillslopes suggest that within Arbor Creek Experimental Catchment, prevalent animal burrowing on the warmer SFS may lead to equivalent sediment transport downslope by bioturbation (e.g., animal burrowing and tree-throw) on the NFS over long time scales. Future research to test this would require quantifying animal burrowing between hillslopes with opposing aspects through field surveys (Dixon et al., 2009) and quantifying the sediment flux due to wind-throw by a tree census (Šamonil et al., 2020) or estimating surface roughness with high resolution topographic data (Doane et al., 2021). Additionally, future work using cosmogenic radionuclides to measure hillslope erosion and soil production rates between hillslopes with opposing aspects over long time scales should be used to determine if rates are similar between hillslopes (Anderson et al., 2021; Granger et al., 1996; Heimsath et al., 1999).

5.2. Legacy Framework: Past Climate and Vegetation Mask the Present-Day Differences in Weathering and Sediment Fluxes

One potential mechanism for hillslope steepness and saprolite symmetry between aspects that our study design did not specifically address is the effect of past climates and vegetation distributions on CZ development.

Specifically, despite the expectation that NFS should have steeper slopes and a thicker saprolite compared to SFS, it is possible that the actively eroding landscapes of central coastal California require longer geologic time under the current climatic conditions to produce the expected topographic and subsurface asymmetries (Figure 9b). This is supported by previous studies that have demonstrated that delayed geomorphic adjustments to climatic fluctuations can lead to complex contemporary observations of soil erosion, soil thickness and topographic gradients (Heimsath et al., 1999; Hudson-Rasmussen et al., 2023; Hughes et al., 2009).

The physical structure of the CZ we observe today is an integration of climatic, hydrologic, vegetative, and lithologic processes that occur across a range of timescales. For example, timescales relevant for vegetation shifts can range from decades to centuries (Corlett & Westcott, 2013), while rock weathering patterns emerge over millennia to hundreds of millennia (Lebedeva & Brantley, 2020). For our study, if we estimate a 0.05–0.10 mm/yr erosion rate in the California Central Coast Ranges (sensu Montgomery, 1993), the maximum and minimum time required to develop the observed 6 m thick saprolite is 60,000–100,000 years. Therefore, we can assume that saprolite thickness is not only dictated by the climatic and vegetative conditions during the present-day Holocene but also by the Late Pleistocene (129 to 11.7 Ka). Paleoclimatic records from across California suggest that during the Pleistocene, climatic conditions were cooler and wetter, with potentially more intense precipitation events compared to the present-day Holocene (Daniels et al., 2005; Kulongoski et al., 2009).

Climatic shifts can have important implications for vegetation dynamics (Heusser, 1998) that can influence soil development and erosion, weathering rates and subsurface water storage (Hagedorn et al., 2019; Ivory et al., 2014; Jackson et al., 2000). The transition from the wetter, cooler Pleistocene to the warmer, drier Holocene contributed to a dramatic shift in dominant vegetation composition across California (Heusser, 1998). Pollen analyses from sediment cores and Neotoma (packrat) middens suggest these landscapes were previously dominated by *Pinus* species and that oak woodlands did not become well-established until the early-mid Holocene (Byrne et al., 1991; Cole, 1983; Heusser, 1998; Mensing, 2005). Furthermore, Mensing (2005) suggested that if oak trees were present during the late Pleistocene, it was “likely on the warmer SFS.” This suggests that the characteristic grass-dominated SFS and oak-tree dominated NFS we observe today may only be a relatively recent (~10,000 years) phenomenon. Therefore, it is plausible that the legacy of pine and oak trees on the SFS, and the associated rock weathering (Hasenmueller et al., 2017; Pawlik et al., 2016), may contribute to the symmetry in hillslope steepness and saprolite thickness between hillslopes with opposing aspects (Figure 9b).

An approach to investigating this could use numerical modeling to assess how variable climatic conditions (e.g., solar radiation and precipitation) influence vegetation compositions and soil moisture between slope-aspects. For example, Zhou et al. (2013) used an ecohydrological Cellular Automata Tree-Grass-Shrub Simulator to model the role of variable precipitation, solar radiation, and soil moisture on the distribution of juniper pine, grass, and creosote bush shrubs between slope-aspects over 10,000 years. We propose that this type of model could be adapted to investigate the distribution of oaks, pines, and grasses across climatic shifts from the wetter, cooler Pleistocene to the warmer, drier Holocene. Specifically, numerical modeling may be able to predict oak and pine vegetation distributions between slope-aspects and the potential effects on soil water balances. While this does not explicitly relate the vegetation distributions to erosion or subsurface weathering, pairing this vegetation distribution model with a landscape evolution model could begin to tease apart the co-evolution of landscapes with variable vegetation distributions.

5.3. Other Considerations

Spatial variability in hydrologic flow due to preferential flowpaths (e.g., rock fractures and macropores) and lithologic heterogeneity (e.g., rock type and bedrock foliation), which may or may not be aspect-dependent, could be contributing to the subsurface weathering patterns observed (Langston et al., 2015; Leone et al., 2020). For example, within a catchment with aspect-dependent differences in vegetation underlain by sedimentary rocks in Arizona, USA, Leone et al. (2020) combined seismic refraction and electrical resistivity tomography to reveal that saprolite on the SFS was thicker than the NFS. They hypothesized that on the SFS, the well-foliated bedrock dips at an angle that increases hydraulic conductivity, and vertical subsurface hydrologic flow promotes saprolite development. This study highlights that other environmental factors (e.g., lithology) may be a stronger control on hydrologic flowpaths and CZ development than microclimate between hillslopes with opposing aspects. A better understanding of how dominant flowpaths and subsurface structure may influence each other could be garnered with the coupling of more vertically resolved hydrologic measurements, high resolution geophysical

techniques (e.g., ground penetrating radar and electrical resistivity tomography), and tracer or irrigation experiments (Cassiani et al., 2009).

Another consideration that warrants future research is the magnitude of asymmetry that should be expected between hillslopes with opposing aspects in regions across the energy to water limitation gradient (Inbar et al., 2018; Nielson et al., 2021). For example, within a snow-dominated region at the semi-arid Reynold Creek CZ observatory underlain by extrusive igneous rock, Nielson et al. (2021) combined snowpack and soil moisture measurements with seismic refraction surveys to investigate saprolite thickness across an elevational gradient with varying snow accumulation. They observed the greatest saprolite asymmetry at the high elevation site where there was the greatest aspect-dependent difference in snow accumulation. In contrast, the low elevation site had similar snow accumulation between slope-aspects and there were nearly identical saprolite weathering thicknesses. They attributed the lack of weathering asymmetry to similarities in soil VWC and water recharge rates between NFS and SFS. These findings demonstrate that variability in soil VWC and recharge dynamics (e.g., magnitude and extent) can exert a strong control on the variability in soil and saprolite weathering.

Another example of variability in physical CZ asymmetry across precipitation gradients occurred in Southeastern Australia (Inbar et al., 2018). Inbar et al. (2018) observed variability in slope and soil depth differences between slope-aspect along a climogradient with mean annual rainfall from 400 to 2,500 mm. Their results revealed that maximum slope and soil depth asymmetry occurred in the transitional “goldilocks” regime between the wet and dry end member conditions. They hypothesized that variability in CZ physical asymmetry was a result of differences in vegetation cover, fire recurrence intervals, and soil hydraulic properties, which were all highly sensitive to differences in precipitation amounts. Therefore, while we observe strong contrasts in vegetation cover between slope-aspects (grass vs. tree) in Arbor Creek Experimental Catchment, the relatively low precipitation inputs (average 600 mm/yr) relative to the region’s high evapotranspiration demand may contribute to the lack of asymmetry observed. This further supports that a one-size-fits all model of aspect controls on hillslope steepness, soil, and saprolite thickness may not capture CZ physical variability across ecoregions important to predict dominant CZ functions.

6. Conclusion

Within a semi-arid, rain-dominated landscape underlain by sedimentary rocks, we used a multidisciplinary approach to investigate the influence of microclimates on CZ structure between hillslopes with opposing aspects. We observed that CZ structure between hillslopes with opposing aspects does not fully align with current conceptual models from the literature that are largely based on snow-dominated landscapes underlain by igneous rocks. We found that on a regional scale, decreased solar radiation correlated with increased tree presence. This aligns with observations within our focus study site, Arbor Creek Experimental Catchment, where the cooler NFS was dominated by oak trees and the warmer SFS was dominated by grasses. However, the hillslope steepness and saprolite thickness was similar between these hillslopes, which was counter to expectations.

We present two frameworks to explain the observed similarity in hillslope steepness, soil and saprolite thickness between hillslopes with opposing aspects. These non-exclusive frameworks highlight the importance of past and present ecohydrologic processes to alter subsurface water storage and movement, which has consequences for long-term CZ development. Further research applying these hypothesized mechanisms across rain-dominated systems with different precipitation magnitudes, vegetation types, and geologic settings can better constrain the prevalence of these potential mechanisms. In addition, the integration of lithologic heterogeneity, paleovegetation distributions and plant-driven alterations in hydrologic flowpaths into numerical models is an exciting frontier in understanding aspect-dependent CZ development. Such research is critically needed to identify the relationship between vegetation, hydrologic flowpaths and weathering, which has important implications for water resource management and ecosystem health in a changing climate.

Data Availability Statement

All data used in the publication are cited in the references and hosted on Consortium of Universities for the Advancement of Hydrologic Science, Inc. (CUAHSI)’s web-based hydrologic information system (HydroShare). A. M. Donaldson (2023). Symmetry in hillslope steepness and saprolite thickness between hillslopes with opposing aspects, HydroShare, <http://www.hydroshare.org/resource/9a9897aa0bb14d20ab4189b98a8439f6>.

The THB rj-MCMC software for active source seismic refraction inversion is available in Zenodo (<https://doi.org/10.5281/zenodo.4590999>; Huang et al., 2021).

Acknowledgments

The authors would like to acknowledge the financial support provided by the Betty and Gordon Moore Foundation under the project title: The California Heartbeat Initiative, National Science Foundation CAREER Grant (Award 2046957), the Instrumentation Discovery Grant through the Consortium of Universities for the Advancement of Hydrologic Sciences, Inc., and the Mildred E. Mathias Graduate Student Research Grant by the University of California Natural Reserve System. The authors would like to acknowledge the financial support granted by the University of California, Santa Cruz through the Kathryn D. Sullivan Impact Award and the Zhen and Wu Memorial Fund Award. The authors thank past and present members of the Zimmer Watershed Hydrology Lab, namely, Chris Causbrook, Peter Willis, Michael Wilshire and Lauren Giggy for support in the lab and field. Members of the California Heartbeat Initiative-Freshwater program, Todd Dawson, Jim Norris, and Collin Bode provided thoughtful guidance and key technical assistance throughout the project. In addition, the authors would like to thank Zac Harlow and Zac Tuthill for land access and troubleshooting enthusiasm. The authors are grateful to Editor Dr. Amy East, Associate Editor Dr. Seunggi Moon, Dr. Brady Flinchum, Dr. Eve-Lyn S. Hinckley, and one anonymous reviewer who provided valuable comments on this manuscript.

References

- Anderson, R. S., Anderson, S. P., & Tucker, G. E. (2013). Rock damage and regolith transport by frost: An example of climate modulation of the geomorphology of the critical zone. *Earth Surface Processes and Landforms*, 38(3), 299–316. <https://doi.org/10.1002/esp.3330>
- Anderson, R. S., Rajaram, H., & Anderson, S. P. (2019). Climate driven coevolution of weathering profiles and hillslope topography generates dramatic differences in critical zone architecture. *Hydrological Processes*, 33(1), 4–19. <https://doi.org/10.1002/hyp.13307>
- Anderson, S. P., Hinckley, E.-L., Kelly, P., & Langston, A. (2014). Variation in critical zone processes and architecture across slope aspects. *Procedia Earth and Planetary Science*, 10, 28–33. <https://doi.org/10.1016/j.proeps.2014.08.006>
- Anderson, S. P., Kelly, P. J., Hoffman, N., Barnhart, K., Befus, K., & Ouimet, W. (2021). Is this steady state? Weathering and critical zone architecture in Gordon Gulch, Colorado Front Range. *Hydrogeology, Chemical Weathering, and Soil Formation*, 231–252. <https://doi.org/10.1002/9781119563952.ch13>
- Armesto, J. J., & Martinez, J. A. (1978). Relations between vegetation structure and slope aspect in the Mediterranean Region of Chile. *Journal of Ecology*, 66(3), 881–889. <https://doi.org/10.2307/2259301>
- Befus, K. M., Sheehan, A. F., Leopold, M., Anderson, S. P., & Anderson, R. S. (2011). Seismic constraints on critical zone architecture, Boulder Creek Watershed, Front Range, Colorado. *Vadose Zone Journal*, 10(3), 915–927. <https://doi.org/10.2136/vzj2010.0108>
- Berkland, J. O., Raymond, L. A., Kramer, J. C., Moores, E. M., & O'Day, M. (1972). What is Franciscan? *American Association of Petroleum Geologists Bulletin*, 56, 2295–2302. <https://doi.org/10.1306/819A421A-16C5-11D7-8645000102C1865D>
- Black, T. A., & Montgomery, D. R. (1991). Sediment transport by burrowing mammals, Marin County, California. *Earth Surface Processes and Landforms*, 16(2), 163–172. <https://doi.org/10.1002/esp.3290160207>
- Bolhar, R., & Ring, U. (2001). Deformation history of the Yolla Bolly terrane at Leech Lake Mountain, Eastern belt, Franciscan subduction complex, California Coast Ranges. *GSA Bulletin*, 113(2), 181–195. [https://doi.org/10.1130/0016-7606\(2001\)113<0181:DHOTYB>2.0.CO;2](https://doi.org/10.1130/0016-7606(2001)113<0181:DHOTYB>2.0.CO;2)
- Brantley, S. L., Lebedeva, M. I., Balashov, V. N., Singha, K., Sullivan, P. L., & Stinchcomb, G. (2017). Toward a conceptual model relating chemical reaction fronts to water flow paths in hills. *Geomorphology*, 277, 100–117. <https://doi.org/10.1016/j.geomorph.2016.09.027>
- Buss, H. L., Chapela Lara, M., Moore, O. W., Kurtz, A. C., Schulz, M. S., & White, A. F. (2017). Lithological influences on contemporary and long-term regolith weathering at the Luquillo Critical Zone Observatory. *Geochimica et Cosmochimica Acta*, 196, 224–251. <https://doi.org/10.1016/j.gca.2016.09.038>
- Byrne, R., Edlund, E., & Mensing, S. A. (1991). Holocene changes in the distribution and abundance of oaks in California. USDA Forest Service General Technical Report PSW-126 (pp. 182–188). Retrieved from <http://treesearch.fs.fed.us/pubs/28418>
- Callahan, R. P., Riebe, C. S., Sklar, L. S., Pasquet, S., Ferrier, K. L., Hahm, W. J., et al. (2022). Forest vulnerability to drought controlled by bedrock composition. *Nature Geoscience*, 15(9), 714–719. <https://doi.org/10.1038/s41561-022-01012-2>
- Cannon, J. B., Peterson, C. J., O'Brien, J. J., & Brewer, J. S. (2017). A review and classification of interactions between forest disturbance from wind and fire. *Forest Ecology and Management*, 406, 381–390. <https://doi.org/10.1016/j.foreco.2017.07.035>
- Cassiani, G., Godio, A., Stocco, S., Villa, A., Deiana, R., Frattini, P., & Rossi, M. (2009). Monitoring the hydrologic behavior of a mountain slope via time-lapse electrical resistivity tomography. *Near Surface Geophysics*, 7(5–6), 475–486. <https://doi.org/10.3997/1873-0604.2009013>
- Chorover, J., Troch, P. A., Rasmussen, C., Brooks, P. D., Pelletier, J. D., Breshears, D. D., et al. (2011). How water, carbon, and energy drive critical zone evolution: The Jemez-Santa Catalina critical zone observatory. *Vadose Zone Journal*, 10(3), 884–899. <https://doi.org/10.2136/vzj2010.0132>
- Cole, K. (1983). Late Pleistocene vegetation of Kings Canyon, Sierra Nevada, California. *Quaternary Research*, 19(1), 117–129. [https://doi.org/10.1016/0033-5894\(83\)90031-5](https://doi.org/10.1016/0033-5894(83)90031-5)
- Corlett, R. T., & Westcott, D. A. (2013). Will plant movements keep up with climate change? *Trends in Ecology & Evolution*, 28(8), 482–488. <https://doi.org/10.1016/j.tree.2013.04.003>
- Crawford, K. E. (1975). The geology of the Franciscan tectonic assemblage near Mount Hamilton, California (Ph.D. thesis), University of California, (p. 137).
- Daniels, M. L., Anderson, R. S., & Whitlock, C. (2005). Vegetation and fire history since the Late Pleistocene from the Trinity Mountains, northwestern California, USA. *The Holocene*, 15(7), 1062–1071. <https://doi.org/10.1191/0959683605hl878ra>
- Desta, F., Colbert, J. J., Rentch, J. S., & Gottschalk, K. W. (2004). Aspect induced differences in vegetation, soil, and microclimatic characteristics of an Appalachian watershed. *Castanea*, 69(2), 92–108. [https://doi.org/10.2179/0008-7475\(2004\)069<0092:aidivs>2.0.co;2](https://doi.org/10.2179/0008-7475(2004)069<0092:aidivs>2.0.co;2)
- Dibblee, T. W., Jr., & Minch, J. A. (2005). *Geologic map of the Diablo quad-range, contra costa and alameda counties*. Dibblee Geological Foundation (Santa Barbara Museum of Natural History). Dibblee Foundation Map DF-162, scale 1:24,000.
- Dixon, J., Heimsath, A., & Amundson, R. (2009). The critical role of climate and saprolite weathering in landscape evolution. *Earth Surface Processes and Landforms*, 34, 155–161. <https://doi.org/10.1002/esp>
- Doane, T. H., Edmonds, D., Yanites, B. J., & Lewis, Q. (2021). Topographic roughness on forested hillslopes: A theoretical approach for quantifying hillslope sediment flux from tree throw. *Geophysical Research Letters*, 48(20), 1–10. <https://doi.org/10.1029/2021GL094987>
- Donaldson, A. M. (2023). *Symmetry in hillslope steepness and saprolite thickness between hillslopes with opposing aspects*. HydroShare. Retrieved from <http://www.hydroshare.org/resource/9a9897aa0bb14d20ab4189b98a8439f6>
- Ernst, W. G. (2011). Accretion of the Franciscan Complex attending Jurassic-Cretaceous geotectonic development of northern and central California. *Bulletin of the Geological Society of America*, 123(9–10), 1667–1678. <https://doi.org/10.1130/B30398.1>
- Fan, Y., Clark, M., Lawrence, D. M., Swenson, S., Band, L. E., Brantley, S. L., et al. (2019). Hillslope hydrology in global change research and Earth system modeling. *Water Resources Research*, 55(2), 1737–1772. <https://doi.org/10.1029/2018WR023903>
- Fan, Y., Grant, G., & Anderson, S. P. (2019). Water within, moving through, and shaping the Earth's surface: Introducing a special issue on water in the critical zone. *Hydrological Processes*, 33(25), 3146–3151. <https://doi.org/10.1002/hyp.13638>
- Ferdowsi, B., Gartner, J. D., Johnson, K. N., Kasprak, A., Miller, K. L., Nardin, W., et al. (2021). Earthcasting: Geomorphic forecasts for society. *Earth's Future*, 9(11), 1–24. <https://doi.org/10.1029/2021EF002088>
- Flinchum, B., Holbrook, W. S., Grana, D., Parsekian, A. D., Carr, B. J., Hayes, J. L., & Jiao, J. (2019). Estimating water holding capacity of the critical zone using near-surface geophysics. *Hydrological Processes*, 32(22), 3308–3326. <https://doi.org/10.1002/hyp.13260>
- Flinchum, B. A., Holbrook, W. S., & Carr, B. J. (2022). What do P-wave velocities tell us about the critical zone? *Frontiers in Water*, 3, 1–15. <https://doi.org/10.3389/frwa.2021.772185>

- Flinchum, B. A., Holbrook, W. S., Rempe, D., Moon, S., Riebe, C. S., Carr, B. J., et al. (2018). Critical zone structure under a granite ridge inferred from drilling and three-dimensional seismic refraction data. *Journal of Geophysical Research: Earth Surface*, 123(6), 1317–1343. <https://doi.org/10.1029/2017JF004280>
- Gabet, E. J., & Mudd, S. M. (2010). Bedrock erosion by root fracture and tree throw: A coupled biogeomorphic model to explore the humped soil production function and the persistence of hillslope soils. *Journal of Geophysical Research*, 115(4), 1–14. <https://doi.org/10.1029/2009JF001526>
- Gabet, E. J., Reichman, O. J., & Seabloom, E. W. (2003). The effects of bioturbation on soil processes and sediment transport. *Annual Review of Earth and Planetary Sciences*, 31(1), 249–273. <https://doi.org/10.1146/annurev.earth.31.100901.141314>
- García-Gamero, V., Peña, A., Laguna, A. M., Giráldez, J. V., & Vanwalleghem, T. (2021). Factors controlling the asymmetry of soil moisture and vegetation dynamics in a hilly Mediterranean catchment. *Journal of Hydrology*, 598, 126207. <https://doi.org/10.1016/j.jhydrol.2021.126207>
- Geldart, L. P., & Sheriff, R. E. (2004). *Problems in exploration seismology and their solutions*. Society of Exploration Geophysicists.
- Götmark, F., & Kiffer, C. (2014). Regeneration of oaks (*Quercus robur*/Q. *petraea*) and three other tree species during long-term succession after catastrophic disturbance (windthrow). *Plant Ecology*, 215(9), 1067–1080. <https://doi.org/10.1007/s11258-014-0365-4>
- Granger, D. E., Kirchner, J. W., & Finkel, R. (1996). Spatially averaged long-term erosion rates measured from in situ-produced cosmogenic nuclides in alluvial sediment. *The Journal of Geology*, 104(3), 249–257. <https://doi.org/10.1086/629823>
- Gu, X., Mavko, G., Ma, L., Oakley, D., Accardo, N., Carr, B. J., et al. (2020). Seismic refraction tracks porosity generation and possible CO₂ production at depth under a headwater catchment. *Proceedings of the National Academy of Sciences of the United States of America*, 117(32), 18991–18997. <https://doi.org/10.1073/pnas.2003451117>
- Gutierrez-Jurado, H., Vivoni, E. R., Harrison, B. J., & Guan, H. (2006). Ecohydrology of root zone water fluxes and soil development in complex semiarid rangelands. *Hydrological Processes*, 20(15), 2267–2274. <https://doi.org/10.1002/hyp.6333>
- Hagedorn, F., Gavazov, K., & Alexander, J. M. (2019). Above- and belowground linkages shape responses of mountain vegetation to climate change. *Science*, 1123, 1119–1123. <https://doi.org/10.1126/science.aax4737>
- Hahn, W. J., Dralle, D. N., Sanders, M., Bryk, A. B., Fauria, K. E., Huang, M. H., et al. (2022). Bedrock vadose zone storage dynamics under extreme drought: Consequences for plant water availability, recharge, and runoff. *Water Resources Research*, 58(4), 1–23. <https://doi.org/10.1029/2021WR031781>
- Hahn, W. J., Rempe, D. M., Dralle, D. N., Dawson, T. E., & Dietrich, W. E. (2020). Oak transpiration drawn from the weathered bedrock vadose zone in the summer dry season. *Water Resources Research*, 56(11), 1–24. <https://doi.org/10.1029/2020WR027419>
- Hahn, W. J., Rempe, D. M., Dralle, D. N., Dawson, T. E., Lovill, S. M., Bryk, A. B., et al. (2019). Hydrologically controlled subsurface critical zone thickness and water storage capacity determine regional plant community composition. *Water Resources Research*, 55(4), 3028–3055. <https://doi.org/10.1029/2018WR023760>
- Hall, K., & Lamont, N. (2003). Zoogeomorphology in the Alpine: Some observations on abiotic–biotic interactions. *Geomorphology*, 55(1–4), 219–234. [https://doi.org/10.1016/S0169-555X\(03\)00141-7](https://doi.org/10.1016/S0169-555X(03)00141-7)
- Hasenmueller, E. A., Gu, X., Weitzman, J. N., Adams, T. S., Stinchcomb, G. E., Eissenstat, D. M., et al. (2017). Weathering of rock to regolith: The activity of deep roots in bedrock fractures. *Geoderma*, 300, 11–31. <https://doi.org/10.1016/j.geoderma.2017.03.020>
- Hayes, J. L., Riebe, C. S., Holbrook, F., Flinchum, S. W. B. A., & Hartsough, P. C. (2019). Porosity production in weathered rock: Where volumetric strain dominates over chemical mass loss. *Science Advances*, 5(9), 1–12. <https://doi.org/10.1126/sciadv.aao0834>
- Heimsath, A. M., Dietrich, W. E., Nishiizumi, K., & Finkel, R. C. (1999). Cosmogenic nuclides, topography, and the spatial variation of soil depth. *Geomorphology*, 27(1–2), 151–172. [https://doi.org/10.1016/S0169-555X\(98\)00095-6](https://doi.org/10.1016/S0169-555X(98)00095-6)
- Heusser, L. (1998). Direct correlation of millennial-scale changes in western North American vegetation and climate with changes in the California current system over the past ~60 Kyr. *Paleoceanography*, 13(3), 252–262. <https://doi.org/10.1029/98PA00670>
- Huang, M. H., Hudson-Rasmussen, B., Burdick, S., Lekic, V., Nelson, M. D., Fauria, K. E., & Scherr, N. (2021). Bayesian seismic refraction inversion for critical zone science and near-surface applications. *Geochemistry, Geophysics, Geosystems*, 22(5), 1–20. <https://doi.org/10.1029/2020GC009172>
- Hudson-Rasmussen, B., Huang, M.-H., Hahn, W. J., Rempe, D., Dralle, D. N., & Nelson, M. D. (2023). Mapping variations in bedrock weathering with slope aspect under a sedimentary ridge–valley system using near–surface geophysics and drilling. *ESS Open Archive*. <https://doi.org/10.22541/essoar.168435460.02903987v1>
- Hughes, M. W., Almond, P. C., & Roering, J. J. (2009). Increased sediment transport via bioturbation at the last glacial-interglacial transition. *Geology*, 37(10), 919–922. <https://doi.org/10.1130/G30159A.1>
- Inbar, A., Nyman, P., Rengers, F. K., Lane, P. N. J., & Sheridan, G. J. (2018). Climate dictates magnitude of asymmetry in soil depth and hillslope gradient. *Geophysical Research Letters*, 45(13), 6514–6522. <https://doi.org/10.1029/2018GL077629>
- Istanbulluoglu, E., Yetemen, O., Vivoni, E. R., Gutiérrez-Jurado, H. A., & Bras, R. L. (2008). Eco-geomorphic implications of hillslope aspect: Inferences from analysis of landscape morphology in central New Mexico. *Geophysical Research Letters*, 35(14), 1–6. <https://doi.org/10.1029/2008GL034477>
- Ivory, S. J., Meglue, M. M., Ellis, G. S., Lézine, A.-M., Cohen, A. S., & Vincens, A. (2014). Vegetation controls on weathering intensity during the last deglacial transition in southeast Africa. *PLoS One*, 9(11), 112855. <https://doi.org/10.1371/journal.pone.0112855>
- Jackson, R. B., Schenk, H. J., Jobbágy, E. G., Canadell, J., Colella, G. D., Dickinson, R. E., et al. (2000). Belowground consequences of vegetation change and their treatment in models. *Ecological Applications*, 10(2), 470–483. [https://doi.org/10.1890/1051-0761\(2000\)010\[0470:BCOVCA\]2.0.CO;2](https://doi.org/10.1890/1051-0761(2000)010[0470:BCOVCA]2.0.CO;2)
- Kanso, T., Gromaire, M. C., Ramier, D., Dubois, P., & Chebbo, G. (2020). An investigation of the accuracy of EC5 and 5TE capacitance sensors for soil moisture monitoring in urban soils-laboratory and field calibration. *Sensors*, 20(22), 6510. <https://doi.org/10.3390/s20226510>
- Kulongoski, J. T., Hilton, D. R., Izibicki, J. A., & Belitz, K. (2009). Evidence for prolonged El Niño-like conditions in the Pacific during the Late Pleistocene: A 43 ka noble gas record from California groundwaters. *Quaternary Science Reviews*, 28(23–24), 2465–2473. <https://doi.org/10.1016/j.quascirev.2009.05.008>
- Kumari, N., Saco, P. M., Rodriguez, J. F., Johnstone, S. A., Srivastava, A., Chun, K. P., & Yetemen, O. (2020). The grass is not always greener on the other side: Seasonal reversal of vegetation greenness in aspect-driven semiarid ecosystems. *Geophysical Research Letters*, 47(15), 1–12. <https://doi.org/10.1029/2020GL088918>
- Langston, A. L., Tucker, G. E., Anderson, R. S., & Anderson, S. P. (2015). Evidence for climatic and hillslope-aspect controls on vadose zone hydrology and implications for saprolite weathering. *Earth Surface Processes and Landforms*, 40(9), 1254–1269. <https://doi.org/10.1002/esp.3718>
- Lebedeva, M. I., & Brantley, S. L. (2013). Exploring geochemical controls on weathering and erosion of convex hillslopes: Beyond the empirical regolith production function. *Earth Surface Processes and Landforms*, 38(15), 1793–1807. <https://doi.org/10.1002/esp.3424>
- Lebedeva, M. I., & Brantley, S. L. (2018). A clarification and extension of our model of regolith formation on hillslopes. *Earth Surface Processes and Landforms*, 43(13), 2715–2723. <https://doi.org/10.1002/esp.4426>

- Lebedeva, M. I., & Brantley, S. L. (2020). Exploring an 'ideal hill': How lithology and transport mechanisms affect the possibility of a steady state during weathering and erosion. *Earth Surface Processes and Landforms*, 45(3), 652–665. <https://doi.org/10.1002/esp.4762>
- Leone, J. D., Holbrook, W. S., Riebe, C. S., Chorover, J., Ferré, T. P. A., Carr, B. J., & Callahan, R. P. (2020). Strong slope-aspect control of regolith thickness by bedrock foliation. *Earth Surface Processes and Landforms*, 45(12), 2998–3010. <https://doi.org/10.1002/esp.4947>
- Lucas, Y. (2001). The role of plants in controlling rates and products of weathering: Importance of biological pumping. *Annual Review of Earth and Planetary Sciences*, 29(1), 135–163. <https://doi.org/10.1146/annurev.earth.29.1.135>
- Ma, L., Oakley, D., Nyblade, A., Moon, S., Accardo, N., Wang, W., et al. (2021). Seismic imaging of a shale landscape under compression shows limited influence of topography-induced fracturing. *Geophysical Research Letters*, 48(17), e2021GL093372. <https://doi.org/10.1029/2021GL093372>
- Marshall, J. A., Roering, J. J., Rempel, A. W., Shafer, S. L., & Bartlein, P. J. (2021). Extensive frost weathering across unglaciated North America during the last glacial maximum. *Geophysical Research Letters*, 48(5), e2020GL090305. <https://doi.org/10.1029/2020GL090305>
- Maxwell, A. E., & Shobe, C. M. (2022). Land-surface parameters for spatial predictive mapping and modeling. *Earth-Science Reviews*, 226, 103944. <https://doi.org/10.1016/j.earscirev.2022.103944>
- McGuire, L. A., Pelletier, J. D., & Roering, J. J. (2014). Development of topographic asymmetry: Insights from dated cinder cones in the western United States. *Journal of Geophysical Research F: Earth Surface*, 119(8), 1725–1750. <https://doi.org/10.1002/2014JF003081>
- McKnight, P., & Najab, J. (2010). Mann-Whitney U test. *Dictionary of Statistics & Methodology*. <https://doi.org/10.4135/9781412983907.n115>
- Mensing, S. (2005). The history of oak woodlands in California, part I: The paleoecologic record.
- Metropolis, N., Rosenbluth, A. W., Rosenbluth, M. N., Teller, A. H., & Teller, E. (1953). Equation of state calculations by fast computing machines. *The Journal of Chemical Physics*, 21(6), 1087–1092. <https://doi.org/10.1063/1.1699114>
- Montgomery, D. R. (1993). Compressional uplift in the central California Coast ranges. *Geology*, 21(6), 543–546. [https://doi.org/10.1130/0091-7613\(1993\)021<0543:CUITCC>2.3.CO;2](https://doi.org/10.1130/0091-7613(1993)021<0543:CUITCC>2.3.CO;2)
- Moon, S., Perron, J. T., Martel, S. J., Holbrook, W. S., & St. Clair, J. (2017). A model of three-dimensional topographic stresses with implications for bedrock fractures, surface processes, and landscape evolution. *Journal of Geophysical Research: Earth Surface*, 122(4), 823–846. <https://doi.org/10.1002/2016JF00415>
- Nielson, T., Bradford, J., Holbrook, W. S., & Seyfried, M. (2021). The effect of aspect and elevation on critical zone architecture in the Reynolds Creek critical zone observatory: A seismic refraction study. *Frontiers in Water*, 1, 670524. <https://doi.org/10.3389/frwa.2021.670524>
- Page, B. M. (1999). Geology of the lick observatory quadrangle, California. *International Geology Review*, 41(4), 355–367. <https://doi.org/10.1080/00206819909465146>
- Pawlik, E., Phillips, J. D., & Samonil, P. (2016). Roots, rock, and regolith: Biomechanical and biochemical weathering by trees and its impact on hillslopes-A critical literature review. *Earth-Science Reviews*, 159, 142–159. <https://doi.org/10.1016/j.earscirev.2016.06.002>
- Pedraza, M. A., Hamm, W. J., Huang, M.-H., Dralle, D., Nelson, M. D., Breunig, R. E., et al. (2021). The relationship between topography, bedrock weathering, and water storage across a sequence of ridges and valleys. *Journal of Geophysical Research: Earth Surface*, 126(4), e2020JF005848. <https://doi.org/10.1029/2020JF005848>
- Pelletier, J. D., Barron-Gafford, G. A., Gutiérrez-Jurado, H., Hinckley, E.-L. S., Istanbuluoglu, E., McGuire, L. A., et al. (2017). Which way do you lean? Using slope aspect variations to understand critical zone processes and feedbacks. *Earth Surface Processes and Landforms*, 43(5), 1133–1154. <https://doi.org/10.1002/esp.4306>
- Perron, J. T. (2017). Climate and the pace of erosional landscape evolution. *Annual Review of Earth and Planetary Sciences*, 45, 1–71. <https://doi.org/10.1146/annurev-earth-060614-105405>
- Poulos, M. J., Pierce, J. L., Flores, A. N., & Benner, S. G. (2012). Hillslope asymmetry maps reveal widespread, multi-scale organization. *Geophysical Research Letters*, 39(6), 6406. <https://doi.org/10.1029/2012GL051283>
- Raymond, L. A. (2014). Designating tectonostratigraphic terranes versus mapping rock units in subduction complexes: Perspectives from the Franciscan Complex of California, USA. *International Geology Review*, 57(5–8), 801–823. <https://doi.org/10.1080/00206814.2014.911124>
- Raymond, L. A. (2018). What is Franciscan?: Revisited. *International Geology Review*, 60(16), 1968–2030. <https://doi.org/10.1080/00206814.2017.1396933>
- Regmi, N. R., McDonald, E. V., & Rasmussen, C. (2019). Hillslope response under variable microclimate. *Earth Surface Processes and Landforms*, 44(13), 2615–2627. <https://doi.org/10.1002/esp.4686>
- Rempe, D. M., & Dietrich, W. E. (2014). A bottom-up control on fresh-bedrock topography under landscapes. *Proceedings of the National Academy of Sciences of the United States of America*, 111(18), 6576–6581. <https://doi.org/10.1073/pnas.1404763111>
- Riebe, C. S., Callahan, R. P., Granke, S. B. M., Carr, B. J., Hayes, J. L., Schell, M. S., & Sklar, L. S. (2021). Anisovolumetric weathering in granitic saprolite controlled by climate and erosion rate. *Geology*, 49(5), 551–555. <https://doi.org/10.1130/G48191.1551-555>
- Riebe, C. S., Kirchner, J. W., Granger, D. E., & Finkel, R. C. (2001). Strong tectonic and weak climatic control of long-term chemical weathering rates. *Geology*, 29(6), 511–514. [https://doi.org/10.1130/0091-7613\(2001\)029](https://doi.org/10.1130/0091-7613(2001)029)
- Roering, J. J., Almond, P., McKean, J., & Tonkin, P. (2002). Soil transport driven by biological processes over millennial timescales. *Geology*, 30(12), 1115–1118. [https://doi.org/10.1130/0091-7613\(2002\)030<1115:STDBBP>2.0.CO;2](https://doi.org/10.1130/0091-7613(2002)030<1115:STDBBP>2.0.CO;2)
- Šamonil, P., Egli, M., Steinert, T., Norton, K., Abiven, S., Daněk, P., et al. (2020). Soil denudation rates in an old-growth mountain temperate forest driven by tree uprooting dynamics, Central Europe. *Land Degradation & Development*, 31(2), 222–239. <https://doi.org/10.1002/ldr.3443>
- Sharp, R. P. (1982). Landscape evolution (A review). *Proceedings of the National Academy of Sciences of the United States of America*, 79(14), 4477–4486. <https://doi.org/10.1073/pnas.79.14.4477>
- Smith, T., & Bookhagen, B. (2020). Climatic and biotic controls on topographic asymmetry at the global scale. <https://doi.org/10.1029/2020JF005692>
- Slyom, P. B., & Tucker, G. (2004). Effect of limited storm duration on landscape evolution, drainage basin geometry, and hydrograph shapes. *Journal of Geophysical Research*, 109(F3), 1–13. <https://doi.org/10.1029/2003JF000032>
- St. Clair, J., Moon, S., Holbrook, W. S., Perron, J. T., Riebe, C. S., Martel, S. J., et al. (2015). Geophysical imaging reveals topographic stress control of bedrock weathering. *Science*, 350(6260), 534–538. <https://doi.org/10.1126/science.122110>
- Szwagrzyk, J., Gazda, A., Dobrowolska, D., Checko, E., Zaremba, J., & Tomski, A. (2018). Natural regeneration following wind disturbance increases the diversity of managed lowland forests in NE Poland. *Journal of Vegetation Science*, 29(5), 898–906. <https://doi.org/10.1111/jvs.12672>
- Übernickel, K., Pizarro-Araya, J., Bhagavathula, S., Paulino, L., & Ehlers, T. A. (2021). Reviews and syntheses: Composition and characteristics of burrowing animals along a climate and ecological gradient, Chile. *Biogeosciences*, 18(20), 5573–5594. <https://doi.org/10.5194/bg-18-5573-2021>
- U.S. Geological Survey. (2020). 3D elevation program. CA LiDar. Distributed by OpenTopography Retrieved from https://portal.opentopography.org/usgsDataset?dsid=CA_SantaClaraCounty_2020

- Wang, W., Chen, P., Dueker, K., Zhang, Y., Lee, E.-J., Mu, D., et al. (2021). Coevolution of weathering front and water table. *Geophysical Research Letters*, *48*(20), e2021GL092916. <https://doi.org/10.1029/2021GL092916>
- Wentworth, C. M., Blake, M. C., McLaughlin, R. J., & Graymer, R. W. (1999). Preliminary geologic description of the San Jose 30 X 60 minute quadrangle, California. *Open-File Report*, 98-795, 1-52.
- West, N., Kirby, E., Nyblade, A. A., & Brantley, S. L. (2019). Climate preconditions the Critical Zone: Elucidating the role of subsurface fractures in the evolution of asymmetric topography. *Earth and Planetary Science Letters*, *513*, 197-205. <https://doi.org/10.1016/j.epsl.2019.01.039>
- Wiekenkamp, I., Huisman, J. A., Bogena, H. R., Lin, H. S., & Vereecken, H. (2016). Spatial and temporal occurrence of preferential flow in a forested headwater catchment. *Journal of Hydrology*, *534*, 139-149. <https://doi.org/10.1016/j.jhydrol.2015.12.050>
- Yazici, B., & Yolacan, S. (2007). A comparison of various tests of normality. *Journal of Statistical Computation and Simulation*, *77*(2), 175-183. <https://doi.org/10.1080/10629360600678310>
- Yetemen, O., Istanbuluoglu, E., Homero Flores-Cervantes, J., Vivoni, E., & Bras, R. (2015). Ecohydrologic role of solar radiation on landscape evolution, 1127-1157. <https://doi.org/10.1002/2014WR016169>
- Zapata-Rios, X., Brooks, P. D., Troch, P. A., McIntosh, J., & Guo, Q. (2016). Influence of terrain aspect on water partitioning, vegetation structure and vegetation greening in high-elevation catchments in northern New Mexico. *Ecohydrology*, *9*(5), 782-795. <https://doi.org/10.1002/eco.1674>
- Zhou, X., Istanbuluoglu, E., & Vivoni, E. R. (2013). Modeling the ecohydrological role of aspect-controlled radiation on tree-grass-shrub coexistence in a semiarid climate. *Water Resources Research*, *49*(5), 2872-2895. <https://doi.org/10.1002/wrcr.20259>